B Physics from the Lattice

John Charles Mehegan

Doctor of Philosophy

The University of Edinburgh

1995

Abstract

Results are presented of a lattice calculation of f_B, the leptonic decay constant of the B meson, and of B_B, the "bag-parameter" of B^0-$\bar{B}^0$ mixing. All the calculations are performed with the heavy quark constituent of the B meson treated in the static approximation and with an $\mathcal{O}(a)$-improved fermion action used for the light quarks. The calculations are performed in the quenched approximation on a $24^3 \times 48$ lattice at $\beta = 6.2$. In simulating the behaviour of B mesons on the lattice one of the most important technical issues is how to correctly isolate the ground state. This is particularly the case when the static approximation is used. Hence several smeared interpolating operators for the B meson are used in these calculations and the results using the various operators are presented and compared. The main findings are

$$\begin{aligned}
f_B^{\rm static} &= 268 \; {}^{+14}_{-11}({\rm stat}) \; {}^{+28}_{-27}({\rm syst}) \;\; {\rm MeV} \\
\frac{f_{B_s}}{f_{B_d}} &= 1.17 \; {}^{+2}_{-2}({\rm stat}) \\
B_{B_d} &= 1.00 \; {}^{+6}_{-6}({\rm stat}) \; {}^{+5}_{-10}({\rm syst}) \\
B_{B_s} &= 1.02 \; {}^{+5}_{-6}({\rm stat}) \; {}^{+5}_{-7}({\rm syst})
\end{aligned}$$

with the greatest uncertainty in the final results coming from one-loop perturbative matching of the lattice and continuum operators.

Declaration

This thesis has been written and composed by me and it contains my own work carried out as a member of the UKQCD Collaboration. The results presented in chapters 3 and 4 used gauge configurations and propagators generated by the UKQCD collaboration. The code to construct the static-light correlators and perform the smearing was written in conjunction with Alistair Ewing. All the analysis of the data was performed by me, though it was also performed independently by Hartmut Wittig and Alistair Ewing. The results are partly presented in

- UKQCD Collaboration, A. K. Ewing *et al.*, submitted to Phys. Rev. D.

Acknowledgements

I would first like to thank Ken Bowler, Richard Kenway and Brian Pendleton for their support, encouragement and no little patience over these last four years. I would also like to thank my collaborators in the University of Southampton, Hartmut Wittig, Chris Sachrajda and, last but not least, Alistair Ewing who shared much of the pleasure and pain of this project with me, and a few beers along the way. Thanks also to Brian Murdoch and Edna Walton of the Edinburgh University Computing Service for putting up with my stupid questions about the now deceased machine, FRINGE, and similarly to David Richards and Dave Henty for always being around at the right times to sort out my physics and computer problems. Finally, I would not have spent these last few years in Edinburgh without the gracious financial support of the British Council and the Particle Physics and Astronomy Research Council.

My time in Edinburgh has been one of the best times of my life and a lot of people have contributed to making that so. In no particular order, Alistair, Harry, Mike and Rajan (the Montague St. Mob), Sinéad, Emma, Henning, Hugh, the two Nicks, Seth, Elana and Mike T and all the guys in the greatest football team in the world (erm), Jurassic Sparks; its been good fun guys !! I would also like to thank my new friends and colleagues in Swansea University Physics Department, especially for their patience with me as I struggled with this beast over the last year.

Finally, I would like to thank my brother and sisters, Catherine, Eugene, Angela and Louisa, and their respective spouses, for their support, with pints and punts, throughout my long academic career. It is very much appreciated. Above all I have to thank my parents for everything. I dedicate this thesis to them.

Contents

Chapter 1

The Standard Model and B Physics

Over the past few decades the $SU(3) \times SU(2) \times U(1)$ Standard Model (SM) of the strong and electroweak interactions of quarks and leptons has provided a comprehensive theoretical description of a wide variety of observed phenomena in high energy physics. However, amongst other things, the parameters governing the weak interactions of quarks are not well determined. Ironically, this has more to do with difficulties with the strong rather than the weak interaction.

One of the main difficulties in studying any of the properties of quarks is that an isolated quark cannot be probed in the same way, for instance, an electron can; quarks only exist in bound states known as hadrons. The theory of the strong interactions of quarks with gluons that hold together these hadrons is Quantum Chromodynamics (QCD). QCD is the $SU(3)$ part of the SM and exhibits the important property of asymptotic freedom – with increasing energy the quark-gluon coupling gets smaller allowing the use of perturbative techniques in calculations of processes at sufficiently high energies. These perturbative calculations have been very successful in the description of high energy hadron scattering processes. However, at low and intermediate energies the quark-gluon coupling is $\mathcal{O}(1)$ and these perturbative techniques cannot be as successfully applied. Hence new calculational tools appropriate to these energy regimes are needed. One such tool is Lattice Field Theory, discussed in the next chapter.

The problem of accurately determining the fundamental parameters governing the weak interactions of quarks can be simply stated. Only the weak interactions of *hadrons* are experimentally observed. How are the unknown parameters in the SM *quark* weak interaction vertices extracted from these measured *hadronic* weak matrix elements? The strongly bound nature of the quark in the hadron is going to influence the relation between the two. From a QCD perspective this is a low energy non-perturbative problem. Hence the claim that the main uncertainty in the determination of weak interactions of quarks has more to do with their strong interactions.

The structure of this thesis is as follows. In this chapter I try to put flesh on the bones of the problem that I have introduced in the last few paragraphs. I discuss the structure of the weak interactions of quarks in the SM, how flavour mixing and CP violation arise via the CKM matrix and in particular the case of neutral meson mixing in the B system. I end the chapter with a section on Heavy Quark Symmetry. Chapter 2 serves as a brief and rather standard introduction to Lattice QCD. In chapter 3 I present results of a calculation of f_B, the leptonic decay constant of the B meson, using the leading order Heavy Quark Effective Theory to describe the heavy quark constituent of the B meson. In chapter 4 I present results of a similar calculation of the bag-parameter, B_B, of $\bar{B}^0 - B^0$ mixing. Finally, in chapter 5 I present a summary of the work and my conclusions.

1.1 The CKM Matrix

In the SM the fermion masses are generated through Yukawa couplings to the scalar Higgs field, Φ_0

$$\mathcal{L}_Y = -\left(\bar{U'_L} m U'_R + \bar{D'_L} \tilde{m} D'_R \;\; + \;\; \text{h.c.}\right)\left(1 + \frac{\Phi_0}{v}\right) \tag{1.1}$$

where v is the vacuum expectation value of the Higgs field, $U'_{L,R}$ and $D'_{L,R}$ are the 3 component vectors in flavour space for the up and down type quarks respectively

$$U'_{L,R} = \frac{1 \mp \gamma_5}{2} \begin{pmatrix} u' \\ c' \\ t' \end{pmatrix} \qquad D'_{L,R} = \frac{1 \mp \gamma_5}{2} \begin{pmatrix} d' \\ s' \\ b' \end{pmatrix} \tag{1.2}$$

and m and $\tilde{m}$ are 3×3 mass matrices of arbitrary complex numbers. In general m and $\tilde{m}$ are not diagonal and their diagonalisation, $m_D = V_L m V_R^\dagger$ and $\tilde{m}_D = \tilde{V}_L \tilde{m} \tilde{V}_R^\dagger$, defines the physical (mass eigenstates) quark fields $U_{L,R} = V_{L,R} U'_{L,R}$ and $D_{L,R} = \tilde{V}_{L,R} D'_{L,R}$ where $V_{L,R}$ and $\tilde{V}_{L,R}$ are unitary matrices. One can use this diagonalisation to transform the entire SM Lagrangian to rewrite everything in terms of the physical quarks. However this gives rise to non-diagonal charged current couplings

$$\mathcal{L}_W = \frac{g}{\sqrt{2}}\left[\bar{U}_L \gamma^\mu W_\mu^+ V_{\text{CKM}} D_L + \bar{D}_L \gamma^\mu W_\mu^- V_{CKM}^\dagger U_L\right] \tag{1.3}$$

where $V_{\text{CKM}} = V_L \tilde{V}_L^\dagger$ is a unitary 3×3 matrix called the Cabibbo-Kobayashi-Maskawa (CKM) matrix [1, 2],

$$V_{\text{CKM}} = \begin{pmatrix} V_{ud} & V_{us} & V_{ub} \\ V_{cd} & V_{cs} & V_{cb} \\ V_{td} & V_{ts} & V_{tb} \end{pmatrix} \tag{1.4}$$

where the elements are written in a form that emphasises their physical significance.

1.1.1 Structure of the CKM Matrix

The elements of V_{CKM} (as well as the masses of the quarks) are not predicted by the SM since the Yukawa couplings, through the matrices m and $\tilde{m}$, are completely arbitrary complex numbers. The only constraint on V_{CKM} is that it is a unitary 3×3 matrix[1]. Any general unitary 3×3 matrix can be parametrised by 3 real numbers and 6 complex phases. However not all these phases in V_{CKM} correspond to physical observables as the phases given to the quark fields are arbitrary. This may appear to eliminate all the 6 phases; in fact it allows for only 5 of the phases to be absorbed through redefinition of the quark fields as a common phase rotation of all the quark fields leaves V_{CKM} unaffected. Hence there are three real angles and one phase to be determined in V_{CKM}.

Kobayashi and Maskawa [2] introduced a parametrisation of these three angles and one phase based on an Eulerian construction of 3 rotation matrices and a phase matrix to give

$$V_{\mathrm{CKM}} = \begin{pmatrix} c_1 & -s_1c_3 & -s_1s_3 \\ s_1c_2 & c_1c_2c_3 - s_2s_3\mathrm{e}^{i\delta} & c_1c_2s_3 + s_2c_3\mathrm{e}^{i\delta} \\ s_1s_2 & c_1s_2c_3 + c_2s_3\mathrm{e}^{i\delta} & c_1s_2s_3 - c_2c_3\mathrm{e}^{i\delta} \end{pmatrix} \tag{1.5}$$

where $c_i = \cos\theta_i$ and $s_i = \sin\theta_i$, $i = 1, 2, 3$ and θ_i and δ are the appropriate angles and phase. One advantage of this representation is that it is clear how to recover the two family case – setting $\theta_2 = \theta_3 = 0$ leaves the third row and column zero[2] with the remaining 2×2 submatrix described by the single angle, $\theta_1 = -\theta_c$, the Cabibbo angle. It is important to note that in this two family case the complex phase is not present and CP violation, as discussed below, is not present.

There are many equivalent parametrisations to this, differing only in what phase conventions are used. Clearly physical observables must be independent of any of these phase conventions. The simplest quantities invariant under any

[1] This is the assumption of three, and only three, families of quarks.

[2] The remaining phase factor in the 33 element can be absorbed, in this limit, through a rephasing of the quark fields.

rephasing of $V_{\rm CKM}$ are the moduli $|V_{ij}|$ and the quartic products $V_{ij}V^*_{ik}V_{lk}V^*_{lj}$ where i,j,k,l are arbitrary. There are other higher order invariants but they are all expressible in terms of these moduli and quartic products. The unitarity of $V_{\rm CKM}$ restricts the number of independent moduli to four, and leaves only one independent quartic product, Δ – the other quartic products can be expressed in terms of Δ and the independent moduli. Unitarity also implies that the imaginary part of all the possible quartic products is the same, which in the above Kobayashi-Maskawa parametrisation can be written as

$$\mathrm{Im}\Delta = s_1^2 c_1 s_2 c_2 s_3 c_3 \sin\delta\,. \tag{1.6}$$

This quantity is the fundamental quantity that arises in the discussion of CP violation in the SM [3]. It can be shown that in this 3 family case a necessary and sufficient condition for the SM Lagrangian to be invariant under CP transformations is that the determinant of the commutator of the mass matrices m and $\tilde{m}$ must be zero [4]. This quantity can be explicitly evaluated and gives

$$\begin{aligned} \det\,[m,\tilde{m}] = 2i\mathrm{Im}\Delta \quad &\times \quad (m_t - m_c)(m_t - m_u)(m_c - m_u) \\ &\times \quad (m_b - m_s)(m_b - m_d)(m_s - m_d). \end{aligned} \tag{1.7}$$

Noting that $\mathrm{Im}\Delta$ is a product of all the CKM angles and the sine of the phase, then for CP violation to occur in the SM requires several conditions; (1) none of the CKM elements is zero, (2) the CKM phase is non-zero and (3) there is no mass degeneracy in the up or down type quarks. The latter two points are intimately related since if there was a mass degeneracy then the phase in $V_{\rm CKM}$ could be absorbed through a redefinition of the quark fields.

One of the current important experimental goals is to test this elegant explanation of CP violation in the SM.

[3] I am ignoring possible strong CP violation here. This is related to the allowed $F\tilde{F}$ term in the QCD Lagrangian. Measurements of the neutron electric dipole moment constrain any such CP violation to be unobservably small in comparison to the weak mixing CP violation discussed here [3].

1.1.2 Current Status of the CKM Matrix – the Unitarity Triangle

Current experimental data coupled with the assumed unitarity of V_{CKM} gives the magnitudes of the elements at the 90% confidence level as [5]

$$\begin{pmatrix} 0.9747 \text{ to } 0.9759 & 0.218 \text{ to } 0.224 & 0.002 \text{ to } 0.005 \\ 0.218 \text{ to } 0.224 & 0.9738 \text{ to } 0.9752 & 0.032 \text{ to } 0.048 \\ 0.003 \text{ to } 0.015 & 0.030 \text{ to } 0.048 & 0.9988 \text{ to } 0.9995 \end{pmatrix}. \tag{1.8}$$

As can be seen the least well known values are those relating to couplings with the third quark family, in particular V_{td} and V_{ub}. The study of B physics can give information on all these third family couplings. In particular the study of B^0-$\bar{B}^0$ mixing, as discussed in the next section, gives information on the elements V_{td} and V_{ts}.

Even though certain of these elements are not very well known, empirically the elements seem to display a hierarchical pattern, with the diagonal elements close to unity, the mixing between the first and second families going as $\lambda \approx \sin\theta_C \approx 0.22$, between second and third families as λ^2 and between first and third families as λ^3, where θ_C is the Cabibbo angle. This was observed by Wolfenstein who introduced the approximate parametrisation [6]

$$V_{\mathrm{CKM}} = \begin{pmatrix} 1-\frac{\lambda^2}{2} & \lambda & A\,\lambda^3(\rho - i\eta) \\ -\lambda & 1-\frac{\lambda^2}{2} & A\,\lambda^2 \\ A\,\lambda^3(1-\rho-i\eta) & -A\,\lambda^2 & 1 \end{pmatrix} + \mathcal{O}(\lambda^4) \tag{1.9}$$

in terms of the three "angles", λ, A and ρ and the phase η. $\lambda \equiv |V_{us}| = 0.2205 \pm 0.0018$ [5] is the best determined of these. Knowing λ, then A is essentially determined by V_{cb} which can be measured in semi-leptonic decays of B mesons into which there has been a lot of study recently. There are still theoretical uncertainties about how to extract V_{cb} from the experimental data – the Particle Data Group [5] quote $|V_{cb}| = 0.040 \pm 0.005$ giving $A = 0.83 \pm 0.08$. The determination of ρ and η are even more fraught with difficulties as they are related to the least well known elements V_{ub} and V_{td}. I shall return to their determination further on. Finally, the advantage of this parametrisation is that it allows the relative sizes of the various combinations of CKM elements to be estimated at a quick glance.

The only assumption about V_{CKM} that has been made is that of unitarity. The experimentally determined values for the elements must be consistent with this or either the assumption of three families or the CKM mechanism is wrong somewhere. The simplest test of unitarity is that the sum of moduli along a given row/column should add to one. This seems to be most accurately obeyed in the couplings to the u quark with [7]

$$|V_{ud}|^2 + |V_{us}|^2 + |V_{ub}|^2 = 0.9965 \pm 0.0032\,. \tag{1.10}$$

However, what are perhaps more interesting tests of unitarity are the off-diagonal unitarity conditions[4]

$$\begin{aligned} V_{ud}^* V_{us} + V_{cd}^* V_{cs} + V_{td}^* V_{ts} &= 0 \\ V_{us}^* V_{ub} + V_{cs}^* V_{cb} + V_{ts}^* V_{tb} &= 0 \\ V_{ub}^* V_{ud} + V_{cb}^* V_{cd} + V_{tb}^* V_{td} &= 0\,. \end{aligned} \tag{1.11}$$

These unitarity relations can be represented as triangles in the complex plane, and it is interesting to note that the area of each of these triangles is the same and equal to $\frac{1}{2}\mathrm{Im}\Delta$. Hence in the absence of CP violation in the SM these triangles would degenerate to lines along the real-axis.

Evaluating the relative sizes of the sides of these unitarity triangles using the Wolfenstein parametrisation shows that the last of the three is perhaps the most interesting – all its sides are of order λ^3 whereas the other two triangles have one side much shorter than the others (λ, λ and λ^5 for the first and λ^2, λ^2 and λ^4 for the second). This unitarity triangle is shown in figure (1.1).

[4]These are for the columns only. The off-diagonal conditions for the rows produce equivalent unitarity triangles.

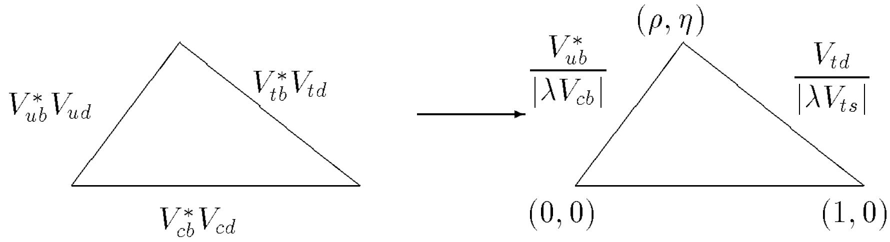

Figure 1.1: The unitarity triangle $V_{ub}^*V_{ud} + V_{cb}^*V_{cd} + V_{tb}^*V_{td} = 0$.

This unitarity triangle is also of great interest as it can be transformed into a triangle in the (ρ,η) plane by dividing out by the length of the $V_{cb}^*V_{cd}$ side of the triangle and using $V_{cd} = \lambda$ and the approximations $V_{cb} \approx V_{ts}$ and $V_{tb} \approx V_{td} \approx 1$. Hence a determination of the two ratios $|V_{ub}|/|V_{cb}|$ and $|V_{td}|/|V_{ts}|$, amongst other things, should provide a good estimation of η and ρ, and determine whether the unitarity triangle is indeed a triangle, whether the $V_{\rm CKM}$ is unitary and whether the SM prescription for CP violation is valid.

The first ratio, $|V_{ub}|/|V_{cb}|$, has been extracted from the semi-leptonic decays of B mesons, again with large theoretical uncertainties, and the Particle Data Group [5] quote

$$\left|\frac{V_{ub}}{V_{cb}}\right| = 0.08 \pm 0.02 \tag{1.12}$$

from recent analyses. This gives the length of the appropriate side of the triangle as

$$\sqrt{\rho^2 + \eta^2} = 0.36 \pm 0.14 \ . \tag{1.13}$$

The other ratio, $|V_{td}|/|V_{ts}|$, can, in principle, be determined from neutral meson mixing in the B system, discussed in the next section. This unitarity triangle can be even more tightly constrained by also measuring the angles. These can be directly determined from the non-leptonic decays of neutral B mesons and are relatively free of the hadronic uncertainties encountered when trying to extract the side lengths. These processes have not yet been measured and are not considered here. For good reviews of the current status and future prospects for the determination of this unitarity triangle see [8, 9, 10, 11, 12].

1.2 Neutral Meson Mixing

Neutral meson mixing can occur in the B, K and D systems. In this section I discuss the mixing in the B system as it is the most relevant to this work. However comparisons are made with the K system, where the phenomenon was first observed, and also with the D system.

1.2.1 Phenomenology

Neutral meson mixing occurs for the same reason that flavour mixing via the CKM matrix occurs – the states B^0 and $\bar{B}^0$ are eigenstates of the strong and electromagnetic interactions but are not mass eigenstates of the weak interactions which are responsible for their decay. Thus a B^0 can be transformed into its antiparticle $\bar{B}^0$ described by some mixing matrix.

The time evolution of an unstable particle can be described by the general Hamiltonian

$$H = M - \frac{i}{2}\Gamma . \tag{1.14}$$

In the B^0-$\bar{B}^0$ basis the 2×2 Hamiltonian describing the evolution of the B^0-$\bar{B}^0$ system can thus be written

$$H = \begin{pmatrix} m & M_{12} \\ M_{12}^* & m \end{pmatrix} - \frac{i}{2} \begin{pmatrix} \gamma & \Gamma_{12} \\ \Gamma_{12}^* & \gamma \end{pmatrix} \tag{1.15}$$

where the mass matrix M and the decay matrix Γ are Hermitian[5] and the diagonal elements of H are equal due to CPT invariance. Diagonalising this Hamiltonian yields the mass eigenstates

$$|B_\pm\rangle = \frac{1}{\sqrt{|p|^2 + |q|^2}} \left[p \left|B^0\right\rangle \pm q \left|\bar{B}^0\right\rangle \right] \tag{1.16}$$

[5] H itself is not Hermitian as the B meson does actually decay.

where

$$\frac{p}{q} = \frac{1+\epsilon}{1-\epsilon} = \sqrt{\frac{M_{12} - \frac{i}{2}\Gamma_{12}}{M_{12}^* - \frac{i}{2}\Gamma_{12}^*}}. \tag{1.17}$$

The strong eigenstates, B^0 and $\bar{B}^0$, are eigenstates of CP, but unless M_{12} and Γ_{12} are real then $p/q \neq 1$ and the mass eigenstates, $B_\pm$, are no longer CP eigenstates. A convenient parameter to describe the extent of this CP violation is ϵ. Observation of a non-zero ϵ signifies CP violation in the state mixing. The other important quantity in this phenomenology of mixing is the difference between the eigenvalues of the mixing matrix, given by

$$\begin{aligned} 2pq &= \Delta m - \frac{i}{2}\Delta\gamma \\ &= 2\sqrt{\left(M_{12} - \frac{i}{2}\Gamma_{12}\right)\left(M_{12}^* - \frac{i}{2}\Gamma_{12}^*\right)} \end{aligned} \tag{1.18}$$

where Δm is the $B_\pm$ mass difference and $\Delta\gamma$ the equivalent decay rate difference. It will be useful later to note that for small CP-violation, $\mathrm{Im}M_{12} \ll \mathrm{Re}M_{12}$ and $\mathrm{Im}\Gamma_{12} \ll \mathrm{Re}\Gamma_{12}$, and

$$\epsilon \approx \frac{\mathrm{Im}M_{12} - \frac{i}{2}\mathrm{Im}\Gamma_{12}}{2(\mathrm{Re}M_{12} - \frac{i}{2}\mathrm{Re}\Gamma_{12})} \tag{1.19}$$

with $\Delta m \approx 2\mathrm{Re}M_{12}$ and $\Delta\Gamma \approx 2\mathrm{Re}\Gamma_{12}$. In both the K and B systems this is the case, but the relative contributions of M_{12} and Γ_{12} differ considerably in both systems.

In order to match the observed Δm, $\Delta\gamma$ and ϵ with the CKM mechanism for quark mixing and CP violation requires knowledge of the exact form of the mixing Hamiltonian, H. This is a non-trivial problem as both long and short distance contributions need to be taken into account.

The short distance contributions come from $\Delta B = 2$ transitions at the quark level within the B meson. These $\bar{b}d \rightleftharpoons b\bar{d}$ transitions occur at the simplest level through box diagrams as in figure 1.2. Long distance contributions come from intermediate mesonic states – the exchange of D and π mesons. The $\Delta B = 2$ flavour change now comes from the action of two $\Delta B = 1$ transitions, those which are responsible for the decay of the meson. These longer distance contributions are the dominant effect in determining Γ_{12}, as this is the only sector of the mixing mechanism which examines the final state phase space available. However it is not as clear what is the relative contribution of short and long distance processes to the mass mixing, M_{12}. This is what makes examination of mixing in the B, K and D systems, although formally the same, phenomenologically very different – the ratio of the short to long distance effects in the mass mixing is quite different in all three cases.

In the B system the short distance box diagram dominates the mass mixing. As is shown in the next section, intermediate t quark exchange dominates this diagram $\sim m_t^2$. The long distance effects of D and π exchange are then suppressed roughly by the factor $(M_B/m_t)^2 \sim \mathcal{O}(10^{-3})$. This is different from the K system where both c and t quark contributions to the box diagram are important and the diagram $\sim m_c^2$. In this case one would naively expect the long distance contribution from pion exchange to be suppressed by a factor $\sim (M_K/m_c)^2 \approx 1/10$. This is not as large a suppression factor, but a suppression nonetheless. However there is a large non-leptonic enhancement of $K \to \pi$ decays from the $\Delta I = 1/2$ rule which overcomes this to leave the ratio of short to long distance contributions $\mathcal{O}(1)$. There is no such enhancement in the B decays. In the D system the longer distance contributions are expected to dominate – the box diagram contribution comes in via the d and s quarks, the b contribution being suppressed by CKM factors, and hence there is no large mass factor in the box contribution to offset the mass of the D in the decay modes.

Finally, it should be noted that the major contribution to ϵ comes from the short distance box diagram in all cases. In the box diagram all quark families contribute, a condition necessary for observation of CP violation as the CP violating parameter ImΔ is a product of all the CKM elements. The longer distance decay channels are dominated by the couplings to the relevant lighter quarks in each case and are less sensitive to the CP violating phase in V_{CKM}. In the following section I outline how to calculate this box diagram amplitude.

1.2.2 The $\Delta B = 2$ Box Diagram

The dominant short distance contribution to the B^0-$\bar{B}^0$ mass mixing comes from the $\Delta B = 2$ box diagram.

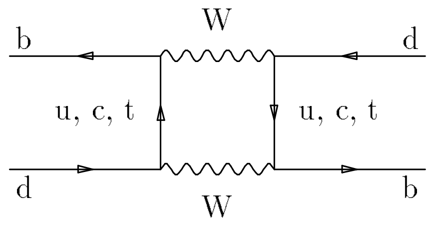

Figure 1.2: $\Delta B = 2$ box diagram for B_d^0–$\bar{B}_d^0$ mixing. This is in fact one of two box diagrams that contributes to the process. The other is the "scattering" version of the above, with the internal box rotated through 90^o. Both contributions are identical.

In order to connect with the phenomenology of the previous section an effective Hamiltonian, H_{eff}, for this $\bar{b}d \rightleftharpoons b\bar{d}$ transition must be derived. This is then measured between the B^0 and $\bar{B}^0$ states giving

$$\Delta m = 2\left|M_{12}\right| = 2\left|\left\langle \bar{B}^0 \right| H_{eff} \left| B^0 \right\rangle\right| \tag{1.20}$$

where the assumption of small CP-violation in the state mixing is implicit.

The characteristic length scale of the box diagram is $\sim 1/M_W$ which is much less than the length scale of the external states, $\sim 1/M_B$. Hence, as far as the external states are concerned, the box diagram transition appears to be a pointlike process. It is much more convenient to measure the matrix element of a pointlike operator than that of a complicated non-local object like the full box diagram. In fact, at the energy scale $\sim M_W$, QCD is in the perturbative regime and it is possible to approximate the box diagram by a pointlike interaction with the corrections to this perturbatively calculable.

The formalism that enables this short distance expansion of currents in terms of a set of local operators to be performed is the Operator Product Expansion

(OPE) – see the treatment in [13] for a good introduction. The basic idea is to "integrate out" the degrees of freedom that are irrelevant at the scales of interest, in other words the W-boson at hadronic energy scales. This leaves one with an *effective* theory in the remaining degrees of freedom. As with all effective theories it is defined at an explicit scale that cannot be removed from the theory. The correspondence with the full theory is ensured by perturbatively matching the full and effective theories at some scale characteristic of the degrees of freedom that have been integrated out, in this case $\sim M_W$. So, the procedure can be summarised in

$$\left\langle \bar{B}^0 \right| H_{eff} \left| B^0 \right\rangle = \sum_i C_i(M_W, g(M_W)) \left\langle \bar{B}^0 \right| \mathcal{O}_i(M_W) \left| B^0 \right\rangle . \tag{1.21}$$

The C_i are the perturbative matching factors and the $\mathcal{O}_i$ are local operators, matrix elements of which need to be determined non-perturbatively. An important point to note is that there must be no scale dependence in the product $C_i\mathcal{O}_i$.

Normally the scale, μ, at which the matrix element is measured is some hadronic scale. One cannot simply use the matching factor calculated at $\mu \approx M_W$ as there will be large logarithms ($\ln M_W/\mu$) in the perturbative expansion of the matrix element of the O_i. The well known solution is to sum up these large logarithms into the C_i using the renormalisation group (RG). This gives

$$C_i(\mu, g(\mu)) = C_i(M_W, g(M_W)) \;\; \exp \int_{g(\mu)}^{g(M_W)} \frac{\gamma_i(g')}{\beta(g')} dg' \tag{1.22}$$

relating C_i at the scale μ to that at M_W, where γ_i is the anomalous dimension of the operator O_i and β is the β-function of QCD. Naturally, any other appropriate scale can be chosen at which to perform the matching and use this as the starting point to the evolution of the RG equation – at any rate the procedure is to calculate the perturbative QCD matching at some scale and the running from this scale to that at which the matrix element is measured is achieved using the RG equation.

One can perform an OPE for the box diagram in figure 1.2. However, this involves the OPE of a product of four weak currents and this direct procedure is rather cumbersome. The usual method employed in the literature is to first ignore the perturbative QCD corrections and evaluate the box diagram between the external free quark states, where the external quark masses and momenta are neglected. The QCD corrections are added later. Proceeding thus gives the effective Hamiltonian [14]

$$H_{eff} = \frac{G_F^2}{16\pi^2} M_W^2 \sum_{i,j} \xi_i \xi_j \, S(x_i, x_j) O_{LL} \tag{1.23}$$

where $x_i = m_i^2/M_W^2$ and $\xi_i = V_{ib}V_{id}^*$ with $i = u, c, t$, and where the four-fermion operator

$$O_{LL} = [\bar{b}\gamma_\mu(1-\gamma_5)d][\bar{b}\gamma^\mu(1-\gamma_5)d] \tag{1.24}$$

is the only local operator to appear at this order. $S(x_i, x_j)$ is an analytic function given by

$$S(x_i, x_j) = \left(1 + \frac{1}{4}x_i x_j\right) A(x_i, x_j) - 2x_i x_j B(x_i, x_j) \tag{1.25}$$

with

$$\begin{aligned} A(x_i, x_j) &= \frac{1}{(1-x_i)(1-x_j)} + \left[\frac{x_i^2 \ln x_i}{(x_i - x_j)(1-x_i)^2} + (i \leftrightarrow j)\right] \\ B(x_i, x_j) &= \frac{1}{(1-x_i)(1-x_j)} + \left[\frac{x_i \ln x_i}{(x_i - x_j)(1-x_i)^2} + (i \leftrightarrow j)\right]. \end{aligned} \tag{1.26}$$

Usually the u quark contribution to the process is eliminated by using the unitarity of the CKM matrix, $\sum_i \xi_i = 0$, and setting $x_u = 0$. This gives rise to the usual form for H_{eff} seen in the literature,

$$H_{eff} = \frac{G_F^2}{16\pi^2} M_W^2 \left[\xi_c^2 \, F(x_c) + \xi_t^2 \, F(x_t) + 2\xi_c \xi_t \, G(x_c, x_t)\right] O_{LL} \tag{1.27}$$

where the Inami-Lim functions [15], F and G, are

$$F(x) \;\; = \;\; x\left[\frac{1}{4} + \frac{9}{4}\frac{1}{1-x} - \frac{3}{2}\frac{1}{(1-x)^2}\right] - \frac{3}{2}\frac{x^3}{(1-x)^3}\ln x$$

$$G(x,y) = xy\left[\frac{1}{x-y}\left(\frac{1}{4}+\frac{3}{2}\frac{1}{1-x}-\frac{3}{4}\frac{1}{(1-x)^2}\right)\ln x + (y \leftrightarrow x) - \frac{3}{4}\frac{1}{(1-x)(1-y)}\right]. \tag{1.28}$$

Now consider the CKM information contained in the above effective Hamiltonian. If the limits[6] $x_c \ll 1$ and $x_t \gg 1$ are taken then $F(x_c) \sim x_c$, $F(x_t) \sim x_t$ and $G(x_c, x_t) \sim \ln(x_t/x_c)$. Hence the t quark internal lines in the box diagram dominate due to the large mass of the top. This is also because all the CKM factors are of $\mathcal{O}(\lambda^6)$. In the K system this is not the case – the c quark CKM factors are at $\mathcal{O}(\lambda^2)$ and the t quark factors at $\mathcal{O}(\lambda^{10})$, and so even though the contribution from the top quark mass is strong it is considerably suppressed by the CKM factors. One can also go through this analysis for the D system – c and u in the external states and d, s and b in the internal quark lines – and show that the b quark contribution is similarly suppressed by CKM factors. This would then demonstrate the small contribution coming from the box diagram to the mass mixing in this system.

So, retaining only the t quark contribution, the effective Hamiltonian can now be written

$$H_{eff} = \frac{G_F^2}{16\pi^2} M_W^2 \eta(x_t,\mu) F(x_t) \left|V_{tb}V_{td}^*\right|^2 O_{LL}(\mu) \tag{1.29}$$

where the QCD corrections have been explicitly introduced – $\eta(x_t,\mu)$ plays the same role as the $C_i(\mu)$ earlier on. It is important to note that renormalisation in the $\overline{MS}$ scheme introduces no new operators beyond the O_{LL} introduced at zeroth order. Now suppose η is calculated at the scale M_W, then the running to a lower scale, μ, is given by equation (1.22). Integrating this equation using the one loop β-function and the one-loop anomalous dimension of $O_{LL}(\mu)$, $\gamma_{LL} = -4\,g^2/16\pi^2$, gives

$$\eta(x_t,\mu) = \eta(x_t, M_W)\left[\frac{\alpha_s(\mu)}{\alpha_s(M_W)}\right]^{-d_{LL}} \equiv \eta(x_t)\left[\alpha_s(\mu)\right]^{-d_{LL}} \tag{1.30}$$

with $d_{LL} = 6/(33-2n_f)$ where n_f is the number of active quark flavours. These

[6]Not strictly true for the mass of the top, but the conclusion stands.

QCD corrections have been extensively studied to leading and next-to-leading order in [16]. An important point in their analysis is that η depends on the *definition* of the top quark mass. This dependence cannot be present in the expression for H_{eff} – in the product $\eta(x_t)F(x_t)$ this dependence is in fact missing. Using five active quarks and a running top quark mass, $m_t = 150$ GeV, they find $\eta(x_t)F(x_t) = 1.113$ at next-to-leading order and using $\Lambda^{(4)}_{\overline{MS}} = 200$ MeV, with the result going up to 1.711 for $m_t = 200$ GeV. Note that to use this result also requires the next-to-leading result for the RG running between scales to be used. In the results quoted later on, only the leading order expressions for the QCD corrections are used.

1.2.3 Vacuum Saturation

The OPE above has lead to an effective local operator, O_{LL}, that must be measured between the B^0 and $\bar{B}^0$ states to make connection with phenomenology as in equation (1.20). The determination of this matrix element requires knowledge of the hadronic wave-function of the B^0 meson. Notwithstanding this, it can be conveniently parametrised using the vacuum saturation approximation. This involves inserting a complete set of states in the four-fermion operator and assuming the vacuum contribution dominates the sum over states,

$$\begin{aligned} \left\langle \bar{B}^0 \right| \mathcal{O}_{LL} \left| B^0 \right\rangle &= \sum_n \left\langle \bar{B}^0 \right| (\bar{b}\gamma_\mu(1-\gamma_5)d) \left| n \right\rangle \left\langle n \right| (\bar{b}\gamma^\mu(1-\gamma_5)d) \left| \bar{B}^0 \right\rangle \\ &\to \left\langle \bar{B}^0 \right| (\bar{b}\gamma_\mu(1-\gamma_5)d) \left| 0 \right\rangle \left\langle 0 \right| (\bar{b}\gamma^\mu(1-\gamma_5)d) \left| B^0 \right\rangle . \end{aligned} \quad (1.31)$$

The two matrix elements in the latter product are just the matrix elements of the axial current between the vacuum and the pseudoscalar meson

$$\left\langle 0 \right| \bar{b}\gamma_\mu\gamma_5 d \left| B^0 \right\rangle = i p_\mu f_B \quad (1.32)$$

used to define f_B, the leptonic decay constant of the B meson, where p_μ is the momentum of the meson. Note that only the axial part of the $V - A$ matrix element survives – this is equivalent to saying there is no overlap between vector and pseudoscalar states.

In principle, f_B can be measured from the total leptonic decay width of charged B mesons, but these measurements are difficult and a reliable experimental measurement of f_B is not currently available. However, if f_B is known then the only theoretical unknown is to what extent the vacuum saturation approximation is wrong. This uncertainty is factored into the above parametrisation using the so-called "bag" parameter B_B. This is defined such that the matrix element can be written as

$$\left\langle \bar{B}^0 \right| \mathcal{O}_{LL}(\mu) \left| B^0 \right\rangle = \frac{8}{3} f_B^2 M_B^2 B_B(\mu) \tag{1.33}$$

where M_B is the mass of the B meson. The factor 8/3 comes from the number of ways the vacuum state can be inserted and the colour singlet property of currents

$$\langle 0| \bar{b}_\alpha \gamma_\mu \gamma_5 d_\beta \left| B^0 \right\rangle = i p_\mu f_B \frac{\delta_{\alpha\beta}}{3}. \tag{1.34}$$

Note that all the scale dependency in $O_{LL}(\mu)$ has been transferred to $B_B(\mu)$. This is because the axial current in the definition of f_B is partially conserved and hence receives no renormalisation. Following the discussion in the previous section, the RG-invariant bag parameter is defined as

$$B_B = [\alpha_s(\mu)]^{-6/23} B_B(\mu) \tag{1.35}$$

in the theory with five active quarks. $B_B = 1$ for complete vacuum saturation.

In this work I present lattice calculations of these two relevant parameters in this parametrisation of the low energy non-perturbative contribution to B^0-$\bar{B}^0$ mixing, namely f_B and B_B.

1.2.4 Relation to Experiment

Gathering together the various strands from the last two sections, the final expression for the mass difference in B^0-$\bar{B}^0$ mixing can be written as

$$\Delta m = \frac{G_F^2}{16\pi^2} M_W^2 \eta(x_t) F(x_t) \frac{8}{3} f_B^2 M_B^2 B_B \, |V_{tb} V_{td}^*|^2 . \tag{1.36}$$

So, a measurement of Δm along with a calculation of $f_B^2 B_B$ should allow the extraction of $|V_{td}|$, if the assumption $V_{tb} \simeq 1$ is made.

In fact it is the quantity $x = \Delta m/\Gamma$ that is extracted from experiment, where $\Gamma = 1/\tau_B$ is the inverse B-lifetime – in most experiments the time-integrated probability for an initially pure B^0 state to decay as a $\bar{B}^0$,

$$\chi = \frac{1}{2}\frac{x^2}{1+x^2} \tag{1.37}$$

is measured. The current world average is [8]

$$x_d = 0.78 \pm 0.05 \tag{1.38}$$
$$\Delta m_d = 0.496 \pm 0.032 \ \ \mathrm{ps}^{-1} \tag{1.39}$$

The subscript d has been appended to these parameters to signify that the quoted values are for B_d^0-$\bar{B}_d^0$ mixing only[7]. One can also observe B_s^0-$\bar{B}_s^0$ mixing and calculate the appropriate mixing parameter, x_s. Unfortunately there are currently no reliable measurements of x_s. Assuming x_s will be accurately measured in the near future, then from the ratio

$$\frac{x_s}{x_d} = \frac{\tau_{B_s} f_{B_s}^2 B_{B_s} M_{B_s}^2}{\tau_{B_d} f_{B_d}^2 B_{B_d} M_{B_d}^2}\left|\frac{V_{ts}}{V_{td}}\right|^2 \tag{1.40}$$

the ratio $|V_{ts}/V_{td}|$ can be extracted and, as was mentioned earlier, this can give an estimate of the length of one side of the unitarity triangle. The advantage of being able to measure this ratio is that certain uncertainties cancel: there is no dependence on the mass of the top for example. The ratios f_{B_s}/f_{B_d} and B_{B_s}/B_{B_d} have been studied in chiral perturbation theory [17]. In this work these ratios are also calculated on the lattice.

In my conclusions I shall return to this issue of relation to experiment and also to the issue of the status of the unitarity triangle.

[7]The mixing parameters x_d and x_s should not be confused with the symbols $x_i = m_i^2/M_W^2$ used earlier on.

1.3 Heavy Quark Symmetry

Consider a meson consisting of a heavy quark, mass $m_Q \gg \Lambda_{QCD}$, and a light quark, mass $m_q < \Lambda_{QCD}$. The heavy and light quark are bound together in this system via the exchange of gluons with energy $\sim \Lambda_{QCD}$. However, since $m_Q \gg \Lambda_{QCD}$ these gluons cannot resolve the structure of the heavy quark. Hence the light degrees of freedom in the meson (the gluons and the light quark – also known as the "brown muck") are relatively insensitive to the mass and spin of the heavy quark and interact with it as if it were a spinless colour source moving with constant velocity. Likewise the heavy quark hardly notices the brown muck and its propagation fluctuates only slightly from that of a free heavy quark. This insensitivity of the brown muck to the heavy quark mass exhibits itself as a flavour symmetry in the heavy quark sector. In other words the physics of heavy-light systems, such as the B and D mesons, should exhibit the same structure.

The obvious analogy with the Hydrogen atom can be drawn. In this system the effect of the proton mass on the atomic energy levels is factored into a reduced mass which is almost equal to the electron mass. Secondly, the hyperfine splitting in Hydrogen is very small. Hence the electron's dynamics are insensitive to the mass and spin of the proton and likewise the proton's dynamics are such that it hardly notices it has an electron bound to it. The flavour symmetry in this analogy is that the energy levels of Hydrogen and Deuterium are almost the same.

These ideas can be incorporated into an effective theory for the heavy quark constituent by taking the limit where $m_Q \to \infty$. Corrections for finite heavy quark mass to the predictions of this effective theory can then be treated as perturbations in Λ_{QCD}/m_Q. In this section I introduce this Heavy Quark Effective Theory (HQET) and show how it is useful in making predictions and performing calculations in B physics – see [18] for a comprehensive review.

1.3.1 Heavy Quark Effective Theory

The construction of an effective theory is very much in the spirit of the OPE described earlier. One wishes to integrate out the degrees of freedom that do not contribute to processes at the energy scales of interest. This procedure generally results in a non-local action functional in the remaining relevant degrees of freedom. This non-local action functional is then expanded in terms of local operators in an OPE and the matching from the full to the effective theory is contained in matching factors analogous to those introduced earlier. Such an approach to the construction of HQET is described by Mannel, Roberts and Ryzak [19]. However here I proceed in a more transparent manner.

I first consider the leading order effective theory. It is convenient to start by writing the momentum of the heavy quark as

$$P_Q^\mu = m_Q v^\mu + k^\mu \tag{1.41}$$

where v^μ is the four-velocity of the hadron, satisfying $v{\cdot}v = 1$, and k^μ is a residual momentum. The residual momentum is of order Λ_{QCD}, so as $m_Q \to \infty$ the heavy quark becomes on-shell. Taking this limit the heavy quark propagator becomes

$$\frac{i\,(\not{P}_Q + m_Q)}{P_Q^2 - m_Q^2} \to \frac{1+\not{v}}{2}\frac{i}{v\cdot k} \tag{1.42}$$

where the factor $(1+\not{v})/2$ is a positive energy projection operator. Similarly, the vertex between a heavy quark and a gluon becomes

$$-ig\frac{1+\not{v}}{2}\gamma^\mu\frac{\lambda_a}{2}\frac{1+\not{v}}{2} \quad = \quad -ig\,v^\mu\frac{\lambda^a}{2}\,\frac{1+\not{v}}{2} \tag{1.43}$$

where λ^a are the Gell-Mann matrices. The projectors $(1+\not{v})/2$ can be moved to the outside of any Feynman graph where they give unity on operating on on-shell spinors. Hence, the heavy quark propagator and heavy quark-gluon vertex in the effective theory are

$$\frac{i}{v\cdot k} \qquad \text{and} \qquad -\,ig\,v^\mu\frac{\lambda^a}{2} \tag{1.44}$$

respectively. So, it can be seen that the propagator of a heavy quark is independent of its mass. The heavy quark-gluon coupling has no gamma matrix structure in it and is thus independent of spin. Hence the flavour and spin symmetries motivated earlier.

These Feynman rules can also be derived from an HQET Lagrangian. Consider just the fermionic part of the QCD Lagrangian with a single heavy quark field, Q,

$$\mathcal{L} = \bar{Q}\,(i\not{D} - m_Q)\,Q \ . \tag{1.45}$$

The factorisation of momentum in equation (1.41) is similarly implemented here by writing the heavy quark field as

$$Q(x) = \mathrm{e}^{-im_Q v\cdot x}\, h_v(x) \tag{1.46}$$

where the on-shell condition constrains h_v to satisfy $\not{v} h_v = h_v$. This allows the HQET Lagrangian to be written as

$$\begin{aligned} \mathcal{L}_v &= \bar{h}_v\,[m_Q(\not{v}-1) + i\not{D}]\,h_v \\ &= \bar{h}_v i\not{D} h_v \\ &= \bar{h}_v \frac{1+\not{v}}{2} i\not{D} \frac{1+\not{v}}{2} h_v \\ &= \bar{h}_v iv\cdot D h_v \end{aligned} \tag{1.47}$$

which gives the same propagator and vertex as above, noting that the D operating on h_v produces a factor of the residual momentum.

There are several points to note about this HQET Lagrangian. Firstly, the quark field is labelled by the velocity of the heavy quark. In the effective theory the QCD interactions cannot change the velocity of the heavy quark – a so-called "velocity super-selection rule" [20]. Some other interaction, such as a weak current, is required to do this. Secondly, the effective theory is not a non-relativistic approximation – there is nothing restricting any of the spatial components of velocity from being of order unity. However, when dealing with just a single heavy quark in the problem it is simplest to treat everything in the rest frame of that heavy quark. Finally, the field h_v annihilates a heavy quark of velocity v but does not create an antiquark. In other words there is no pair creation in this effective theory and the quark and antiquark fields are distinct.

Further on in this work the real-space propagator of the heavy quark in this effective theory is used. This is most easily arrived at by solving the equation of motion

$$v \cdot D h_v = 0 \tag{1.48}$$

for the heavy quark field. In the particular case of a static quark where $v = (1,0,0,0)$ the time evolution of the quark field is given by

$$\frac{\partial}{\partial t} h_0(\vec{x},t) = igA_0(\vec{x},t)h_0(\vec{x},t) \tag{1.49}$$

which gives the propagator as

$$P_{\vec{x}}(t_x,t_y) = \mathcal{T}\exp\left(ig\int_{t_y}^{t_x} dt' A_0(\vec{x},t')\right) \tag{1.50}$$

where $\mathcal{T}$ denotes time ordering. So, as the static quark propagates forward in time it just picks up the phase of the gauge field – in other words its propagator is a Wilson line in the time direction. Mapping back to the propagator in terms of the fields Q gives [21]

$$\begin{aligned} G_{(Q)}(\vec{x},t_x;\vec{y},t_y) &= \left[\mathrm{e}^{im_Q(t_x-t_y)}\frac{1+\gamma_0}{2}\Theta(t_x-t_y) + \mathrm{e}^{-im_Q(t_x-t_y)}\frac{1-\gamma_0}{2}\Theta(t_y-t_x)\right] \\ &\times \; P_{\vec{x}}(t_x,t_y)\delta^3(\vec{x}-\vec{y}) \end{aligned} \tag{1.51}$$

where Θ is just the Heaviside step function. This form is very useful in simulating the leading order (static) HQET on the lattice since for a given gauge configuration the propagator of a heavy quark in that background gauge field is trivial to calculate.

1.3.2 Explicit $1/m_Q$ Corrections

So far the effective theory has been formulated in terms of an on shell heavy quark effective field, $h_v(x)$. The first step in considering corrections to this leading order effective theory is to allow the heavy quark to go slightly off shell. This is achieved by a decomposition of the heavy quark field similar to equation (1.46),

$$Q(x) = \mathrm{e}^{-im_Q v\cdot x}\ [h_v(x) + H_v(x)] \tag{1.52}$$

where the new field H_v, satisfying $\not{v} H_v = -H_v$, has been introduced to describe the off-shell behaviour. Note that in the rest frame of the heavy quark h_v corresponds to the upper components of $Q(x)$ and H_v to the lower components :

$$Q(x)_{\text{rest frame}} = \mathrm{e}^{-im_Q t} \begin{pmatrix} h_v(x) \\ H_v(x) \end{pmatrix} \ . \tag{1.53}$$

Also note that this new field does not represent antiquark degrees of freedom.

The field, H_v, corresponds to the heavy degrees of freedom which one wishes to integrate out of the problem. This can be achieved by expanding H_v in terms of h_v from the equation of motion

$$[m_Q(\not{v} - 1) + i\not{D}]\,[h_v + H_v] = 0 \tag{1.54}$$

which gives

$$H_v = \left[1 - \frac{i\not{D}}{2m_Q}\right]^{-1} \frac{i\not{D}}{2m_Q} h_v \ . \tag{1.55}$$

The inverse operator here is clearly a non-local object, but it can be expanded in terms of a set of local operators with operators of increasing dimension being suppressed by increasing powers of m_Q – this exemplifies the connection with the OPE commented on earlier. Expanding just to leading order gives

$$H_v = \frac{1}{2m_Q} i\not{D} h_v + \mathcal{O}(\frac{1}{m_Q^2}) \tag{1.56}$$

and hence the heavy quark field can now be written as

$$Q(x) = \mathrm{e}^{-im_Q v\cdot x} \left[1 + \frac{i\not{D}}{2m_Q}\right] h_v(x) + \mathcal{O}(\frac{1}{m_Q^2}) \tag{1.57}$$

and putting this into the Lagrangian of equation (1.45) gives

$$\mathcal{L}_v = \bar{h}_v iv\cdot Dh_v + \frac{\bar{h}_v}{2m_Q}\left[(iD)^2 - \frac{1}{2}g\sigma_{\mu\nu}F^{\mu\nu}\right]h_v + \mathcal{O}(\frac{1}{m_Q^2}) \ . \tag{1.58}$$

So, two terms come into the Lagrangian at $\mathcal{O}(1/m_Q)$, a kinetic energy term, $(iD)^2$, describing the off-shell motion of the heavy quark, and a chromomagnetic term, $\sigma_{\mu\nu}F^{\mu\nu}$. The first term breaks the flavour symmetry of the lowest order Lagrangian while the second term breaks both the flavour and spin symmetry.

It should be noted that this Lagrangian is non-renormalisable. However, this is not a problem. In as far as one is interested in corrections of $\mathcal{O}(1/m_Q)$ then this restricts one to a single insertion of the appropriate operators in the graphs of interest. The generalisation of this is also true: at a given order in $1/m_Q$ there are only a finite number of insertions of non-renormalisable operators in the renormalisable leading order theory, leaving the theory renormalisable [22].

These operators have been introduced by expanding the off-shell field H_v in terms of h_v from the equation of motion. This again is purely a tree-level matching with the gluons treated as a background field. Introducing loop corrections gives rise to renormalisation of the operators arising at order $\mathcal{O}(1/m_Q)$. Introducing appropriate matching factors gives the Lagrangian as

$$\mathcal{L}_v = \bar{h}_v iv\cdot Dh_v + \frac{\bar{h}_v}{2m_Q}\left[C_{kin}(\mu)\,(iD)^2 - C_{mag}(\mu)\frac{1}{2}g\sigma_{\mu\nu}F^{\mu\nu}\right]h_v \ . \tag{1.59}$$

From reparametrisation invariance[8] it can be shown to all orders in perturbation theory that the kinetic energy operator receives no renormalisation [23] and hence $C_{kin}(\mu) = 1$. Matching to leading order at the scale m_Q and using the renormalisation group to run to arbitrary scale μ gives [22]

$$C_{mag}(\mu) = \left[\frac{\alpha_s(m_Q)}{\alpha_s(\mu)}\right]^{-9/(33-2n_f)} \tag{1.60}$$

[8]An arbitrariness in how the decomposition of the heavy quark momentum in equation (1.41) is achieved.

in the leading log approximation.

I have introduced the procedure for including $1/m_Q$ corrections for completeness sake. In the rest of what follows I restrict attention to the leading order effective theory.

1.3.3 Scaling Law for the Pseudoscalar Decay Constant

HQET can be used to make predictions about the structure of weak matrix elements of heavy-light mesons. Here I simply concentrate on the matrix element for the heavy-light pseudoscalar decay constant,

$$\langle 0|\, \bar{h}_v^{(i)} \gamma_\mu \gamma_5 q \,|P_i(p)\rangle = i p_\mu f_{P_i} \tag{1.61}$$

as in equation (1.32), where P_i is the pseudoscalar heavy-light meson with heavy quark constituent, $h_v^{(i)}$, and momentum p. In the effective theory it is appropriate to label the meson state by its velocity. The conventional normalisation for meson states, $|P\rangle$, is

$$\langle P(p')|P(p)\rangle = 2E\delta^3(\vec{p}\,' - \vec{p}) \tag{1.62}$$

but in the effective theory a mass independent normalisation of states is appropriate. Factoring the meson mass, M_P, out of the δ-function gives the mass independent normalisation of the meson states labelled by velocity as

$$\langle P(v')|P(v)\rangle = \frac{2E}{M_P}\delta^3(\vec{v}\,' - \vec{v}) \tag{1.63}$$

and hence

$$|P(v)\rangle = M_P^{-1/2}\,|P(p)\rangle \ . \tag{1.64}$$

Now using this in equation (1.61) gives

$$\langle 0|\, \bar{h}_v^{(i)} \gamma_\mu \gamma_5 q \,|P_i(v)\rangle = i v_\mu f_{P_i}\sqrt{M_{P_i}} \ . \tag{1.65}$$

The matrix element on the left of this equation is independent of the heavy meson mass and hence $f_{P_i}\sqrt{M_{P_i}}$ is independent of the flavour, i, of the heavy quark constituent of the meson. In particular, if the b and c quarks can be described by the lowest order HQET then this gives the relation

$$f_B = \sqrt{\frac{M_D}{M_B}} f_D \tag{1.66}$$

between the leptonic decay constants of the B and D mesons.

1.3.4 Renormalisation and Matching

So far the effective theory has been introduced by matching tree level graphs in the full theory with tree level graphs in the heavy quark limit. However, the effective theory doesn't describe the short distance behaviour of QCD properly – high energy gluons can resolve the structure of the heavy quark. Fortunately this discrepancy between full QCD and the effective theory can be handled in perturbation theory since the problem lies in the short distance perturbative regime. This perturbative matching between the theories has been introduced to a certain extent in the discussion of $1/m_Q$ corrections to the effective Lagrangian. Here I just briefly consider the matching of the axial current in the leading order effective theory to that in the full theory. This is also discussed in chapter 3. The matching of O_{LL} between the full and effective theory is treated in chapter 4.

The axial current in the full theory is partially conserved and hence receives no renormalisation. Consider the heavy-light axial current in the full theory, $A_\mu = \bar{Q}\gamma_\mu\gamma_5 q$. This is a local dimension-three operator and in order to match to the effective theory all local dimension-three operators in the effective theory with the same quantum numbers must be considered. There are two such operators in HQET,

$$J_1 = \bar{h}_v \gamma_\mu \gamma_5 q \qquad \text{and} \qquad J_2 = \bar{h}_v v_\mu \gamma_5 q \tag{1.67}$$

where v_μ is the heavy quark velocity. The matching can be written as

$$A_\mu \cong C_1(\mu) J_1 + C_2(\mu) J_2 \tag{1.68}$$

where the symbol $\cong$ means that this equation holds on the level of matrix elements. These matching coefficients have been calculated at one-loop in the $\overline{\mathrm{MS}}$ scheme giving [24]

$$
\begin{aligned}
C_1(\mu) &= 1 + \frac{\alpha_s}{\pi}\left(\ln\frac{m_Q}{\mu} - \frac{4}{3}\right) \\
C_2(\mu) &= -\frac{2\alpha_s}{3\pi}\,.
\end{aligned}
\tag{1.69}
$$

This matching procedure is applied at scales $\mu \sim m_Q$. Using the RG to run to arbitrary scale in the leading-log approximation gives[9] [25, 26]

$$
\begin{aligned}
C_1(\mu) &= \left[\frac{\alpha_s(m_Q)}{\alpha_s(\mu)}\right]^{-2/\beta_0} \\
C_2(\mu) &= 0
\end{aligned}
\tag{1.70}
$$

where $\beta_0 = (11 - 2n_f/3)$ is the usual one loop factor from β_{QCD}. The main point to note is that the matching modifies the scaling behaviour in equation (1.66) to

$$
f_B = \sqrt{\frac{M_D}{M_B}}\left[\frac{\alpha_s(M_B)}{\alpha_s(M_D)}\right]^{-6/25} f_D \tag{1.71}
$$

with four active quarks in the region between M_B and M_D and using $m_b \approx M_B$ and $m_c \approx M_D$. So the scaling law for f_P has a weak logarithmic dependence on M_P from the perturbative matching to the full theory.

[9] C_2 only runs in the next-to-leading log approximation. However, I still quote the result in equation (1.69) as it will be useful later on.

Chapter 2

Lattice Field Theory

Lattice Field Theory is a first principles approach to the determination of the Green functions of a given theory. Consider for example the case of a theory with a single scalar field, ϕ. The approach takes as its starting point the path integral representation of these Green functions,

$$\begin{aligned} G^{(n)}(x_1, \ldots, x_n) &= \langle 0|\, T(\phi(x_1)\ldots\phi(x_n))\,|0\rangle \\ &= \frac{1}{Z}\int [d\phi]\,(\phi(x_1)\ldots\phi(x_n))\,\mathrm{e}^{iS[\phi]} \end{aligned} \tag{2.1}$$

where T denotes time ordering and

$$Z = \int [d\phi]\ \mathrm{e}^{iS[\phi]} \tag{2.2}$$

with

$$S[\phi] = \int d^4x \mathcal{L}(\phi(x)) \tag{2.3}$$

the action functional of the field ϕ, where the field theory is defined through the Lagrange density, $\mathcal{L}$. The functional integration is over all possible configurations of the field ϕ with functional measure $[d\phi] = \prod_x d\phi(x)$. This product is over all possible space-time points and is thus an uncountably infinite product. It is difficult to give a precise mathematical meaning to this. One way, if not the only way, is as the limit of a countable product over a discrete set of space-time points. Hence one is naturally lead to the idea of formulating field theory on a lattice of space-time points. Furthermore, if this lattice is restricted to a finite volume then the number of degrees of freedom in the functional integral is no longer merely countable but finite. This opens the way to the use of numerical techniques for the determination of the Green functions of the theory.

There are three basic questions that are addressed in this chapter : (1) How is QCD formulated on a lattice ? (2) How are calculations performed in Lattice QCD and what are the technical issues involved ? (3) How are these quantities calculated on the lattice related to the required quantities in continuum QCD ? All these issues are interrelated and I don't necessarily discuss them individually.

2.1 QCD on a Lattice

In this section I present the steps involved in formulating QCD on a 4-dimensional hypercubic lattice and outline how expectation values (Green functions) are evaluated in this lattice theory. The procedure is relatively straightforward. Space-time is considered to consist of a set of discrete points separated by a lattice spacing a. The quark fields exist only on these lattice points and the gauge fields exist on the links connecting adjacent points. The idea is to construct a lattice action from these lattice fields such that in the limit $a \to 0$ the lattice action becomes the continuum action.

2.1.1 Euclidean QCD

In Lattice Field Theory it is more convenient to work with the field theory defined in Euclidean space rather than Minkowski space. The most practical reason for this comes from the path integral in equation (2.1). The integrand is a wildly oscillating function of the action and so in the functional integral there are large cancellations between different, and possibly widely separated, areas of the configuration space of the functions ϕ. This renders numerical procedures unreliable for sampling the configuration space. Going to the Euclidean theory the action becomes $S_E = iS$ and so the integrand is now exponentially damped and much easier to handle numerically. Also the Euclidean functional integral

$$Z = \int [d\phi] \; \mathrm{e}^{-S_E[\phi]} \tag{2.4}$$

can be interpreted as the partition function of a classical statistical mechanical system. Hence the calculation of quantities in lattice field theory is no more than the evaluation of expectation values in a classical statistical mechanical system and this has the advantage of enabling the use of the vast array of techniques already well developed in this field.

A crucial question arises as to whether Green functions calculated in the Euclidean theory actually yield any information at all about the Minkowski theory. This issue is at the very heart of constructive quantum field theory – see [27]. The essential question is this: is knowledge of the Euclidean Green functions sufficient to enable a reconstruction of the Hilbert space of the Minkowski theory? The answer is yes, if the Euclidean Green functions satisfy a condition known as *reflection positivity*. The reflection positivity condition requires a special “time” direction to be singled out in the otherwise $SO(4)$ invariant Euclidean theory. If the Euclidean theory is reflection positive then the generator of translations in this “time” direction, τ, is $\exp(-H\tau)$ with H having the same spectrum of states on the Hilbert space of the Minkowski theory as the Hamiltonian. For a complete discussion of reflection positivity see [28, 27].

The QCD action in Minkowski space with the signature $(1,-1,-1,-1)$ is [5]

$$S = \int d^4x \left[-\frac{1}{4} F_a^{\mu\nu} F_{\mu\nu}^a + \sum_{f=1}^{n_f} \bar{\psi}_j^{(f)} \left(i \not{D}_{jk} - m^{(f)} \delta_{jk} \right) \psi_k^{(f)} \right] . \tag{2.5}$$

The field strength tensor is

$$F_{\mu\nu}^a = \partial_\mu A_\nu^a - \partial_\nu A_\mu^a + g f^{abc} A_\mu^b A_\nu^c \tag{2.6}$$

and the covariant derivative

$$(D_\mu)_{jk} = \delta_{jk} \partial_\mu - i g A_\mu^a \frac{\lambda_{jk}^a}{2} \tag{2.7}$$

where g is the strong coupling constant. f^{abc} are the (antisymmetric) structure constants of $SU(3)$ and the λ^a are the generators for the fundamental representation (the Gell-Mann matrices). Note that $a = 1, \ldots, 8$ and $j, k = 1, \ldots, 3$ in the above and repeated index summation is used. n_f is the number of quark flavours in the theory.

The question is how to write this Lagrangian in Euclidean space with a signature $(1,1,1,1)$? The rotation to Euclidean space is defined through $t \rightarrow -i\tau$ with Euclidean four-vectors related to their Minkowski counterparts through

$$B^E = (\vec{B}^E, B_4) \equiv (\vec{B}, -iB_0) \; . \tag{2.8}$$

Following this convention easily leads to the Euclidean QCD action (suppressing flavour and colour indices)

$$S_E = \int d^4x_E \left[\frac{1}{4}F^{\mu\nu}F_{\mu\nu} + \bar{\psi}\left(\not{D}_E + m\right)\psi\right] \tag{2.9}$$

with $\not{D}_E = \gamma^E_\mu D_\mu$ where the Euclidean gamma matrices are defined as

$$\gamma_4 = \gamma_0 \, , \quad \gamma^E_i = i\gamma_i \, , \quad \gamma^E_5 = \gamma_5 \tag{2.10}$$

satisfying

$$\{\gamma^E_\mu, \gamma^E_\nu\} = 2\delta_{\mu\nu} \, , \qquad \gamma^{E\,\dagger}_\mu = \gamma^E_\mu \; . \tag{2.11}$$

The definition of D_μ and $F_{\mu\nu}$ used in the above is the same in both Minkowski and Euclidean space, where it is understood that the Euclidean four-vector A_μ is used in the Euclidean definition. Note that the Euclidean action is $S_E = i\,S$ as required.

2.1.2 Discretising Gauge Fields

The action S_E is a local action and is invariant under local $SU(3)$ gauge transformations. However, when discretising the action on the lattice, the derivatives are replaced by finite differences, e.g.

$$\partial_\mu\psi(x) \longrightarrow \frac{1}{2a}\left[\psi(x + a\hat{\mu}) - \psi(x - a\hat{\mu})\right] \tag{2.12}$$

and hence terms in the action involving derivatives are now non-local[1]. The question is how to preserve the invariance of the action under local gauge transformations in the presence of these non-local terms?

The solution comes from the very concept of the gauge field. The gauge field $A_\mu(x)$ is a element of the Lie algebra $su(3)$. A *group* element, $U(x+dx,x)$, is associated with this gauge field through the infinitesimal transport $x \to x+dx$,

$$U(x+dx,x) = \mathbf{1} + igA_\mu(x)dx^\mu \tag{2.13}$$

where $\mathbf{1}$ is the identity of the group. This can be generalised to the transport along a finite path $\mathcal{C}$ from x to y as

$$U(y,x;\mathcal{C}) = \mathrm{e}^{ig\mathcal{P}\int_x^y A_\mu(z)dz^\mu} \tag{2.14}$$

where $\mathcal{P}$ denotes path ordering.

The important point to note is that the quantity $\bar{\psi}(y)U(y,x;\mathcal{C})\psi(x)$ is invariant under local gauge transformations. This gives a prescription for constructing a lattice covariant derivative as

$$D_\mu(x)\psi(x) \longrightarrow \frac{1}{2a}\left[U_\mu(x)\psi(x+a\hat{\mu}) - U_\mu^\dagger(x-a\hat{\mu})\psi(x-a\hat{\mu})\right] \tag{2.15}$$

with the link variables $U_\mu(x)$ related to the continuum gauge fields through

$$U_\mu(x) \equiv U(x+a\hat{\mu},x) = e^{ig\mathcal{P}\int_0^1 A_\mu(s)ds} \tag{2.16}$$

where s parametrises the path along the link. These link variables are considered the fundamental gauge objects in gauge theories on the lattice. Note that the

[1]Forward or backward finite differences for the derivatives could equally well be used. This symmetric derivative is however preferable as it preserves the anti-hermitian nature of the continuum $\not{D}$ operator.

link matrices satisfy

$$U_{-\mu}(x) = U_{\mu}^{\dagger}(x - a\hat{\mu}) \, , \qquad U_{\mu}(x) U_{\mu}^{\dagger}(x) = \mathbf{1} \ . \tag{2.17}$$

The next issue is how to construct the pure gauge part of the action from these link variables.

Here the important point to note is that the group element $U(x, x; \mathcal{C})$ coming from transport around a closed path is also invariant under local gauge transformations. The shortest closed path on the lattice is the plaquette, $\Box$. In the (μ, ν) plane the plaquette from the point x can be defined as the path

$$x \rightarrow x + a\hat{\mu} \rightarrow x + a\hat{\mu} + a\hat{\nu} \rightarrow x + a\hat{\nu} \rightarrow x$$

with the corresponding plaquette variable then defined as

$$P_{\mu\nu}^{\Box}(x) \equiv U(x, x; \Box) = U_{\mu}(x) U_{\nu}(x + a\hat{\mu}) U_{\mu}^{\dagger}(x + a\hat{\nu}) U_{\nu}^{\dagger}(x) \ . \tag{2.18}$$

Taking the trace of the plaquette variable so as to get a gauge invariant quantity it can be shown that

$$\mathrm{Re}\ \mathsf{Tr} P_{\mu\nu}^{\Box}(x) = N_c - \frac{g^2}{2} a^4 \mathsf{Tr}(F_{\mu\nu}^2(x)) + \mathcal{O}(a^6) \tag{2.19}$$

where $F_{\mu\nu} = F_{\mu\nu}^a \frac{\lambda^a}{2}$. $N_c = 3$ is the number of colours and the trace (Tr) is over the implicit colour indices. This then leads to a lattice version of the pure gauge action

$$\begin{aligned} S_G &= \int d^4x \frac{1}{2} F^{\mu\nu} F_{\mu\nu} \longrightarrow a^4 \sum_x \frac{1}{2} \mathsf{Tr}(F_{\mu\nu}^2(x)) \\ &= \sum_x \sum_{\Box} \frac{2}{g^2} \Big(N_c - \mathrm{Re} \mathsf{Tr} P_{\mu\nu}^{\Box}(x) \Big) + \mathcal{O}(a^2) \end{aligned} \tag{2.20}$$

where the $\Box$ under the sum stands for $1 \leq \nu < \mu \leq 4$. The factor of two arises because of the mismatch between the number of plaquettes per site, 6, and the number of terms in the sum over $\mu\nu$, 12. The constant term is irrelevant and it is conventional to use the notation, $\beta = 2N_c/g^2$, giving

$$S_G = -\beta \sum_{x,\Box} \frac{\mathrm{Re}\mathsf{Tr}P_{\mu\nu}^{\Box}}{N_c} \tag{2.21}$$

which is known as the Wilson pure gauge action [29]. This gives the pure gauge contribution to the partition function as

$$Z_G = \int \prod_{x,\mu} dU_\mu(x) \exp\left(\beta \sum_{x,\Box} \frac{\mathrm{Re}\mathsf{Tr}P_{\mu\nu}^{\Box}}{N_c}\right) . \tag{2.22}$$

This is gauge invariant if the so-called Haar measure [30] is used for integration over each link variable. For any compact group G the Haar measure is the unique measure dU on G which satisfies

$$\int_G f(U)dU = \int_G f(VU)dU = \int_G f(UV)dU \quad \text{for all} \quad V \in G \tag{2.23}$$

where f is some function and $\int_G dU = 1$. It is neither necessary here nor straightforward to express the Haar measure for $SU(3)$ – I refer the reader to [31].

2.1.3 Discretising Fermion Fields – Wilson Fermions

Using the lattice covariant derivative from equation (2.15) it is straightforward to arrive at a discretised version of the fermionic part of the action,

$$\begin{aligned} S_{NF} &= \int d^4x\, \bar{\psi}(x)\, (\not{D} + m)\, \psi(x) \\ &\longrightarrow \sum_x a^4 \{ m\bar{\psi}(x)\psi(x) \\ &+ \sum_\mu \frac{1}{2a} \bar{\psi}(x)\gamma_\mu \left[U_\mu(x)\psi(x + a\hat{\mu}) - U_\mu^\dagger(x - a\hat{\mu})\psi(x - a\hat{\mu}) \right] \} . \end{aligned} \tag{2.24}$$

This is known as the "naive" fermion action. Unfortunately there is a problem with this action in that it represents 16 continuum fermions of the same mass, rather than just one – the famous fermion doubling phenomenon.

Wilson [32] suggested a way around this by simply adding an extra term to the action,

$$S_W = -\sum_x a^4 \sum_\mu \frac{r}{2a} \bar{\psi}(x) \left[U_\mu(x)\psi(x+a\hat{\mu}) - 2\psi(x) + U_\mu^\dagger(x-a\hat{\mu})\psi(x-a\hat{\mu}) \right] \tag{2.25}$$

where r is an arbitrary constant – in general one chooses[2] $r = 1$. This term is no more than the lattice equivalent of $a\bar{\psi}\Box\psi$ where $\Box$ is the d'Alembert operator. This term goes as $\mathcal{O}(a)$ and so the continuum form for the action is still retrieved as $a \to 0$. The action with this term leads to 15 of the 16 doublers being decoupled from the theory in the continuum limit.

There is, however, a serious drawback in using this Wilson term – the resulting fermionic action is not invariant under chiral transformations even if $m = 0$. QCD with zero fermion masses is a chiral invariant theory, and left handed and right handed fermions are treated differently in the SM, so Wilson fermions would appear to be singularly inappropriate for the formulation of the SM on the lattice.

A common alternative approach is to keep the naive action, which still has the correct chiral behaviour, but perform a transformation on the fermionic degrees of freedom to reduce the number of doublers. The transformation that leads to "staggered" fermions [33] essentially shares out the spinor degrees of freedom amongst the sites of an elementary hypercube of the lattice so that the fermion field is now only a single component field at each site. The doubling problem still remains in that the continuum limit of this single component field is 16 one component fermions. In staggered fermions these sixteen fermionic degrees of freedom are interpreted as four degenerate flavours of Dirac fermions, with the flavours also spread over a hypercube. In other words the approach of staggered fermions is to reduce the number of doublers at the price of mixing up the spin and flavour degrees of freedom and spreading them over a hypercube. The technical details are quite involved, and as only actions based on Wilson fermions are used in this work, I refer the reader to [31, 28] for further details.

[2]The Wilson action then satisfies reflection positivity.

However, regardless of the approach taken, the doubler problem has not been avoided without introducing new problems. In fact it turns out that it is not possible to formulate a chiral theory on a regular lattice without introducing extra unwanted states (the doublers) [34, 35]. In the Wilson approach one breaks chiral symmetry to overcome the problem, in the staggered approach one keeps chiral symmetry but also the doublers, albeit a reduced number of them.

2.1.4 Improved Fermionic Action – the Clover Action

The Wilson fermion action has corrections in lattice spacing at $\mathcal{O}(a)$ as distinct from $\mathcal{O}(a^2)$ for the naive action and also $\mathcal{O}(a^2)$ for the pure gauge action. Addition of the term [36]

$$\begin{aligned}\Delta S^{\mathrm{II}} &= a^4\sum_{x,\mu}\left\{\frac{r}{8a}\left[\bar{\psi}(x)U_\mu(x)U_\mu(x+a\hat{\mu})\psi(x+2a\hat{\mu})\right.\right.\\ &+ \left.\left.\bar{\psi}(x)U_\mu^\dagger(x-a\hat{\mu})U_\mu^\dagger(x-2a\hat{\mu})\psi(x-2a\hat{\mu})-2\bar{\psi}(x)\psi(x)\right]\right\} \qquad (2.26)\end{aligned}$$

to the Wilson fermion action reduces the discretisation error back to $\mathcal{O}(a^2)$, while leading to the removal of 15 of the doublers from the theory in the same manner as the Wilson action. The fermion action with this term is the so-called "two-link action". It can be shown [36, 37] that matrix elements calculated using this action have no corrections of $\mathcal{O}(a)$ or $\mathcal{O}((g^2)^n\ln^n a)\sim\mathcal{O}(a)$. The leading discretisation errors in these matrix elements occur at $\mathcal{O}(g^2a)$.

However, it is not convenient to use this two-link action in simulations as it contains next-to-nearest neighbour interactions and this increases the computational cost of the problem. Heatlie *et al.* [37] observed that by transforming the quark fields as

$$\psi \longrightarrow \left(1-\frac{ar}{4}(\overrightarrow{\not{D}}-m)\right)\psi+\mathcal{O}(a^2) \qquad (2.27)$$

$$\bar{\psi} \longrightarrow \bar{\psi}\left(1+\frac{ar}{4}(\overleftarrow{\not{D}}+m)\right)+\mathcal{O}(a^2) \qquad (2.28)$$

then one can arrive at an action with only nearest neighbour interactions,

$$S_F = S_{NF} + S_W - a^4 \sum_{x,\mu,\nu} ig\frac{ar}{4}\bar{\psi}(x)\sigma_{\mu\nu}F_{\mu\nu}(x)\psi(x)\,. \tag{2.29}$$

This action was originally introduced by Sheikholeslami and Wohlert [38], though it is also known as the "clover" action.

If the quark fields are treated according to this action and they are rotated as in equations (2.27) and (2.28) in operators such as $O_\Gamma = \bar{\psi}\Gamma\psi$, then matrix elements of these operators, as for the case of the two-link action, have leading discretisation errors at $\mathcal{O}(g^2 a)$, at worst [37]. Note that the bare mass in the clover action (m') is related to the bare mass in the two-link action (m) by $m' = m(1 + mra/2)$. For this improvement procedure using m or m' as the mass in the action and rotations is irrelevant to $\mathcal{O}(a^2)$. Moreover, in calculating on-shell hadronic matrix elements, as in this work, the rotations can be simplified using the equation of motion to give

$$\psi \longrightarrow \left(1 - \frac{ar}{2}\overrightarrow{\not{D}}\right)\psi, \qquad \bar{\psi} \longrightarrow \bar{\psi}\left(1 + \frac{ar}{2}\overleftarrow{\not{D}}\right)\,. \tag{2.30}$$

So, the procedure is to use the clover action to describe the lattice quark fields, and on-shell improvement of matrix elements is ensured by rotating currents as

$$\Gamma \longrightarrow \left(1 + \frac{ar}{2}\overleftarrow{\not{D}}\right)\Gamma\left(1 - \frac{ar}{2}\overrightarrow{\not{D}}\right)\,. \tag{2.31}$$

The term "clover" comes from the lattice definition of the field strength tensor,

$$iga^2 F_{\mu\nu}(x) = \frac{1}{4}\sum\left[\frac{P^{\Box}_{\mu\nu}(x) - P^{\Box\dagger}_{\mu\nu}(x)}{2}\right] \tag{2.32}$$

with $P^{\Box}_{\mu\nu}$ as defined earlier. The sum is over the four plaquettes in the (μ,ν) plane around the point x – the four leaves of the clover.

2.1.5 The Partition Function of Lattice QCD

The partition function of lattice QCD can now be written down. First, it is convenient to write the fermion action in the general form

$$S_F = \sum_{x,y} \sum_{f} \bar{\psi}^{(f)}(x) M^{(f)}(x,y)[U] \psi^{(f)}(y) \,. \tag{2.33}$$

The fermion matrix, M, for SW-clover fermions can be written as

$$M^{(f)}(x,y)[U] = A(x)\delta_{x,y} - \kappa_f \sum_{\mu} \left[(r-\gamma_\mu) U_\mu(x) \delta_{x+\hat{\mu},y} + (r+\gamma_\mu) U_\mu^\dagger(y) \delta_{x-\hat{\mu},y} \right] \tag{2.34}$$

for fermion flavour f and where

$$A(x) = \left(1 - i \frac{r\kappa_f}{2} \sum_{\mu\nu} \sigma_{\mu\nu} \frac{1}{4} \left[\frac{P_{\mu\nu}^{\square}(x) - P_{\mu\nu}^{\square\dagger}(x)}{2i} \right] \right) \,. \tag{2.35}$$

It should be noted that for both Wilson and clover fermions M satisfies the hermiticity relation

$$M(y,x) = \gamma_5 M^\dagger(x,y) \gamma_5 \,. \tag{2.36}$$

The hopping parameter, κ_f, is defined as

$$\kappa_f = \frac{1}{8r + 2m_f a} \tag{2.37}$$

and the fields have been rescaled as $\psi^{(f)}(x) \rightarrow a^{-3/2}\sqrt{2\kappa_f}\psi^{(f)}(x)$. So, the partition function can be written as

$$Z = \int [dU] \prod_f [d\psi^{(f)}][d\bar{\psi}^{(f)}] \, \mathrm{e}^{-S_G[U] - \sum_{x,y} \sum_f \bar{\psi}^{(f)}(x) M^{(f)}(x,y)[U] \psi^{(f)}(y)} \tag{2.38}$$

where $[d\psi] = \prod_x d\psi(x)$ etc. Using the rules for integrating Grassman variables this becomes

$$Z = \int [dU] \prod_f \det M^{(f)}[U] \, \mathrm{e}^{-S_G[U]} \,. \tag{2.39}$$

The vacuum expectation value of any operator, $\mathcal{O}[\psi, \bar{\psi}, U]$, is then calculable as

$$\langle 0 \,|\mathcal{O}|\, 0\rangle = \frac{1}{Z}\int [dU]\, \mathcal{O}[U] \prod_f \det M^{(f)}[U]\, \mathrm{e}^{-S_G[U]} \,. \tag{2.40}$$

The question is how is this integral evaluated in practice ?

2.1.6 Numerical Techniques and the Quenched Approximation

Restricting the lattice to a finite volume allows the numerical evaluation of the action for a given gauge and quark field configuration. In order to do this appropriate boundary conditions on the fields must be set. A standard choice, and the one used in this work, is periodic boundary conditions for the gauge fields, periodic boundary conditions in the space directions and anti-periodic in time for the fermion fields. The anti-periodicity condition arises as a result of the anti-commuting nature of the fermion fields.

The numerical evaluation of the path integral still requires the "discretisation" of the space of these gauge and quark field configurations. By "discretisation" it is meant an approximation of the full configuration space by a finite ensemble of configurations, thus allowing the integral to be approximated by a sum over this ensemble. The issue of practical importance is how to construct this ensemble such that the ensemble sum is a good approximation to the integral. All of the methods used in lattice field theory are based on Monte Carlo integration with importance sampling. The basic idea is to generate the ensemble $\{U^i\}$ so that each member of the ensemble occurs with probability

$$P(U^i)dU^i = [dU^i] \prod_f \det M^{(f)}[U^i]\, \mathrm{e}^{(-S_G[U^i])} \tag{2.41}$$

– see [31, 28] for details of the various algorithms used to do this. Having thus generated the ensemble $\{U^i\}$ the expectation value of any operator $\mathcal{O}$ is

$$\langle \mathcal{O} \rangle \approx \frac{1}{N}\sum_{i=1}^{N} \mathcal{O}(U_i) \tag{2.42}$$

where N is the number of configurations in the ensemble. For sufficiently large N the measurements $\mathcal{O}(U_i)$ will be Gaussian distributed about the mean with variance

$$\sigma_{\mathcal{O}}^2 = \frac{1}{N-1}\left(\langle \mathcal{O}^2\rangle - \langle \mathcal{O}\rangle^2\right) . \tag{2.43}$$

This presumes that the ensemble consists of statistically independent configurations. Using the Metropolis [39] or related algorithms to generate the configuration ensemble involves generating successive configurations along a Markov chain. Successive configurations are highly correlated and hence for the uncorrelated set used for measurements only widely separated configurations along the chain are saved. However, there may still be some latent correlations in the measurements. Similarly, measurements on different timeslices and different κ values are often highly correlated and these correlations must be taken into account when analysing the statistical errors. I discuss statistical fitting procedures in appendix A.

The presence of the fermion determinant gives rise to some problems. Firstly $\prod_f \mathsf{det}\, M^{(f)}[U]$ is only necessarily positive for degenerate pairs of fermion flavours, for Wilson or clover fermions. This positivity is necessary if the weight $P(U)$ is to be considered as a probabilistic weight. Secondly, the dimension of the fermion matrix is enormous and calculating its determinant is the most numerically intensive part in generating the configuration ensemble. In contrast, generating just a pure gauge ensemble of configurations, i.e. with weight $[dU]\exp(-S_G[U])$, is considerably faster. Setting $\mathsf{det}\, M^{(f)}[U] = \mathsf{constant}$ overcomes both problems. This is known as the *quenched* or *valence* approximation. Taking this approximation amounts to ignoring closed quark loops in the gluon propagator. It is an uncontrolled approximation and it is not clear a priori that calculations in quenched QCD should yield predictions close to full QCD. Nonetheless, quenched QCD retains all the important features of QCD, namely confinement, chiral symmetry breaking and asymptotic freedom. So far quenched QCD simulations of the light hadron spectrum seem to suggest that the effect of quenching is not too drastic [40]. In this work the quenched approximation is used. Until further calculations are performed in unquenched QCD the exact effect of quenching on the results will not be known. For more details on the effects of quenching see the discussion in [41] and references therein.

2.2 Hadron Correlation Functions and Smearing

2.2.1 Two-Point Functions

In the last chapter the leptonic decay constant of the B meson was introduced, defined by the matrix element (rotated to Euclidean space)

$$\langle 0|A_\mu(0)|B_0(p)\rangle = f_B p_\mu \tag{2.44}$$

where p_μ is the momentum of the meson. This matrix element can be extracted from the study of the Euclidean correlator

$$C_{AB}(t;\vec{p}) = \int d^3x \, \langle 0| \, A_\mu(\vec{x},t)\chi_B^\dagger(0) \, |0\rangle \, \mathrm{e}^{i\vec{p}.\vec{x}} \tag{2.45}$$

where $\chi_B^\dagger(0)$ is some operator that produces a state at the origin with the same quantum numbers as the B meson. The procedure is as follows: (1) insert a complete set of states $\left|M(\vec{k},n)\right\rangle$ with energy $E_n(\vec{k})$ between the A_μ and $\chi_B^\dagger$, with the states normalised such that the completeness relation is[3]

$$\mathbf{1} = \sum_n \int \frac{d^3k}{(2\pi)^3 2E_n(\vec{k})} \left|M(\vec{k},n)\right\rangle \left\langle M(\vec{k},n)\right| , \tag{2.46}$$

(2) translate the operator A_μ to the origin using

$$A_\mu(\vec{x},t) = \mathrm{e}^{Ht+i\vec{p}.\vec{x}} A_\mu(0) \mathrm{e}^{-Ht-i\vec{p}.\vec{x}} \tag{2.47}$$

where H is the Hamiltonian, and (3) finally use the fact that

$$\int \frac{d^3x}{(2\pi)^3} \mathrm{e}^{i(\vec{p}-\vec{k}).\vec{x}} = \delta(\vec{p}-\vec{k}) \tag{2.48}$$

[3]For convenience I'm assuming a discrete set of energy states.

to give

$$C_{AB}(t;\vec{p}) = \sum_n \langle 0|\, A_\mu(0)\,|M(\vec{p},n)\rangle \, \langle M(\vec{p},n)|\, \chi_B^\dagger(0)\,|0\rangle \, \frac{\mathrm{e}^{-E_n(\vec{p})t}}{2E_n(\vec{p})}. \tag{2.49}$$

So, if the state with lowest energy in this sum is the state $|B(\vec{p})\rangle$ then at large Euclidean times the contribution of this state will dominate,

$$C_{AB}(t;\vec{p}) \xrightarrow{t\gg 0} \langle 0|\, A_\mu(0)\,|B(\vec{p})\rangle \, \langle B(\vec{p})|\, \chi_B^\dagger(0)\,|0\rangle \, \frac{\mathrm{e}^{-E_B(\vec{p})t}}{2E_B(\vec{p})} \tag{2.50}$$

where $E_B^2(\vec{p}) = M_B^2 + |\vec{p}|^2$.

Hence by studying the large Euclidean time behaviour of this correlator the matrix element $\langle 0|\, A_\mu(0)\,|B(\vec{p})\rangle$, and consequently f_B, can be extracted. The contribution of $\langle B(\vec{p})|\, \chi_B^\dagger(0)\,|0\rangle$ can be factored out by also studying the correlator

$$C_{BB}(t;\vec{p}) \xrightarrow{t\gg 0} |\, \langle B(\vec{p})|\, \chi_B^\dagger(0)\,|0\rangle \,|^2 \frac{\mathrm{e}^{-E_B(\vec{p})t}}{2E_B(\vec{p})} \tag{2.51}$$

or equally well just studying the correlator

$$C_{AA}(t;\vec{p}) \xrightarrow{t\gg 0} |\, \langle 0|\, A_\mu(0)\,|B(\vec{p})\rangle \,|^2 \frac{\mathrm{e}^{-E_B(\vec{p})t}}{2E_B(\vec{p})} \tag{2.52}$$

would suffice. At any rate the point is that calculation of correlators of the form in equation (2.45) allows the extraction of the phenomenological parameters of interest. Note also that the mass of the excitation can, in principle, be extracted from these correlators.

Several points are worth noting before proceeding further. Firstly, reflection positivity has allowed the identification of H in the above as the Hamiltonian. Secondly, on the lattice the integral over x is clearly a sum over x. I could equally well have proceeded entirely on the lattice and used lattice completeness relations to arrive at the same result. Finally, it should be noted that the expressions are modified in the case of a lattice of finite temporal extent, T say. Then the asymptotic behaviour is replaced by

$$C_{AB}(t;\vec{p}) \xrightarrow{t\gg 0} c_+\,\mathrm{e}^{-E_B(\vec{p})t} + c_-\,\mathrm{e}^{-E_B(\vec{p})(T-t)} \tag{2.53}$$

where

$$c_+ = \frac{1}{2E_B(\vec{p})}\,\langle 0|\,A_\mu(0)\,|B(\vec{p})\rangle\,\langle B(\vec{p})|\,\chi_B^\dagger(0)\,|0\rangle \tag{2.54}$$

$$c_- = \frac{1}{2E_B(\vec{p})}\,\langle 0|\,\chi_B(0)\,|B(\vec{p})\rangle\,\langle B(\vec{p})|\,A_\mu^\dagger(0)\,|0\rangle\ . \tag{2.55}$$

It is assumed that periodic or anti-periodic boundary conditions for the fields are being used.

2.2.2 Interpolating Operators and Quark Propagators

In the above $\chi_B^\dagger$ was introduced as some operator that created a state with the same quantum numbers as the B meson. So, the obvious question is what is a good interpolating operator in terms of its constituent quark and gluon fields to use as the creation operator for the B meson? By convention the neutral B meson has quark constituents $\bar{b}q$ where q is a light quark (d,s). The simplest operator with this quark constituent that reproduces the correct J^{PC} for the B meson is the local operator $\chi_B^\dagger(x) = \bar{q}(x)\,\gamma_5\,b(x)$. Note that this is a spinor-colour singlet. With this and using $A_\mu(x) = \bar{b}(x)\gamma_\mu\gamma_5 q(x)$ allows the two-point correlation function, equation (2.45), to be written in terms of the basic fields as

$$C_{AB}(t;\vec{p}) = \sum_{\vec{x}} \mathrm{e}^{i\vec{p}.\vec{x}}\,\langle 0|\,\bar{b}(\vec{x},t)\Gamma_1 q(\vec{x},t)\bar{q}(0)\Gamma_2 b(0)\,|0\rangle \tag{2.56}$$

where $\Gamma_1 = \gamma_\mu\gamma_5$ from the axial current and $\Gamma_2 = \gamma_5$ from the pseudoscalar interpolating operator. In the path integral representation this correlator becomes, after the Wick contractions,

$$C_{AB}(t;\vec{p}) = \int [dU]\,\prod_f \mathsf{det}\,M^{(f)}[U]\,\mathrm{e}^{-S_G[U]}\,\sum_{\vec{x}} \mathrm{e}^{i\vec{p}.\vec{x}}\left\{-\mathsf{Tr}\left[G^{(b)}(0,x)\Gamma_1 G^{(q)}(x,0)\Gamma_2\right]\right\} \tag{2.57}$$

where the G are the quark propagators calculated in the given background gauge configuration, U, and the trace is over the implicit spinor and colour indices. The G can be calculated by solving

$$\sum_x M_{ki}^{(f)}(z,x)[U]G_{ij}^{(f)}(x,y) = \delta(z-y)\delta_{kj} \tag{2.58}$$

for each flavour, f, in the given background gauge configuration, U, – note i, j, k are spinor-colour indices. This amounts to the inversion of a very large sparse matrix (M) and there are various algorithms for doing this [42]. In practice on the lattice only propagators from the origin to all other points are calculated, $G(x,0)$. The propagator $G(0,x)$ is related to this from the hermiticity relation, $G(0,x) = \gamma_5 G^\dagger(x,0)\gamma_5$. So, in summary, the procedure is to calculate the spatial sum of the trace,

$$\sum_{\vec{x}} \mathrm{e}^{i\vec{p}.\vec{x}} \left\{ -\mathsf{Tr}\left[\gamma_5 {G^{(b)}}^\dagger(x,0)\gamma_5\Gamma_1 G^{(q)}(x,0)\Gamma_2 \right] \right\} \tag{2.59}$$

on each configuration and average over the configuration sample to evaluate the two-point correlator.

A final point to note concerns clover fermions. Recall that for on-shell improvement the operators must be rotated as

$$\Gamma \longrightarrow \left(1 + \frac{1}{2}\overleftarrow{\not{D}}\right)\, \Gamma\, \left(1 - \frac{1}{2}\overrightarrow{\not{D}}\right) . \tag{2.60}$$

If these rotations are introduced into the correlator in equation (2.59) then from the trace it can be seen that the effect of these rotations can be absorbed by rotating the ends of the propagators as

$$G(x,0) \longrightarrow \left(1 - \frac{1}{2}\overrightarrow{\not{D}}\,(x)\right) G(x,0) \left(1 + \frac{1}{2}\overleftarrow{\not{D}}\,(0)\right) . \tag{2.61}$$

So for on-shell improved correlators, the effective propagators, G, are calculated by inverting the clover fermion matrix and performing the rotations at each end as above.

2.2.3 Smearing

The lowest lying energy state dominates the sum in equation (2.49) for large Euclidean times, as has been noted. There are two points to emphasise about using this fact to extract information from lattice correlators. Firstly, on a lattice of finite temporal extent, T, this asymptotic behaviour must be reached for times less than $T/2$. Secondly, for some correlators the correlator signal-to-noise ratio, coming from the Monte-Carlo simulation, decreases with increasing Euclidean time. So clearly one would like to have operators A_μ and $\chi_B^\dagger$ that have a strong overlap with the lowest energy state (or whatever state of interest for that matter) in order that this state dominates the sum over states at relatively small Euclidean times. In general, just using the local forms of these operators, as in the previous subsection, is not good enough.

One method of constructing better operators is to "smear" the local operators. This involves constructing an effective local operator from a linear combination of non-local ones. Take for example the local operator, $\mathcal{O}^L(\vec{x},t) = \bar{h}(\vec{x},t)\,\Gamma\,l(\vec{x},t)$, for the quark fields h and l. Then a corresponding smeared operator is

$$\mathcal{O}^S(\vec{x},t) = \sum_{\vec{y}} \bar{h}(\vec{y},t)\,f(\vec{y},\vec{x})\,\Gamma\,l(\vec{x},t) \tag{2.62}$$

where the spatial weighting $f(\vec{y},\vec{x})$ is called the smearing function. A judicious choice of smearing function can radically improve the overlap of the operator with the lowest energy state. The motivation for smearing is intuitive – the meson has finite extent and so by smearing the meson operator with a spatial weighting of roughly the same size and shape as the ground state wave function one expects the smeared operator to have very good overlap with that ground state. The task is then to construct smearing functions that achieve this. There are several approaches that can be taken depending on the system being investigated – see [43] for example. A major aspect of this work is the investigation of the efficiency of various smearing functions in isolating the ground state in B meson correlation functions.

An important point to note about the smearing technique is that it breaks the gauge invariance of the fermion bilinear unless the smearing function is itself gauge covariant. So the smearing function must be constructed to be explicitly gauge covariant or otherwise everything must be performed in a fixed gauge. In the latter case the Coulomb gauge is the most common choice. In a smooth gauge like the Coulomb gauge explicit functional forms for the smearing functions, such as hydrogen-like wavefunctions, can be chosen. In the next chapter I describe the exact smearing functions, both gauge covariant and in a fixed gauge, used in this work, and I also elaborate on some of the more technical details involved.

Finally, a useful diagnostic for checking how well the lightest state dominates the correlator is the effective mass plot. In the asymptotic region $C(t) = A\exp(-mt)$ and so it is expected that

$$m_{\text{eff}}(t) = \ln\left(\frac{C(t)}{C(t+1)}\right) = \mathsf{constant} = m\,. \tag{2.63}$$

Hence the onset and persistence of a plateau in a plot of $m_{\text{eff}}(t)$ versus t is a good sign of ground state domination and the effectiveness of the smearing function used.

2.2.4 Three-Point Functions

In the last sections it has been illustrated how f_B can be extracted by studying the large time behaviour of two-point correlation functions. In order to extract a meson-to-meson amplitude, such as that describing B^0-$\bar{B}^0$ mixing,

$$\left\langle \bar{B}^0 \right| \mathcal{O}_{LL}(0) \left| B^0 \right\rangle,$$

requires the study of three-point correlation functions. Consider the three-point function

$$C_{\text{3pt}}(t_x, t_y; \vec{p_x}, \vec{p_y}) = \sum_{\vec{x},\vec{y}} \mathrm{e}^{i(\vec{p_x}.\vec{x}+\vec{p_y}.\vec{y})} \left\langle 0\right| \chi_B^\dagger(\vec{x},t_x)\, O_{LL}(\vec{0},0)\chi_B^\dagger(\vec{y},t_y) \left|0\right\rangle \tag{2.64}$$

with $t_y < 0 < t_x$. Again proceeding via the insertion of a complete set of states the large Euclidean time behaviour ($t_y \ll 0$ and $t_x \gg 0$) of this correlator is found to be

$$\begin{aligned} C_{3\mathrm{pt}}(t_x, t_y; \vec{p_x}, \vec{p_y}) \quad &\longrightarrow \quad \frac{Z_B(\vec{p_x}) Z_B(\vec{p_y})}{4E_B(\vec{p_x}) E_B(\vec{p_y})} \, \mathrm{e}^{-E_B(\vec{p_x}) t_x} \, \mathrm{e}^{E_B(\vec{p_y}) t_y} \\ &\times \quad \left\langle \bar{B}^0(\vec{p_x}) \right| O_{LL}(0) \left| B^0(\vec{p_y}) \right\rangle \end{aligned} \tag{2.65}$$

where

$$Z_B(\vec{q}) = \langle 0 | \, \chi_B^\dagger(0) \left| \bar{B}^0(\vec{q}) \right\rangle . \tag{2.66}$$

The Z_B and E_B can be extracted from the study of the appropriate two-point correlation functions and hence the required matrix element can be extracted from the three-point function. Writing out the three-point function in terms of the constituent quark fields and performing the Wick contractions is rather involved. The details are given in appendix B.

2.3 The Continuum Limit

What has been described so far in this chapter is the explicit regularisation of QCD by formulating it on a regular lattice and the basics of how to perform calculations in this regularised theory have been sketched. The whole aim of the exercise is the extraction of continuum physics from these calculations. The issues surrounding this are discussed here.

2.3.1 Scaling

In order to extract continuum results one would like to be in a regime where physical quantities calculated on the lattice are independent of the regulator. The final expressions for the lattice QCD functional integral contain only dimensionless quantities – there is no explicit scale in the lattice theory. The only free parameters are the bare coupling, $g_0^2 = 2N_c/\beta$, and the hopping parameter(s), κ. The only physical predictions of the lattice theory are ratios of physical observables of the same dimension. For such a ratio, $R(a, g_0)$ say, to be independent of

a then

$$-a\frac{d}{da}R(a,g_0) \equiv \left[-a\frac{\partial}{\partial a} + \beta_{\rm latt}(g_0)\frac{\partial}{\partial g_0}\right] R(a,g_0) = 0 \tag{2.67}$$

where $\beta_{\rm latt} \equiv -a\partial g_0/\partial a$ specifies how g_0 must be tuned with lattice spacing such that this *scaling* behaviour is achieved. As g_0 is the explicit parameter in the theory, and not a, the functional dependence in $\beta_{\rm latt}$ should be thought of as being the other way around – $\beta_{\rm latt}$ specifies how a depends on the choice of the bare coupling g_0.

The asymptotic freedom of QCD implies that the continuum limit, $a \to 0$, is recognised as the point where $g_0 \to 0$. The perturbative expansion of $\beta_{\rm latt}$ near this limit is well known,

$$\beta_{\rm latt}(g_0) = -\frac{\beta_0}{16\pi^2}g_0^3 - \frac{\beta_1}{(16\pi^2)^2}g_0^5 + \ldots \tag{2.68}$$

with $\beta_0 = 11$ and $\beta_1 = 102$ the first two (universal) coefficients[4]. This can be integrated to give the functional dependence of a on g_0 in this *asymptotic scaling regime* as

$$a\Lambda_{\rm latt} = \left(\frac{\beta_0 g_0^2}{16\pi^2}\right)^{-\beta_1/2\beta_0^2} \mathrm{e}^{-16\pi^2/2\beta_0 g_0^2}[1 + \mathcal{O}(g_0^2)]\,. \tag{2.69}$$

$\Lambda_{\rm latt}$ is the single renormalisation group invariant parameter with dimensions of mass that appears in the theory. Although RG invariant it is scheme dependent and hence depends on the actual discretisation of the action used.

In principle $\Lambda_{\rm latt}$ carries the dimension of all dimensionful quantities in the theory. However, in practice, it is not used to set the scale. Normally some other dimensionful observable, say the mass of the rho meson, is used. Its value in lattice units is calculated and this is compared to its experimental value – a is then just the ratio of the lattice to physical mass.

If the scaling behaviour in equation (2.67) is exactly obeyed then it is immaterial which dimensionful observable is used to set the lattice spacing. In practice,

[4] I'm assuming the quenched theory here so the effective number of quark flavours is zero.

unfortunately, the RHS of equation (2.67) will not be zero but instead $\mathcal{O}(a^n)$, for some power n, reflecting the presence of discretisation errors in the lattice action. These scaling violating terms are known as lattice artifacts. The size of the lattice artifacts not only depends on the discretisation of the action, but also on the actual quantity being measured on the lattice. So, in practice, scaling is only achieved up to the presence of these lattice artifacts. Hence to accurately extract continuum (renormalised) observables from lattice calculations requires the simulation to be performed at several values of the bare coupling and the results extrapolated to $a \to 0$. Care must also be taken to to set the scale from a quantity which is relatively insensitive to lattice artifacts.

2.3.2 The Chiral Limit

From equation (2.37) the bare quark mass is given by

$$am_0 = \frac{1}{2}\left(\frac{1}{\kappa} - \frac{1}{\kappa_{\text{crit}}}\right) \tag{2.70}$$

where κ_{crit} is the value of the hopping parameter that corresponds to zero quark mass. In equation (2.37) $\kappa_{\text{crit}} = 1/8$. However, this is only valid for free fermions. The Wilson term breaks chiral symmetry so there is nothing special about the value $m_0 = 0$. The bare quark mass corresponding to a continuum massless fermion is shifted by the introduction of interactions and hence the value of critical hopping parameter corresponding to zero renormalised quark mass is likewise changed. It should be noted that in the continuum limit the bare coupling goes to zero and so the theory approaches that of a free theory. Hence, as the continuum limit is approached, $\kappa_{\text{crit}} \to 1/8$.

For sufficiently small a then κ_{crit} can be calculated perturbatively. However it is more common in lattice simulations to determine κ_{crit} non-perturbatively. Zero renormalised quark mass implies zero pion mass, so the procedure is to calculate the pion mass on the lattice (à la some of the techniques described earlier) and find the value of κ where it vanishes. In practice the pion mass is calculated at several values of κ_q. The PCAC relation [44] between the mass of the light pseudoscalar, P, of quark content $\bar{q}q$, and the quark mass m_q is given by $m_P^2(m_q) \propto m_q$, or on the lattice

$$m_P^2(\kappa_q) = a_P \left(\frac{1}{\kappa_q} - \frac{1}{\kappa_{\text{crit}}} \right) \tag{2.71}$$

where a_P is a constant. So, the value of κ_{crit} is determined from the intercept of $m_P^2(\kappa_q)$ versus $1/\kappa_q$.

2.3.3 Finite Volumes and Light Quarks

In order to perform simulations it is necessary to work with a lattice of finite extent. The number of lattice sites that can be fitted into this volume is restricted by the available computing power. Given an upper limit on the number of lattice sites, then choosing the lattice spacing fixes the volume and vice-versa. Clearly it is necessary to choose the lattice spacing to be in the scaling regime. However, one also wants to work with a lattice volume bigger than the size of the lightest particle in the spectrum, namely the pion. Current lattice spacings are ranged around $a^{-1} \sim 1.5$–3.5 GeV, with the number of spatial lattice points 16^3–32^3. This gives lattice spatial volumes in the range $(1.5\,\text{fm})^3$ to $(3\,\text{fm})^3$ compared to the Compton wavelength of the pion ~ 1.5fm. Hence current lattice sizes are barely bigger than the size of the pion and so finite size effects are expected to be important. On a periodic lattice the effect can be thought of as being due to the pion interacting with itself across the boundaries of the lattice. In order to suppress this effect requires the lattice to be several times bigger than the size of the pion.

One way of getting around the problem is guided by equation (2.71) above. Light κ-values are chosen which correspond to unphysically large pion masses (thus fitting more easily on the lattice) and as long as these κ-values are not so large as to violate the behaviour in equation (2.71) then the extrapolation of results to the correct u and d quark masses is straightforward. In practice the approximation $\kappa_u = \kappa_d = \kappa_{\text{crit}}$ is made. Also this approach overcomes another problem in that fermion matrix inversions with light quarks take longer to converge [42].

The light κ values used in simulations are generally around the mass of the strange quark. The actual value of κ corresponding to the strange quark mass, κ_s, is determined as follows. According to PCAC the variation of the light vector mass with quark mass is (on the lattice)

$$m_V(\kappa_1, \kappa_2) = a_V + b_V \left(\frac{1}{2\kappa_1} + \frac{1}{2\kappa_2} - \frac{1}{\kappa_{\text{crit}}} \right) \tag{2.72}$$

where a_V, b_V are constants and the vector meson consists of quarks q_1, q_2. The mass of the rho meson, m_ρ, in lattice units is $m_\rho = m_V(\kappa_{\text{crit}}, \kappa_{\text{crit}}) = a_V$. The generalisation of equation (2.71) to non-degenerate light quarks gives

$$m_P^2(\kappa_1, \kappa_2) = a_P \left(\frac{1}{2\kappa_1} + \frac{1}{2\kappa_2} - \frac{1}{\kappa_{\text{crit}}} \right) \tag{2.73}$$

and so the mass of the K meson in lattice units is given by $m_K^2 = m_P^2(\kappa_s, \kappa_{\text{crit}})$. By studying the ratio $m_K^2/m_\rho^2 = m_P^2(\kappa_1, \kappa_{\text{crit}})/m_V^2(\kappa_{\text{crit}}, \kappa_{\text{crit}})$ and finding the value of κ_1 that gives this ratio as its experimental value determines κ_s. It should be noted that simulations show that these PCAC relations are in fact valid up to the strange quark mass [45, 46].

Finally, similar to the elimination of lattice artifacts, the only consistent way to remove finite volume errors is to perform simulations at a fixed lattice spacing and for different volumes and extrapolate the results to the infinite volume limit.

2.3.4 Matching Continuum and Lattice Operators

In the OPE long and short distance behaviour is separated into operators, $\mathcal{O}_i(\mu)$, matrix elements of which need to be determined non-perturbatively, and perturbative coefficient functions $C_i(\mu)$. The product $C_i(\mu)\mathcal{O}_i(\mu)$ must be both scale and scheme independent. So, in principle, if matrix elements are to be measured on the lattice, the OPE and RG should also be performed on the lattice. However this is inconvenient in practice. Firstly, performing the OPE on an electroweak process with a regulator that breaks chiral symmetry is problematic. Secondly, lattice Feynman rules are more complicated than their continuum counterparts.

It is much more convenient to perform the OPE and RG in a continuum scheme such as the $\overline{MS}$ scheme. This gives coefficient functions $C_i^{\overline{MS}}(\mu)$ and operators $\mathcal{O}_i^{\overline{MS}}(\mu)$. The problem is now to match these $\mathcal{O}_i^{\overline{MS}}(\mu)$ to the corresponding lattice $\mathcal{O}_j^{\rm latt}(a)$. This matching can be written as

$$\mathcal{O}_i^{\overline{MS}}(\mu) = \sum_j Z_{ij}(a\mu)\mathcal{O}_j^{\rm latt}(a)\,. \tag{2.74}$$

It is important to note that Z_{ij} does not have to be diagonal – extra operators can come into this matching step. This is because of the different symmetries in the two schemes. In particular consider the case of the four-fermion operator O_{LL}. On the lattice, because of the Wilson term, there is nothing preventing such a purely left-handed operator from mixing with operators of different chiralities. The presence of the Wilson term also means that the axial current on the lattice receives a non-trivial renormalisation. As noted in the last chapter, in the continuum the axial current is partially conserved and hence receives no renormalisation. This no longer holds on the lattice with the Wilson term.

The difference between the two schemes lies in the ultraviolet behaviour of the operators and hence one expects to be able to perform the matching perturbatively. For convenience consider a simple quark bilinear operator $\mathcal{O} = \bar{\psi}\Gamma\psi$. The one-loop matrix element of this operator between external free quark states in the two schemes is easily calculable as

$$\begin{aligned}
\langle\psi|\,\mathcal{O}^{\rm latt}(a)\,|\psi\rangle &= A\left(1 + \frac{g_0^2(a)}{16\pi^2}\left(-\gamma\ln a^2p^2 + c_{\rm latt}\right)\right) && (2.75)\\
\langle\psi|\,\mathcal{O}^{\overline{MS}}(a)\,|\psi\rangle &= A\left(1 + \frac{g_{\overline{MS}}^2(\mu)}{16\pi^2}\left(-\gamma\ln p^2/\mu^2 + c_{\overline{MS}}\right)\right) && (2.76)
\end{aligned}$$

where p is some infrared cutoff and γ is the one-loop anomalous dimension of the operator. The c's are constants that depend on the actual operator being considered. So the matching factor to one-loop can be written as

$$Z(a\mu) = \frac{\langle\psi|\,\mathcal{O}^{\overline{MS}}(a)\,|\psi\rangle}{\langle\psi|\,\mathcal{O}^{\rm latt}(a)\,|\psi\rangle} = 1 + \frac{g^2}{16\pi^2}\left(-\gamma\ln\frac{a^{-2}}{\mu^2} + c_{\overline{MS}} - c_{\rm latt}\right) \tag{2.77}$$

since the matching is independent of the external states. An ambiguity arises as to what coupling to use in the final expression.

The two couplings actually differ considerably. The correspondence between the couplings in the two schemes can be computed similarly to above giving ($n_f = 0$)

$$g^2_{\overline{MS}}(\mu) = g_0^2(a)\left(1 - \beta_0\frac{g_0^2}{16\pi^2}\left(\ln\frac{a^{-2}}{\mu^2} - \ln C^2\right)\right) \tag{2.78}$$

to one-loop and where one can make the identification $C = \Lambda_{\overline{MS}}/\Lambda_{\rm latt}$. Numerically $\ln C^2 = 6.7217$ and hence

$$\Lambda_{\overline{MS}} = 28.81\Lambda_{\rm latt}\,. \tag{2.79}$$

Thus the perturbative expansions of a high energy process in the lattice and $\overline{MS}$ schemes are expected to differ considerably at the same scales.

Most perturbative expansions in the $\overline{MS}$ scheme converge quite well. The same cannot be said of the bare lattice scheme where large corrections at second order can contribute. Lepage and Mackenzie [47] suggest a way of improving the convergence of lattice perturbation series by instead using a "boosted" coupling,

$$\tilde{g}^2 = g_0^2/u_0^4 \tag{2.80}$$

where u_0 is a measure of the average link variable. This procedure sums the large contributions from "tadpole diagrams" to the bare perturbation theory. These diagrams are predominantly responsible for the large value of the ratio $\Lambda_{\overline{MS}}/\Lambda_{\rm latt}$. u_0 can be measured as

$$u_0 = \langle\frac{1}{3}\mathsf{Tr}P^{\Box}\rangle^{1/4}\,. \tag{2.81}$$

For the action with just the Wilson term this procedure can be thought of as simply rescaling the gauge fields $U_\mu \to U_\mu/u_0$ and compensating for this by rescaling the bare coupling as above and the hopping parameters to $\tilde{\kappa} = \kappa u_0$. With this improved perturbation theory the critical hopping parameter is expected to be close to its continuum value, $\tilde{\kappa}_{\rm crit} \approx 1/8$. Hence an estimate $u_0 = 1/(8\kappa_{\rm crit})$ is often used instead of the measure above [47]. This is used in this work.

The matching between lattice and continuum operators is further complicated in this work in that a matching step between full QCD and HQET is also necessary. The actual matching factors used for the axial current and O_{LL} are given at the appropriate junctures in chapters 3 and 4.

2.4 Heavy Quarks on the Lattice

The mass of the b quark is $m_b \sim 5$ GeV. Current lattice spacings lie in the range $a^{-1} = 1.5$–3.5 GeV and so $m_b a > 1$ on these lattices. Hence the simulation of a b quark on current lattices using Wilson fermions, or even SW-clover fermions, will be plagued by large lattice artifacts. Several ways around this have been suggested.

2.4.1 Static Quarks on the Lattice

Eichten [21] first proposed simulating the leading order HQET on the lattice, in particular where the heavy quark is treated in its rest frame – the static approximation. The advantage of using this approach is that the large $m_b a$ effects are bypassed since the "dynamical" degrees of freedom of the heavy quark have been explicitly integrated out of the problem. Following equation (1.51), the static propagator on the lattice is given by

$$G_{(b)}(\vec{x}, t_x; \vec{0}, 0) = \left[\mathrm{e}^{-m_b t_x} \frac{1+\gamma_4}{2} \Theta(t_x) + \mathrm{e}^{m_b t_x} \frac{1-\gamma_4}{2} \Theta(-t_x) \right] P_{\vec{0}}(t_x, 0) \delta^3(\vec{x}) \tag{2.82}$$

where

$$\begin{aligned} P_{\vec{0}}(t_x, 0) &= U_4^\dagger(\vec{0}, t_x - 1) U_4^\dagger(\vec{0}, t_x - 2) \cdots U_4^\dagger(\vec{0}, 0) \qquad t_x > 0 && (2.83) \\ &= U_4(\vec{0}, t_x) U_4(\vec{0}, t_x + 1) \cdots U_4(\vec{0}, -1) \qquad t_x < 0\,. && (2.84) \end{aligned}$$

So for a given gauge configuration the static propagator is easy to compute – no computationally intensive fermion matrix inversions are required. Note that this propagator satisfies the usual hermiticity relation $G(0,x) = \gamma_5 G^\dagger(x,0)\gamma_5$.

Most of the important points about using this approach can be best explained in the context of the calculation of the two point correlator,

$$C^{\mathrm{LL}}(t) = \sum_{\vec{x}} \langle 0|\, A_4^L(\vec{x},t) A_4^{L\,\dagger}(\vec{0},0)\,|0\rangle \xrightarrow{t\gg 0} \frac{f_B^2 M_B^2}{2M_B} \mathrm{e}^{-\mathcal{E}t} \tag{2.85}$$

where the local static-light axial current is

$$A_4^L(\vec{x},t) = b^\dagger(\vec{x},t)\gamma_4\gamma_5 q(\vec{x},t)\,. \tag{2.86}$$

The first point is that static quark and static antiquark fields are distinct. The static quark field b annihilates a quark but does not create an antiquark. Similarly $b^\dagger$ in the above expression creates a quark but does not annihilate an antiquark. One must be careful that one uses the correct fields in operators. For example, the interpolating operator for the B meson with a static quark constituent is $\chi_B^\dagger = \bar{q}\gamma_5 \tilde{b}^\dagger$ where $\tilde{b}^\dagger$ creates an antiquark – the corresponding field $\tilde{b}$ annihilates an antiquark. Only Wick contractions of b with $b^\dagger$, or $\tilde{b}$ with $\tilde{b}^\dagger$, can be performed. This is of particular importance in the three-point function for B^0-$\bar{B}^0$ mixing – see appendix B.

Secondly, the static quark propagator has discretisation errors $\mathcal{O}(a^2)$. So, to obtain $\mathcal{O}(a)$ improved matrix elements of static-light bilinears only the light quark field needs to be improved à la Sheikholeslami and Wohlert. In other words only rotation of the light quark fields in the bilinear is required,

$$b^\dagger\,\Gamma\, q \longrightarrow b^\dagger\,\Gamma\,\left(1 - \frac{1}{2}\overrightarrow{\not{D}}\right)\, q\,. \tag{2.87}$$

As noted before, this rotation is absorbed at the ends of the light quark propagator.

Thirdly, the correlator falls off exponentially as $\exp(-\mathcal{E}t)$ and not $\exp(-M_B t)$, where $\mathcal{E} = M_B - m_b$ is the binding energy of the heavy quark in the meson. $\mathcal{E}$ is not a physical observable. However its calculation is useful. In particular calculation of $\mathcal{E}$ at $\kappa_{\rm crit}$ and κ_s, $\mathcal{E}_d$ and $\mathcal{E}_s$ respectively, allows an estimate of the mass splitting

$$M_{B_s} - M_{B_d} = \mathcal{E}_d - \mathcal{E}_s \tag{2.88}$$

to be extracted. Results for this are presented in the next chapter.

Fourthly, I have deliberately specified the calculation of the two-point function with both operators local. This is to illustrate the need for smearing in static-light systems. Figure 2.1 is an effective mass plot for the case where both operators are local, with figure 2.2 the corresponding plot where the operator at the source is smeared with a cubic smearing function in the Coulomb gauge. The details of the simulation from which these results are extracted are given in the next chapter. These plots illustrate two things. Firstly, the LL effective mass plot exhibits no plateau. Secondly smearing with a relatively primitive guess for the smearing function (a cube) drastically improves the situation. Also it can be seen that

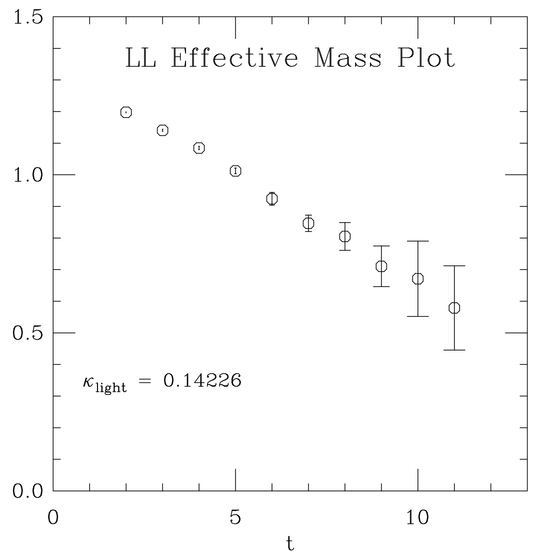

Figure 2.1: Effective mass plot, $\ln[C(t)/C(t+1)]$, for LL correlator at light $\kappa = 0.14226$ on 60 quenched configurations at $\beta = 6.2$.

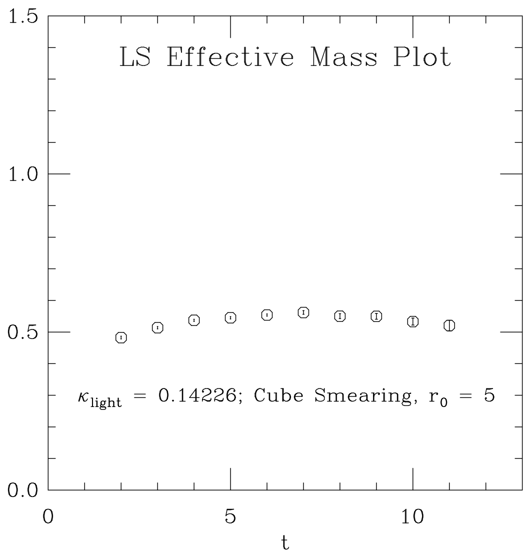

Figure 2.2: Effective mass plot, $\ln[C(t)/C(t+1)]$, for LS correlator at light $\kappa = 0.14226$ on 60 quenched configurations at $\beta = 6.2$, using cubic smearing function at the source of size $r_0 = 5$.

the signal from the LL correlator rapidly descends into noise. This is a generic problem with static-light correlators which even smearing cannot overcome – the signal-to-noise ratio decreases exponentially with time [48, 49].

Finally, what is (in principle) extracted from the calculation of this two-point function is the quantity $f_P\sqrt{M_P}$ in the limit $M_P \to \infty$, where P is a generic heavy-light meson. As discussed in chapter 1, HQET predicts that this quantity should obey the scaling law $f_P\sqrt{M_P} = \mathsf{constant}$, up to mild logarithmic corrections. If this scaling law is obeyed then this calculation in the static approximation gives f_B. Unfortunately, lattice simulations show that this scaling law is badly violated by $1/M_P$ corrections [50, 51], $\sim 10\%$ for the B meson and $\sim 30\%$ for the D meson. The scaling behaviour can be generalised to include these corrections,

$$f_P\sqrt{M_P} = A + \frac{B}{M_P} + \frac{C}{M_P^2} + \mathcal{O}(\frac{1}{M_P^3}) . \tag{2.89}$$

Simulations in the static approximation allow the extraction of the parameter A in this relation. The corrections cannot be perturbatively calculated, so lattice simulations using other approaches are needed to determine them. Before briefly discussing these other approaches, it should be noted that $1/M_P$ corrections are not expected to be as important in ratios such as f_{B_s}/f_{B_d} and B_B.

2.4.2 Other Approaches

Although Wilson or SW-clover fermions cannot be used to simulate the b quark on current lattices, they can be used to simulate heavy quarks up to the mass of the c quark, $m_c \sim 1.5$GeV. This is about the limit of the applicability of these actions to heavy quark simulations. In particular Wilson fermions already have severe lattice artifacts for $m_c a \sim 1/2$. A rescaling of the Wilson quark field as $\sqrt{1-6\tilde{\kappa}}$ as distinct from the standard normalisation $\sqrt{2\kappa}$ can account for a large part of these $m_c a$ corrections [52, 53, 50]. However, to properly reduce these lattice artifacts it is preferable to use a systematically improved lattice fermion action, such as the SW-clover action.

Simulating heavy quarks around the c quark mass allows the extraction of f_D and hence allows the corrections to the scaling behaviour to be estimated. In practice one simulates at several values of the heavy quark mass and plots $f_P\sqrt{M_P}$ versus $1/M_P$. A fit to this behaviour, using some functional form[5] as in equation (2.89), and including the static point ($1/M_P = 0$), can then allow an estimate of f_B to be extracted. In these fits it is also important to show that fitting with and without the static point included gives consistent results. This is not always clear, due to both uncertainties in the static point and also $m_Q a$ effects in the "propagating" results.

Another approach to the b quark on the lattice is to use Non-Relativistic QCD (NRQCD). The motivation behind NRQCD is essentially the same as HQET. For $m_Q \gg \Lambda_{QCD}$, then in its couplings to low-momentum gluons the heavy quark can be treated non-relativistically. As in HQET, the effect of high-momentum gluons

[5]... including the logarithmic corrections also.

can be included perturbatively. The lowest order NRQCD Lagrangian is

$$\mathcal{L}_{\mathrm{NRQCD}} = \psi^\dagger \left(D_t + \frac{1}{2m_Q}\vec{D}^2 + c_1(g^2)\frac{g}{2m_Q}\vec{\sigma}\cdot\vec{B} + \mathcal{O}(\frac{1}{m_Q^2}) + \dots \right)\psi \tag{2.90}$$

where ψ is a two-component field. The coefficient c_1 is obtained by perturbative matching with QCD. As in the discussion of HQET in the last chapter one has integrated out the "heavy" degrees of freedom to arrive at an effective theory. The matching to the full theory is performed at m_Q and the theory is only valid for scales $\mu < m_Q$. This is ideal for the b quark on the lattice where $m_b > a^{-1}$. Like the static approximation, this does not lead to discretisation errors $\mathcal{O}(m_Q a)$ but rather $\mathcal{O}(pa)$ where p is a typical value for the residual momentum of the heavy quark, $p \sim \Lambda_{QCD}$. Note that for $m_Q \to \infty$ the static limit is retrieved. NRQCD is well established in simulations of $\bar{b}b$ systems [54, 55] and has only recently been applied to simulations of the B meson system [56, 57, 58].

So, combining results from all these methods should eventually allow f_B, and other results in B-physics, to be accurately extracted. In the rest of this work I deal only with the simulations in the static theory.

Chapter 3

Calculation of f_B in the Static Limit

In this chapter the results of a calculation of f_B^{static} are presented. Results in the static approximation for the mass splitting, $M_{B_s} - M_{B_d}$, and the ratio, f_{B_s}/f_{B_d}, are also presented. A major aspect of the calculation is the study of a wide variety of smearing techniques in order to optimise the overlap of interpolating operators with the ground state of the B meson. In the first two sections I outline the details of the simulation and the smearing used and in the remaining section I present and discuss the results.

3.1 Simulation Details

The calculation was performed on 60 $SU(3)$ gauge configurations generated in the quenched approximation on a lattice of size $24^3 \times 48$ at $\beta = 6.2$. The configurations were generated using the hybrid over-relaxed algorithm as described in [59]. The heavy quark propagator was treated in the static approximation, equation (2.82), with the light quark described by the SW-clover action, equation (2.29). $\mathcal{O}(a)$ improvement of static-light matrix elements was ensured by rotating the ends of the light quark propagator, equation (2.61). Light quark propagators were calculated at three κ-values, κ = 0.14144, 0.14226 and 0.14262, using an over-relaxed minimal residual algorithm [42]. On this configuration set the value of κ corresponding to the strange quark mass was determined as $\kappa_s = 0.1419(1)$ with $\kappa_{\text{crit}} = 0.14315(2)$ [45].

The heavy-light leptonic decay constant in the static approximation is determined via

$$f_B^{\rm static} = \sqrt{\frac{2}{M_B}}\, Z_A\, Z_L\, a^{-3/2} \tag{3.1}$$

where M_B is the experimental value of the mass of the B meson, a is the lattice spacing, Z_A the perturbative matching coefficient between the axial current in the lattice static theory and the continuum full theory, and where the matrix element

$$Z_L = \langle 0|A_\mu^L(0)|B_0\rangle \tag{3.2}$$

must be extracted from the lattice simulation.

3.1.1 The Lattice Spacing

Several quantities can be used to determine the lattice spacing, a, corresponding to $\beta = 6.2$. Table 3.1 shows various estimates for a^{-1} from the calculation of mass of the ρ meson, m_ρ, the pion decay constant, f_π, the string tension, $\sqrt{K}$, and the related hadronic observable R_0 [60]. The numbers from [45] are based on a study on the 60 configurations used in this work. The results from [61] are based on a more recent study on a larger set of 101 configurations. Finally, the result from f_π is changed from that in [45] by instead using a non-perturbative estimate of the matching coefficient for the axial current from [62]. Most of the

	a^{-1} GeV	Ref.
m_ρ	$2.7\ ^{+1}_{-1}$	[45]
$\sqrt{K}$	$2.77\ ^{+4}_{-6}$	[61]
f_π	$3.1\ ^{+2}_{-1}$	[45, 62]
R_0	$2.95\ ^{+7}_{-11}$	[61]

Table 3.1: Determinations of the lattice spacing at $\beta = 6.2$ by the UKQCD collaboration.

published work to date using this configuration set has used $a^{-1} = 2.7(1)$ GeV as set from m_ρ [45]. However, in this work, to be consistent with [63] and taking account of the more recent estimates of a^{-1}, a value $a^{-1} = 2.9(2)$ GeV is used. This encompasses the spread of values quoted in the above table.

3.1.2 The Matching Coefficient

In order to extract a physical value for f_B from the lattice calculation, the axial current in the lattice static theory must be matched to the axial current in the full continuum theory (which is protected from renormalisation) at the scale a^{-1}. This is done in two stages. First the matching between the lattice static theory and the continuum static theory is calculated, and then this is combined with the matching between the continuum static theory and the continuum full theory. This two-stage matching process was first presented in [64, 65] for Wilson fermions, and later in [66, 67] for SW-clover fermions, in all cases only to one-loop order. The matching coefficient with the light quark treated by the SW-clover action is [66]

$$Z_A = 1 + \frac{\alpha_{\overline{MS}}(a^{-1})}{4\pi}\left[2\ln(a^2 m_b^2) - \frac{8}{3}\right] - 15.02\,\frac{\alpha_{\rm latt}(a^{-1})}{3\pi} \tag{3.3}$$

at the scale a^{-1}. The first term arises from matching the continuum full and static theories at m_b, as described in chapter 1 (equation (1.69)), with the second term coming from matching the lattice and continuum static theories.

In order to evaluate this numerically the one-loop expression

$$\alpha_{\overline{MS}}(a^{-1}) = \frac{2\pi}{\beta_0 \ln(a^{-1}/\Lambda_{\overline{MS}})} \tag{3.4}$$

is used, with $\beta_0 = 11 - \frac{2}{3}n_f$. At the scale $a^{-1} = 2.9$ GeV the number of active quark flavours is $n_f = 4$ and $\Lambda_{\overline{MS}} = 250$ MeV is an appropriate value to use. A "boosted" lattice coupling is used,

$$\alpha_{\rm latt}(a^{-1}) = \frac{6}{4\pi\beta u_0^4} \tag{3.5}$$

with $u_0 = 1/(8\kappa_{\rm crit})$ chosen as a measure of the average link variable. Using these expressions and a value $m_b = 5$ GeV then the matching coefficient is determined as

$$Z_A = 0.78\,. \tag{3.6}$$

The major contribution to this result comes from matching the lattice static theory to the continuum static theory. It should be noted that the actual number of active quark flavours is used, $n_f = 4$, although the simulations are performed in the quenched approximation. At any rate, changing n_f has little effect on the numerical value of Z_A. Also, if instead $\Lambda_{\overline{MS}} = 200$ MeV at $n_f = 4$ is used the value of Z_A changes only in the third decimal place. The error in Z_A due to the error in the scale is of a similar order. Finally, if instead $u_0 = 0.88506$ [68] from the average plaquette is used in the boosted lattice coupling the value gets shifted to $Z_A = 0.79$.

3.1.3 Calculating Z_L

As illustrated in the last chapter, correlation functions of static-light bilinears need at least one of the bilinears to be smeared if asymptotics are to be reached. Defining operators

$$A_4^L(\vec{x},t) = b^\dagger(\vec{x},t)\gamma_4\gamma_5 q(\vec{x},t) \tag{3.7}$$

$$A_4^S(\vec{x},t) = \sum_{\vec{y}} b^\dagger(\vec{y},t) f(\vec{y},\vec{x})\gamma_4\gamma_5 q(\vec{x},t) \tag{3.8}$$

then the following correlators

$$\begin{aligned} C^{\rm SS}(t) &= \sum_{\vec{x}} \langle 0|A_4^S(\vec{x},t) A_4^{\dagger S}(\vec{0},0)|0\rangle \stackrel{t\gg 0}{\longrightarrow} (Z_S)^2\, \mathrm{e}^{-\mathcal{E}\,t}, \\ C^{\rm LS}(t) &= \sum_{\vec{x}} \langle 0|A_4^L(\vec{x},t) A_4^{\dagger S}(\vec{0},0)|0\rangle \stackrel{t\gg 0}{\longrightarrow} Z_S Z_L\, \mathrm{e}^{-\mathcal{E}\,t}, \\ C^{\rm SL}(t) &= \sum_{\vec{x}} \langle 0|A_4^S(\vec{x},t) A_4^{\dagger L}(\vec{0},0)|0\rangle \stackrel{t\gg 0}{\longrightarrow} Z_S Z_L\, \mathrm{e}^{-\mathcal{E}\,t}, \end{aligned} \tag{3.9}$$

were calculated for various ground state smearing functions, $f(\vec{y},\vec{x})$, with Z_L as in equation (3.2) and Z_S analogously defined. The aim is the extraction of Z_L from the asymptotic behaviour of these correlators. The different smearing methods used to achieve this and the various fitting methods used to extract Z_L are described further on.

In order to enhance the signal in the correlators, time-reversal symmetry can be exploited. In extracting the asymptotic behaviour the "folded" correlators

$$C^{\text{folded}}(t) = \frac{1}{2}\left[C(t) + C(T-t)\right] \tag{3.10}$$

are used. Finally, because of the limits of time and computational facilities, only correlators on the timeslices $2 \leq t \leq 12$ and $36 \leq t \leq 46$ were calculated. At any rate the results presented later suggest that outside these ranges the signal-to-noise ratio becomes prohibitively small on the configuration sample available for the study.

3.2 Smearing Details

3.2.1 Implementing Smearing

The SS two-point correlator above is the configuration average of the quantity

$$\sum_{\vec{x}} \left\{ \mathsf{Tr} \left[G^{(b)}{}_{SS}(\vec{0},0;\vec{x},t)\gamma_4\gamma_5 G^{(q)}(\vec{x},t;\vec{0},0)\gamma_4\gamma_5 \right] \right\} \tag{3.11}$$

where the smearing of the operators has been absorbed into a smeared propagator

$$G^{(b)}{}_{SS}(\vec{0},0;\vec{x},t) = \sum_{\vec{y},\vec{z}} f_2(\vec{0},\vec{y})\, G^{(b)}(\vec{y},0;\vec{z},t)\, f_1(\vec{z},\vec{x}) \tag{3.12}$$

for smearing functions f_1 and f_2 at the sink and source respectively. In principle the smearing could equally well have been absorbed by smearing the heavy propagator at one end and the light quark propagator at the other, or vice versa. Similarly just smearing the light quark propagator at both ends should be equivalent. However, in practice, the way the smearing is applied is important. For static-light systems it is always better to absorb the smearing in the static quark propagator.

Inserting the form of the static propagator in the above gives $(t > 0)$

$$G^{(b)}{}_{SS}(\vec{0},0;\vec{x},t) = \mathrm{e}^{-m_b|t|}\frac{1-\gamma_4}{2}P^{SS}_{\vec{x}}(0,t) \tag{3.13}$$

where

$$\begin{aligned}
P^{SS}_{\vec{x}}(0,t) &= \sum_{\vec{y},\vec{z}} f_2(\vec{0},\vec{y}) P_{\vec{y}}(0,t) \delta^3(\vec{y}-\vec{z}) f_1(\vec{z},\vec{x}) \\
&= \sum_{\vec{y}} f_2(\vec{0},\vec{y}) P_{\vec{y}}(0,t) f_1(\vec{y},\vec{x}) \qquad (3.14)
\end{aligned}$$

is the equivalent smeared Wilson line. This illustrates several things. Firstly, just smearing at the sink, $f_2(\vec{0},\vec{y}) = \delta^3(\vec{y})$, then only the Wilson line $P_{\vec{0}}(0,t)$ contributes to P^{SL}. However, smearing at the source only, $f_1(\vec{z},\vec{x}) = \delta^3(\vec{z}-\vec{x})$, then the Wilson lines for all $\vec{y}$, $P_{\vec{y}}(0,t)$, contribute to P^{LS}. Hence LS correlators are expected to be less noisy than SL correlators, though formally the two correlators should give the same results. The data confirms this – see figure 3.1. Hence only LS correlators are used in the extraction of Z_L. The second point is related to this. Smearing only the light quark propagators again results in only the single Wilson line $P_{\vec{0}}(0,t)$ contributing to correlation functions. Again these will be noisier than correlators where all the Wilson lines contribute.

In summary, the Wilson lines, $P_{\vec{y}}(t,0)$, on a given gauge configuration are calculated, from which smeared Wilson lines (SL, LS and SS) as in equation (3.14) are constructed using various smearing functions which are described in the following sections. On each configuration the quantity in equation (3.11) is calculated using these smeared static propagators, and averaging over configurations finally gives the correlation functions of equation (3.9).

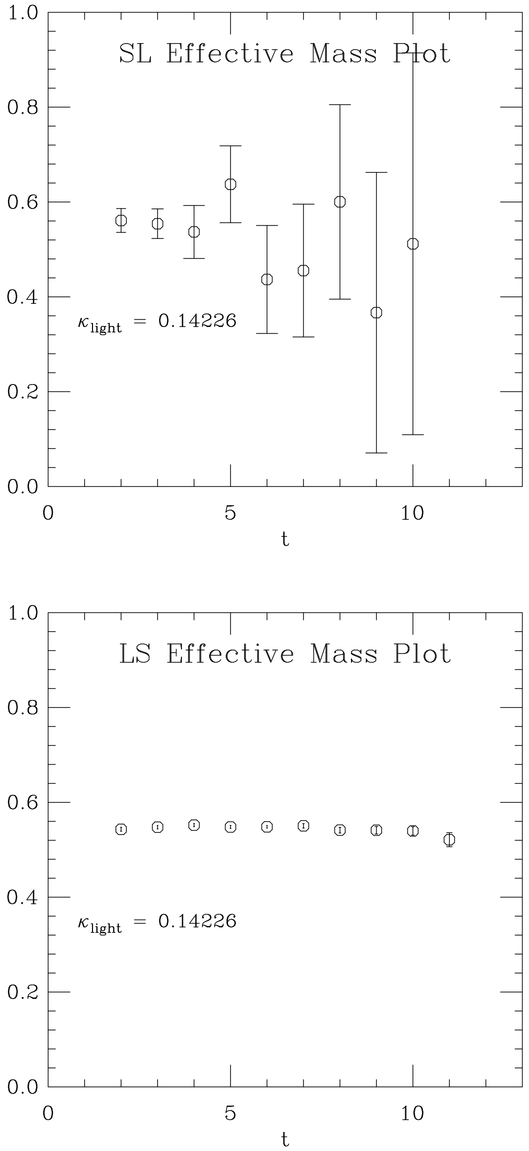

Figure 3.1: Effective mass plots, $\ln[C(t)/C(t+1)]$, for LS and SL correlators at light $\kappa = 0.14226$ on 60 quenched configurations at $\beta = 6.2$, using exponential smearing function of size $r_0 = 5$.

3.2.2 Gauge Invariant Smearing

The idea is to construct a smearing function $f(\vec{x},\vec{y})$ which models the shape and size of the ground state wave function of the B meson. One suggestion for doing this in an explicitly gauge covariant way is to use the 3D scalar propagator as the smearing function [69]. The motivation behind this is that the free field continuum scalar propagator behaves $\sim \exp(-|\vec{x}-\vec{y}|/r_0)$ for some size r_0. It is expected that such a hydrogen-like wavefunction should give a good overlap with the ground state.

The 3D scalar propagator, S, on a given timeslice can be easily calculated on the lattice from

$$\sum_{\vec{x}} K(\vec{x},\vec{y})S(\vec{y},\vec{z}) = \delta_{\vec{x},\vec{z}}, \tag{3.15}$$

where

$$\begin{aligned} K(\vec{x},\vec{y}) &= \delta_{\vec{x},\vec{y}} - \kappa_{\rm sc}\Delta(\vec{x},\vec{y}) \\ \Delta(\vec{x},\vec{y}) &= \sum_{i=1}^{3}\left[\delta_{\vec{y},\vec{x}-\hat{\imath}}U_i^\dagger(\vec{x}-\hat{\imath}) + \delta_{\vec{y},\vec{x}+\hat{\imath}}U_i(\vec{x})\right] \end{aligned} \tag{3.16}$$

is a discretised version of the 3D Klein-Gordon equation. The only free parameter is $\kappa_{\rm sc}$ and this can be varied to change the size of the smearing function. This is measured as the rms radius

$$r_0 = \sqrt{\frac{\sum_{\vec{x}} |\vec{x}|^2 |S(\vec{x},\vec{0})|^2}{\sum_{\vec{x}} |S(\vec{x},\vec{0})|^2}}\,. \tag{3.17}$$

Using this method to generate the smearing function is known as Wuppertal smearing.

Another approach based on this Wuppertal smearing method is to solve for S from equation (3.15) as a power series in $\kappa_{\rm sc}$, stopping at some finite power, N,

$$S(\vec{y},\vec{z}) = \sum_{n=0}^{N}\sum_{\vec{y}} \kappa_{\rm sc}^n \Delta^n(\vec{x},\vec{y})\delta_{\vec{y},\vec{z}}\,. \tag{3.18}$$

When $\kappa_{\rm sc}$ is smaller than some critical value, $\kappa_{\rm sc}^{\rm crit}$, then this power series converges. However for $\kappa_{\rm sc}$ greater than this critical value the series diverges. This gives a greater freedom in varying the smearing radius while retaining the essential shape of the smearing function. The smearing function is equation (3.18) can be generated via Jacobi iteration. That is, each term in the series is generated from the previous one by acting on it with the operator

$$e^{-4(\kappa_{\rm sc}-\kappa_{\rm sc}^{\rm crit})}\,(1+\kappa_{\rm sc}\Delta(\vec{x},\vec{y})) \tag{3.19}$$

where the exponential factor is a convenient normalisation. In order to generate a smearing function with a given r_0 then one can choose $\kappa_{\rm sc}$ such that a minimum number of iterations, N, is needed. In general the calculation of a smearing function of a given size can thus be achieved much quicker than with the Wuppertal method. In this work this Jacobi smearing [46] is used. An illustration of the shape of a Jacobi smearing function is given in figure 3.2 – this is taken from [70]. Also shown is a plot of the variation of smearing radius with N for fixed $\kappa_{\rm sc}$ on a single configuration. As can be seen the variation is roughly linear at this $\kappa_{\rm sc}$.

One technical point should be noted. The LS and SL Wilson lines are easy to generate using this method as only the scalar propagator from the spatial origin of any timeslice is required, $S(\vec{x},\vec{0})$. However, for SS Wilson lines it may appear at first glance that the scalar propagator from all spatial points to all other spatial points on the sink timeslice is needed. Fortunately this isn't the case;

$$\begin{aligned} P^{SS}_{\vec{x}}(t,0) &= \sum_{\vec{y}} S(t;\vec{x},\vec{y})P_{\vec{y}}(t,0)S(0;\vec{y},\vec{0}) \\ &= \sum_{\vec{y}} S(t;\vec{x},\vec{y})P^{LS}_{\vec{y}}(t,0) \end{aligned} \tag{3.20}$$

and so, comparing with equation (3.18), it can be seen that P^{SS} can be generated by simply using P^{LS} instead of the δ-function on the RHS of this equation. The computational cost of generating SS Wilson lines is thus much the same as for SL Wilson lines.

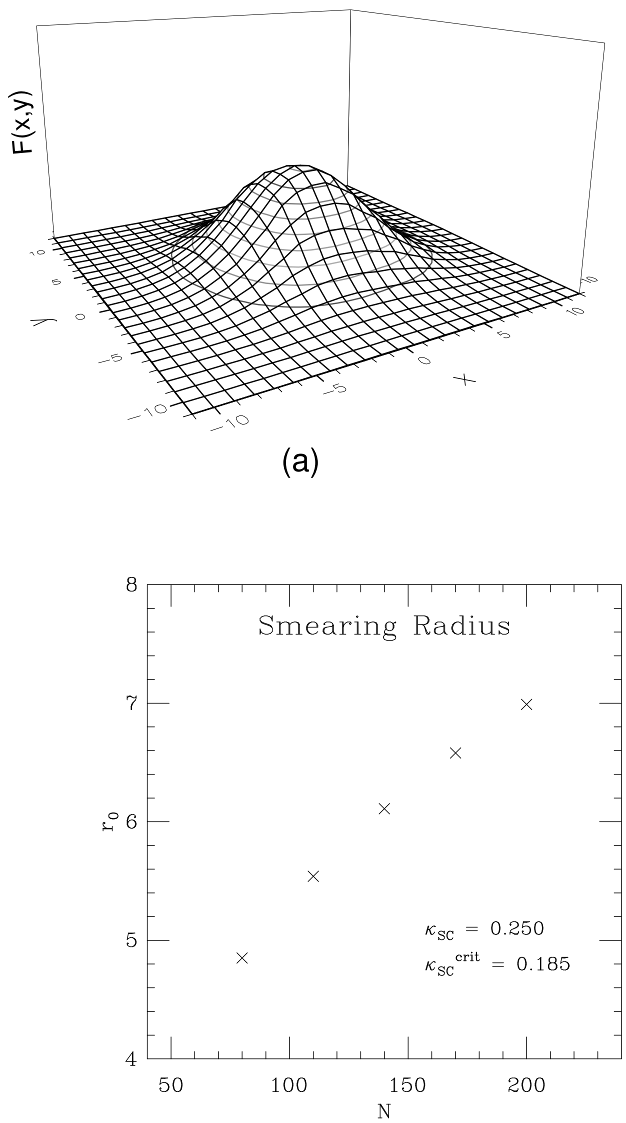

Figure 3.2: (a) The smearing functions $F(x,y) = \sqrt{|S|^2}\,\Big|_{z=0}$, normalised to unit volume, on a $24^3 \times 48$ lattice using Jacobi smearing with $N = 50$. (b) Variation of smearing radius with number of Jacobi iterations, N. Everything is measured on the source timeslice of a single configuration, with $\kappa_{\rm sc} = 0.250$ and with $\kappa_{\rm sc}^{\rm crit} = 0.185$.

3.2.3 Gauge Fixed Smearing

Another approach is to use explicit functional forms for the smearing functions. However, as noted earlier, this breaks the gauge invariance of the quark bilinears. This is not a problem if everything is done in a fixed gauge, such as the Coulomb gauge.

In the Coulomb gauge the following functions were used as ground state smearing functions :

$$\begin{aligned}
\text{Cube (CUB)}: \quad f(\vec{x},\vec{y}) &= \prod_{i=1}^{3} \Theta(r_0 - |x_i - y_i|) \\
\text{Double Cube (DCB)}: \quad f(\vec{x},\vec{y}) &= \prod_{i=1}^{3} \left(1 - \frac{|x_i - y_i|}{2r_0}\right) \Theta(2r_0 - |x_i - y_i|) \\
\text{Exponential (EXP)}: \quad f(\vec{x},\vec{y}) &= \exp\left\{-|\vec{x} - \vec{y}|/r_0\right\} . \qquad (3.21)
\end{aligned}$$

A hydrogen-like wavefunction, the exponential, is expected to give a good overlap with the ground state. The cubic smearing function was one of the first shapes to be used for smearing [71]. The original thinking was to use the simplest shape with the symmetries of the lattice, in other words a cube. Another simple shape with cubic symmetry is the double cube, a convolution of a cube with itself. This gives a pyramid-like shape.

Using explicit functional forms for the smearing functions allows the construction of functions that produce a good overlap with some higher excited state rather than just the ground state. The idea here is that one might then be able to isolate and eliminate the influence of higher excited states in correlators, thus achieving asymptotics at earlier timeslices. To this end the smearing function

$$\text{EXP2S}: \quad f(\vec{x},\vec{y}) = |\vec{x} - \vec{y}| \exp\left\{-|\vec{x} - \vec{y}|/r_0\right\} \qquad (3.22)$$

was also used. The expectation is that this should give a good overlap with the first radial excited state of the B meson.

A 2×2 matrix of SS correlators, C_{ij}, was constructed using the EXP and

EXP2S smearing functions, i.e. the four combinations of smearing at the source and sink with the two smearing functions. Each of these smearing functions induces a different overlap with the ground state and first excited state of the system. This acts as a variational basis and determining the eigenvalues and -vectors allows, in principle, the extraction of operators which have an improved overlap with the ground state. On each timeslice the eigenvalue equation

$$[C_{ij}(t) - \lambda^{\alpha}(t)]\, v_j^{(\alpha)} = 0 \tag{3.23}$$

is solved. This gives eigenvalues

$$\lambda_+(t) \quad \stackrel{t>>0}{\longrightarrow} \quad C_+ \mathrm{e}^{-\mathcal{E}} \tag{3.24}$$

$$\lambda_-(t) \quad \stackrel{t>>0}{\longrightarrow} \quad C_- \mathrm{e}^{-\mathcal{E}^*} \tag{3.25}$$

where $C_\pm$ are constants and $\mathcal{E}$ and $\mathcal{E}^*$ are the binding energies corresponding to the ground and first excited state, assuming this 2×2 variational basis is sufficient to correctly isolate the contribution of the first excited state. Hence calculating

$$\Delta E(t) = \ln \frac{\lambda_+(t)}{\lambda_-(t)} \tag{3.26}$$

allows the extraction of the splitting $\Delta E = \mathcal{E}^* - \mathcal{E}$ at sufficiently large times.

The eigenvectors can be used to construct "best" LS and SS correlators from the original EXP and EXP2S LS and SS correlators. This can be easily seen. Consider a general system with n states. In order to isolate these n states needs at least n operators, O_i, $i = 1, \ldots, n$. Using these operators the correlator matrix

$$\begin{aligned} C_{ij}(t) &= \sum_{\mathbf{x}} \langle 0|\, O_i(\vec{x}, t) O_j^\dagger(\vec{0}, 0)\, |0\rangle \\ &= Z_{in} M_n\, \mathrm{e}^{-E_n t} \delta_{nm} Z^*_{mj} \end{aligned} \tag{3.27}$$

can be constructed, for constants Z_{in} and where the E_n are the energies of the states. If each of these operators has a non-zero overlap with only a single distinct state then this correlator matrix will be diagonal. Suppose the set of operators that achieves this is $\{\tilde{O}_i\}$. This optimal set can be written in terms of the original set as

$$\tilde{O}_i = Y_{ij}\, O_j \tag{3.28}$$

and the diagonal optimal correlator matrix is

$$\begin{aligned}\tilde{C}_{ij}(t) &= Y_{ik} Z_{kn} M_n\, \mathrm{e}^{-E_n t} \delta_{nm} Y_{jp} Z^*_{mp} \\ &= Y_{ik} C_{kp}(t) Y_{jp}\,,\end{aligned} \tag{3.29}$$

or in matrix notation $\tilde{C} = Y\,C\,Y^T$. It is easy to show that for the diagonalisation of a matrix written in this form, the rows of the matrix Y correspond to the eigenvectors of C. Hence knowing the eigenvectors then the Y_{ij} and hence the optimal set of operators (smearing functions, correlators) can be reconstructed.

3.2.4 Fixing to the Coulomb Gauge

The lattice analogue of the continuum Coulomb gauge condition, $\partial_i A_i(x) = 0$, is

$$\theta(x) = \mathsf{Tr}[\Delta(x)\Delta^\dagger(x)] = 0 \tag{3.30}$$

where

$$\Delta(x) = \sum_i^3 \Big(U_i(x) + U_i^\dagger(x-i) \quad - \quad \text{h.c.} \Big)_{\text{traceless}} \tag{3.31}$$

with the index i signifying spatial components only. This gauge condition can be achieved by iteratively applying gauge transformations that increase the value of the function

$$F[U^g] = \frac{1}{N_t} \sum_{t=1}^{N_t} f[U^g](t) \tag{3.32}$$

where

$$f[U^g](t) = \frac{1}{V_s} \sum_{\vec{x}} \sum_i^3 \mathsf{Tr}[U_i^g(\vec{x},t) + U_i^{g\dagger}(\vec{x},t)]\,. \tag{3.33}$$

and where V_s is the lattice spatial volume. The gauge transformed links are

$$U_i^g(\vec{x},t) = g(\vec{x},t) U_i(\vec{x},t) g^\dagger(\vec{x}+\hat{\imath},t) \tag{3.34}$$

for a local gauge transformation g. f is the lattice equivalent of $\int d^3x A_i(x)A^i(x)$. Maximising this function is equivalent to fixing the gauge. The procedure for doing this is described in [72, 73]. At each iteration of the gauge fixing procedure the average value of θ was calculated, $\langle\theta\rangle = \sum_x \theta(x)/V$, where V is the total lattice volume. For each gauge configuration the gauge was fixed to a precision $\langle\theta\rangle \sim 10^{-4}$.

An important issue when transforming to a fixed gauge is the problem of Gribov copies [74]. The problem is that only a local maximum of the function F is needed to satisfy the gauge fixing condition, and there may be many such local maxima. So, given a set of equivalent gauge configurations, differing only by global gauge transformations, then applying a gauge fixing algorithm to each of the configurations in this set should give the same gauge fixed configuration, up to a global gauge transformation. However if F has many maxima then this may not happen. It is possible that this may add an extra "gauge noise" to gauge fixed correlators beyond the normal Monte-Carlo noise. In particular for the Coulomb gauge, different timeslices may be fixed to different Gribov copies. The study in [72] suggests that for static-light correlators calculated on a limited configuration set, such as in this work, this "gauge noise" will be much less than the statistical noise, even when the gauge is only fixed to a moderate degree of precision.

3.2.5 Choosing the Smearing Radius

Having decided what shapes to use for the smearing functions, the next issue to decide is what sizes to use for each shape. In order to do this a subsidiary study was performed on a subset of 29 of the configurations for the Coulomb gauge smearing functions using radii $r_0 = 4, 5, 6$. For the gauge invariant smearing the study was performed on 30 configurations using a single $\kappa_{\rm sc} = 0.25$ and the smearing radius was varied by changing the number of iterations of the Jacobi algorithm, N. The values $N = 80, 110, 140, 170$, and 200 were used. It should be noted that the study in [46] shows that for $\kappa_{\rm sc} \geq 0.25$ the smearing radius depends mostly on N.

The results of this study are presented in Appendix C. Based on this, for the calculation on the full set of 60 configurations, the value $r_0 = 5$ was used for all the Coulomb gauge smearing functions and $N = 140$ as the number of iterations of the Jacobi algorithm (with $\kappa_{\rm sc} = 0.25$ and $\kappa_{\rm sc}^{\rm crit} = 0.185$) for gauge invariant smearing. This corresponds to an rms radius of 6.4.

3.3 Results and Discussion

There are several ways of extracting Z_L from the correlators defined in equation (3.9) :

- **Method I :** Fit $C^{\rm SS}(t)$ to an exponential form in the asymptotic region to extract Z_S^2. Fit the ratio $C^{\rm LS}(t)/C^{\rm SS}(t)$ to a constant also in this region giving $R = Z_L/Z_S$ and so finally giving $Z_L = R \times \sqrt{Z_S^2}$.
- **Method II :** Fit $C^{\rm LS}(t)$ to an exponential in the asymptotic region to extract $Z_S Z_L$. Again fit the ratio $C^{\rm LS}(t)/C^{\rm SS}(t)$ to a constant also in this region giving $R = Z_L/Z_S$ and so finally giving $Z_L = \sqrt{R \times Z_S Z_L}$.
- **Method III :** Fit simultaneously to $C^{\rm SS}(t)$ and $C^{\rm LS}(t)$ in the asymptotic region, constraining the binding energy, $\mathcal{E}$, to be the same for both correlators. This gives Z_L directly from the fit.
- **Method IV :** Fit the ratio

$$R_{Z_L}(t_1, t_2) = \frac{C^{LS}(t_1)\, C^{LS}(t_2)}{C^{SS}(t_1 + t_2)} \longrightarrow (Z^L)^2 \qquad (3.35)$$

  to a constant which again directly gives Z_L.

This last method was used in [75]. However, in order to implement it requires a large time extent over which both $C^{\rm LS}(t)$ and $C^{\rm SS}(t)$ have a plateau. This requires good smearing and, more importantly, large statistics – the study in [75] used 220 configurations. Given the limited time extent and statistics in this study, it was not feasible to use this method to extract Z_L.

In the following, results are presented using both methods I and II. In the course of this study fits with method III were also performed, but the results proved to be very similar to those from method II for all the smearings. In other words the constrained fits always seemed to be dominated by the LS signal.

All the fits presented are taken from bootstrap fits using 250 bootstrap samples. Unless otherwise stated all the fits use a correlated χ^2 – see Appendix A. Errors on data points in the graphs come from a jackknife estimate of the covariance matrix. Finally, all the errors quoted are at the 68% confidence level.

The fit ranges for the exponential fits to the LS and SS correlators were chosen by observing where there was a plateau in the corresponding effective mass plots, shown in figures 3.3 and 3.4 respectively at a single light κ-value. As can be seen from these that CUB gives the worst plateaux in both the LS and SS correlators, whereas EXP and INV seem to give reasonably good plateaux in both. In order to choose the best fit range in some more systematic way, and also to compare the different smearing methods, the sensitivity of the binding energy extracted from the exponential fits to the fit range used, was investigated. This was done by holding the largest time in the fit range fixed and performing the fits with varying minimum time. Plots illustrating this behaviour at a single light κ-value are given in figures 3.6 and 3.7. These confirm the basic picture one can deduce from the effective mass plots, namely fits to CUB smeared correlators are not as stable as for the other smearings. Again EXP and INV give reasonable stable fits for both LS and SS correlators. DCB is slightly worse than EXP and INV, more so in the LS signal than the SS one. This general behaviour varies little among the different light κ-values.

Examples of plots of the ratio $R(t) = C^{\mathrm{SL}}(t)/C^{\mathrm{SS}}(t)$ are shown in figure 3.5. The behaviour of these plots also bears out the main points discussed in the last paragraph. Again the general behaviour of the ratio varies little across κ-values.

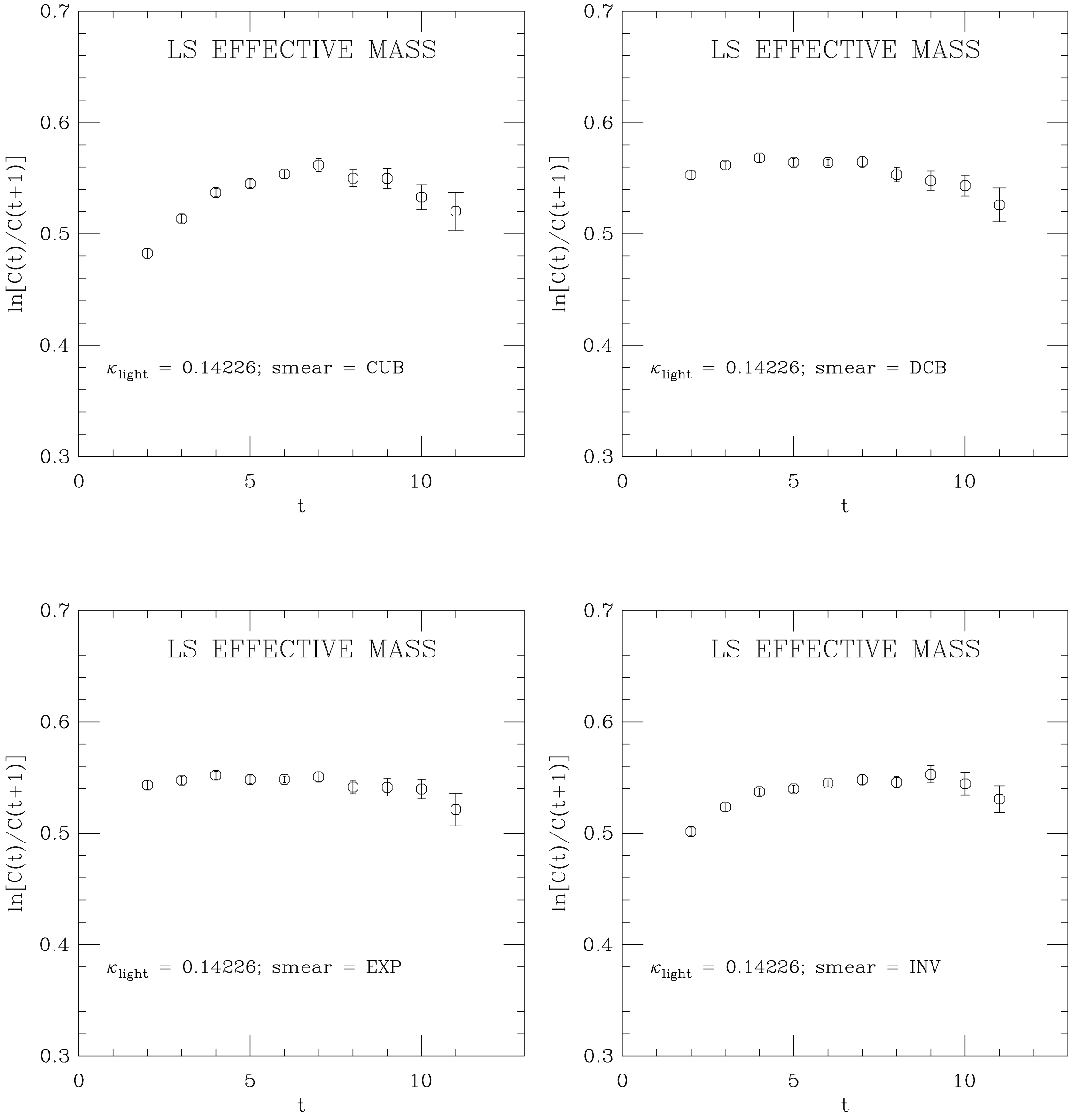

Figure 3.3: Effective mass plots, $\ln[C(t)/C(t+1)]$ versus t, for LS correlators using all four smearing types and at light $\kappa = 0.14226$.

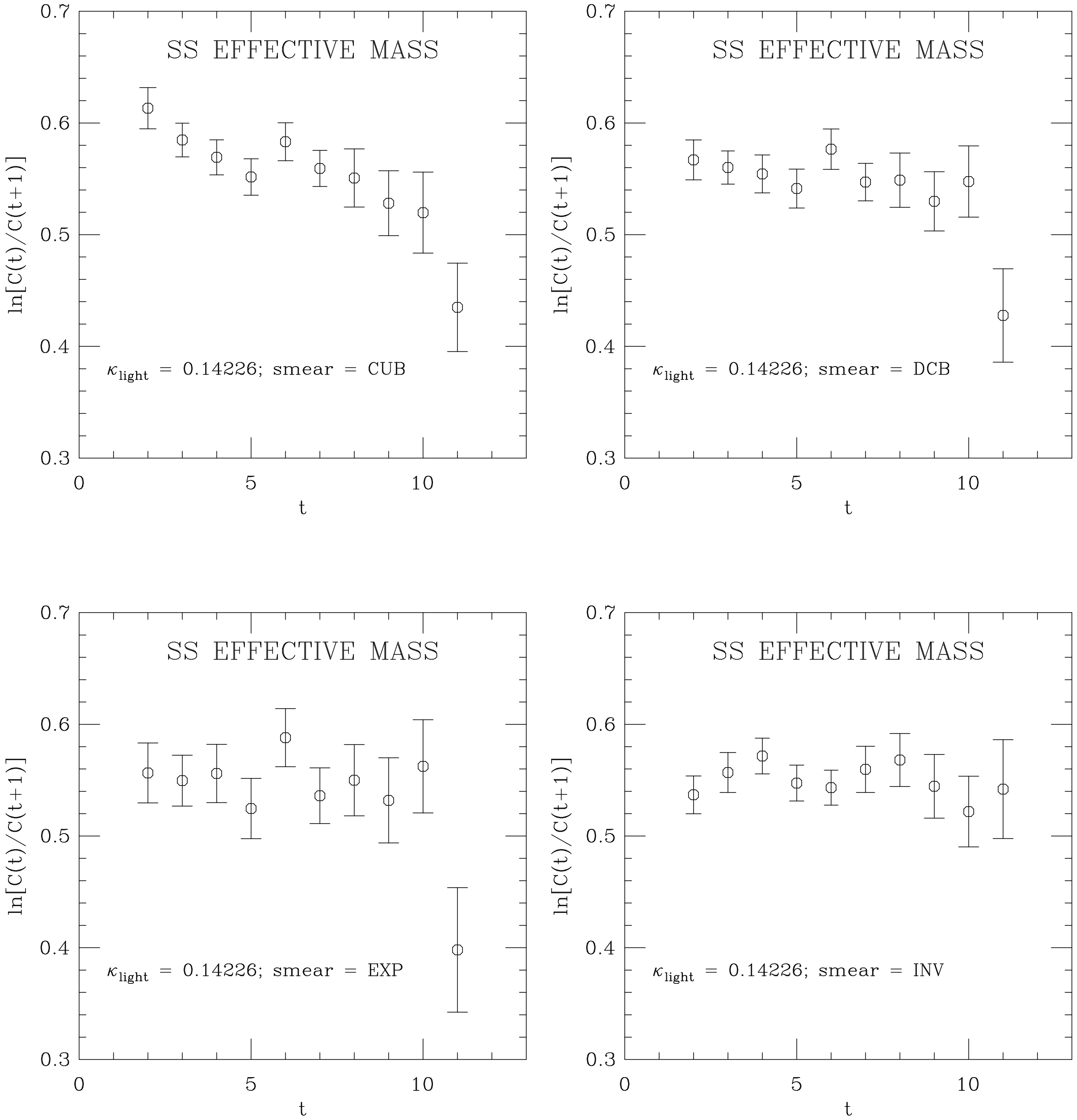

Figure 3.4: Effective mass plots, $\ln[C(t)/C(t+1)]$ versus t, for SS correlators using all four smearing types and at light $\kappa = 0.14226$.

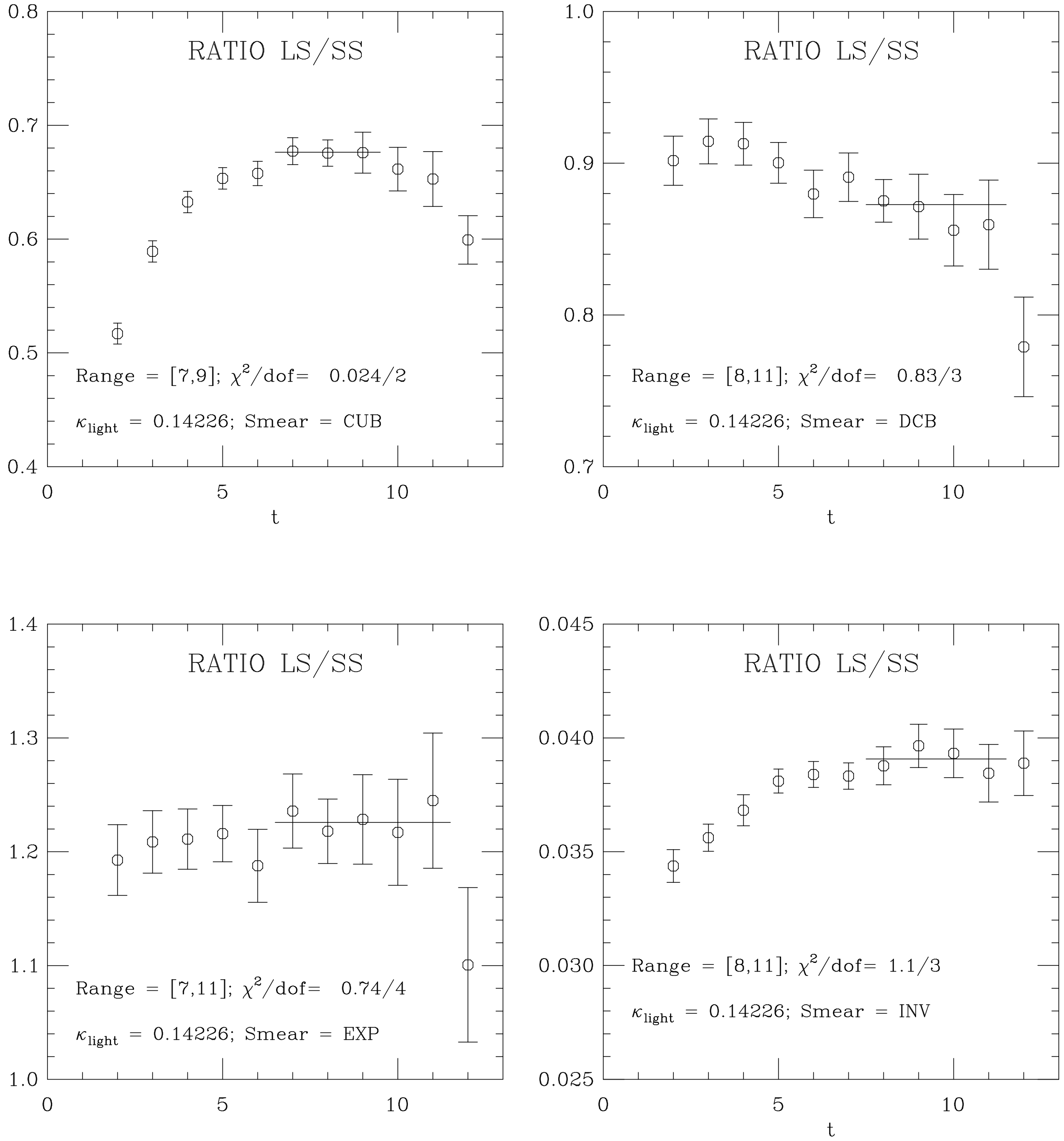

Figure 3.5: Ratio plots, $R(t) = C^{\mathrm{LS}}(t)/C^{\mathrm{SS}}(t)$ versus t, for all four smearing types and at light $\kappa = 0.14226$.

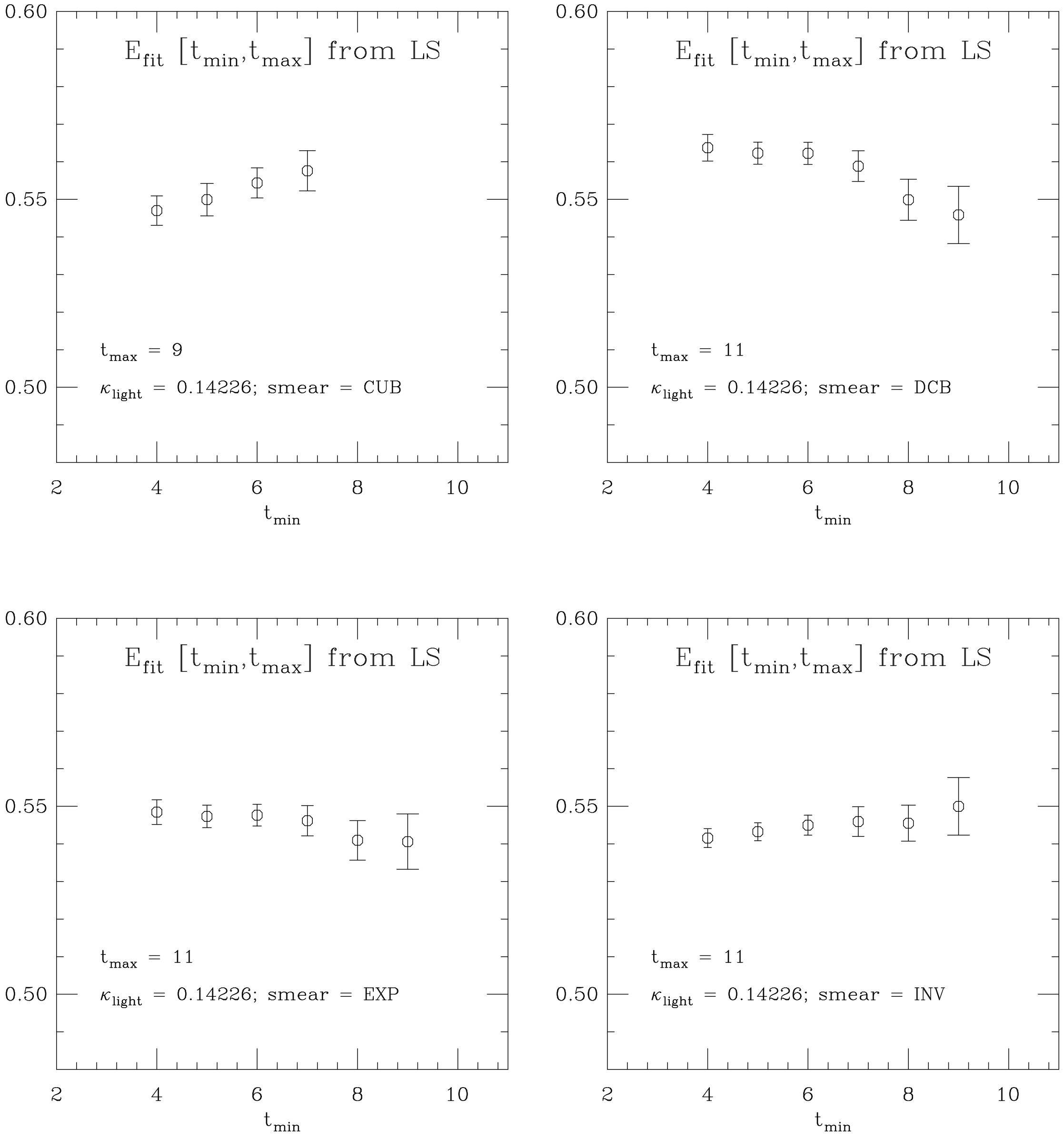

Figure 3.6: Sensitivity of the value for the binding energy, $\mathcal{E}$ coming from exponential fits to the LS correlators. The maximum time in the fit range is fixed and the variation of the fit value with the minimum time is investigated. These fits are for light $\kappa = 0.14226$.

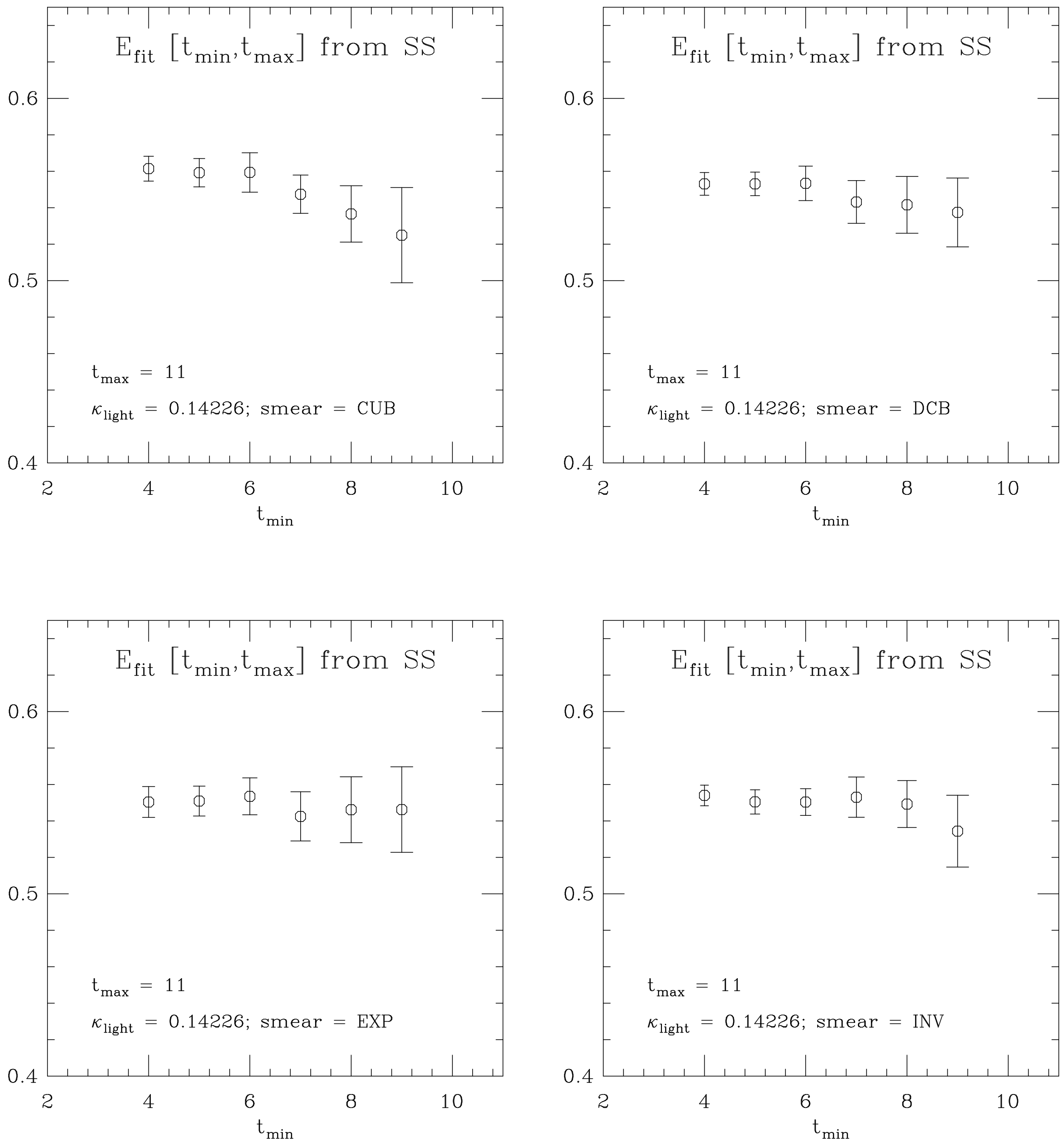

Figure 3.7: Sensitivity of the value for the binding energy, $\mathcal{E}$ coming from exponential fits to the SS correlators. The maximum time in the fit range is fixed and the variation of the fit value with the minimum time is investigated. These fits are for light $\kappa = 0.14226$.

The EXP2S smearing function was implemented with the expectation that it would have a good overlap with the first radial excited state. The LS and SS effective mass plots using just this smearing function are given in figure 3.8, as ever at just a single light κ-value. At first glance this doesn't seem to be very promising. The SS signal is very similar to the SS signal for the other smearing functions already discussed, albeit a bit noisier. The same is true of the LS signal, although it never clearly reaches a plateau.

The effective masses of the eigenvalues of the correlator matrix constructed from the EXP and EXP2S smearing functions are shown in figure 3.9 with the corresponding mass difference $\Delta E(t)$ shown in figure 3.10. These are all at a single light κ-value. So, using this smearing function does in fact result in some overlap with the first excited state. A correlator matrix was also constructed from the DCB and EXP smearing functions. As shown in figure 3.10 this leads to a similar mass difference to that when using the EXP$\times$EXP2S basis. However, this gives a noisier signal, as one might expect from using a smearing function that is not supposed to have as good an overlap with the first excited state. For both correlator matrices the computed ΔE seems to be reasonably constant with time, but the signal falls quickly into noise.

Ideally it was hoped that the eigenvectors of the correlator matrix could be used to project out a best ground state smearing function. Using the eigenvectors of the EXP2S $\times$ EXP matrix the LS and SS correlators corresponding to this "best" smearing function were computed. At a single light κ-value, the corresponding effective masses and ratio $C^{\mathrm{LS}}/C^{\mathrm{SS}}$ are shown in figure 3.11. The effective mass plots show little change from the corresponding plots for EXP smearing. More disappointing is the ratio plot which exhibits a worse plateau than for straightforward smearing with EXP.

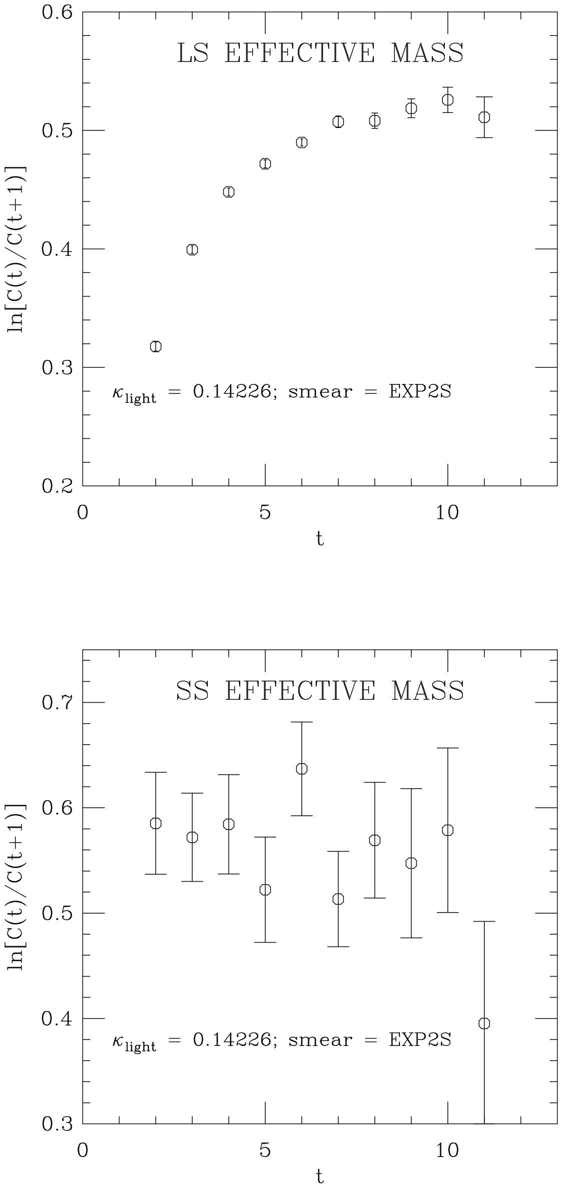

Figure 3.8: Effective mass plots for LS and SS correlators for EXP2S Smearing at light $\kappa = 014226$.

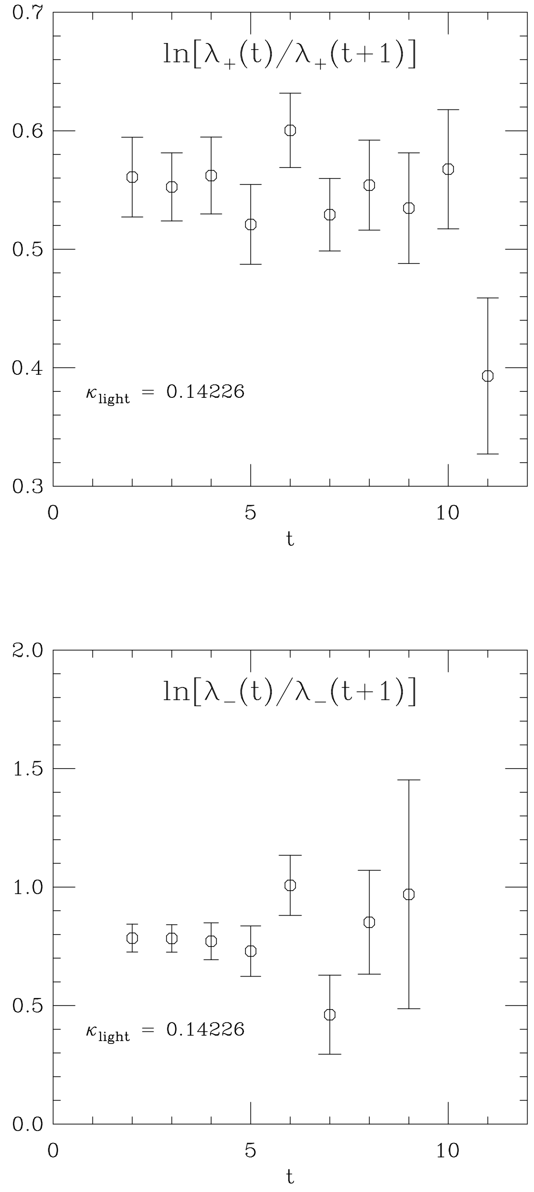

Figure 3.9: The effective masses of the eigenvalues of the 2×2 correlator matrix constructed from the EXP and EXP2S smearing functions in the Coulomb gauge. This is for light $\kappa = 0.14226$.

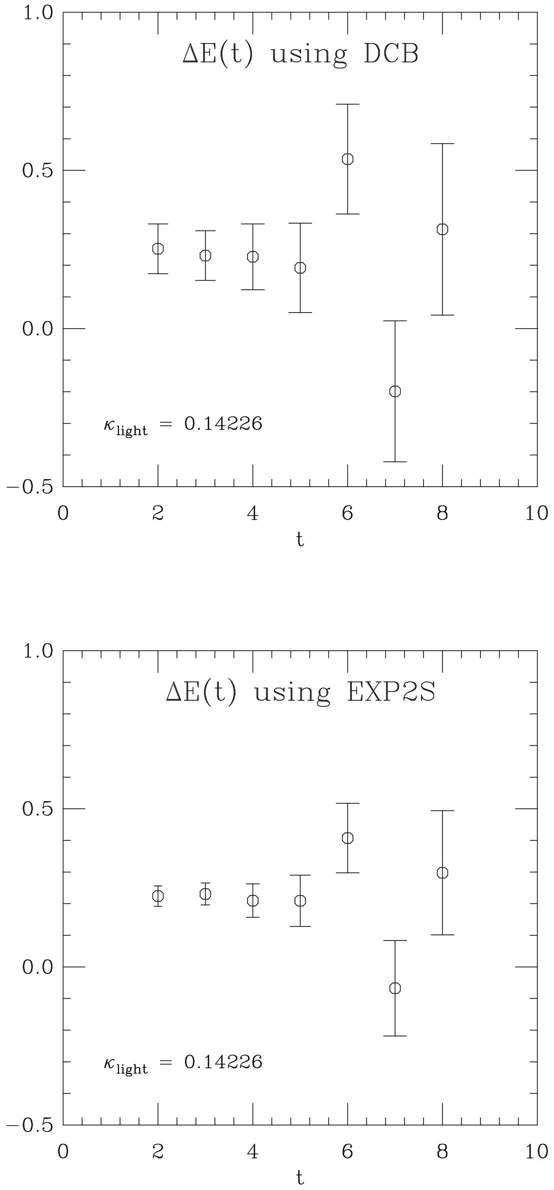

Figure 3.10: The mass difference, $\Delta\mathcal{E}$, between the eigenvalues of the correlator matrix constructed from EXP and (a) DCB and (b) EXP2S smearing functions in the Coulomb gauge. Again this is for light $\kappa = 0.14226$.

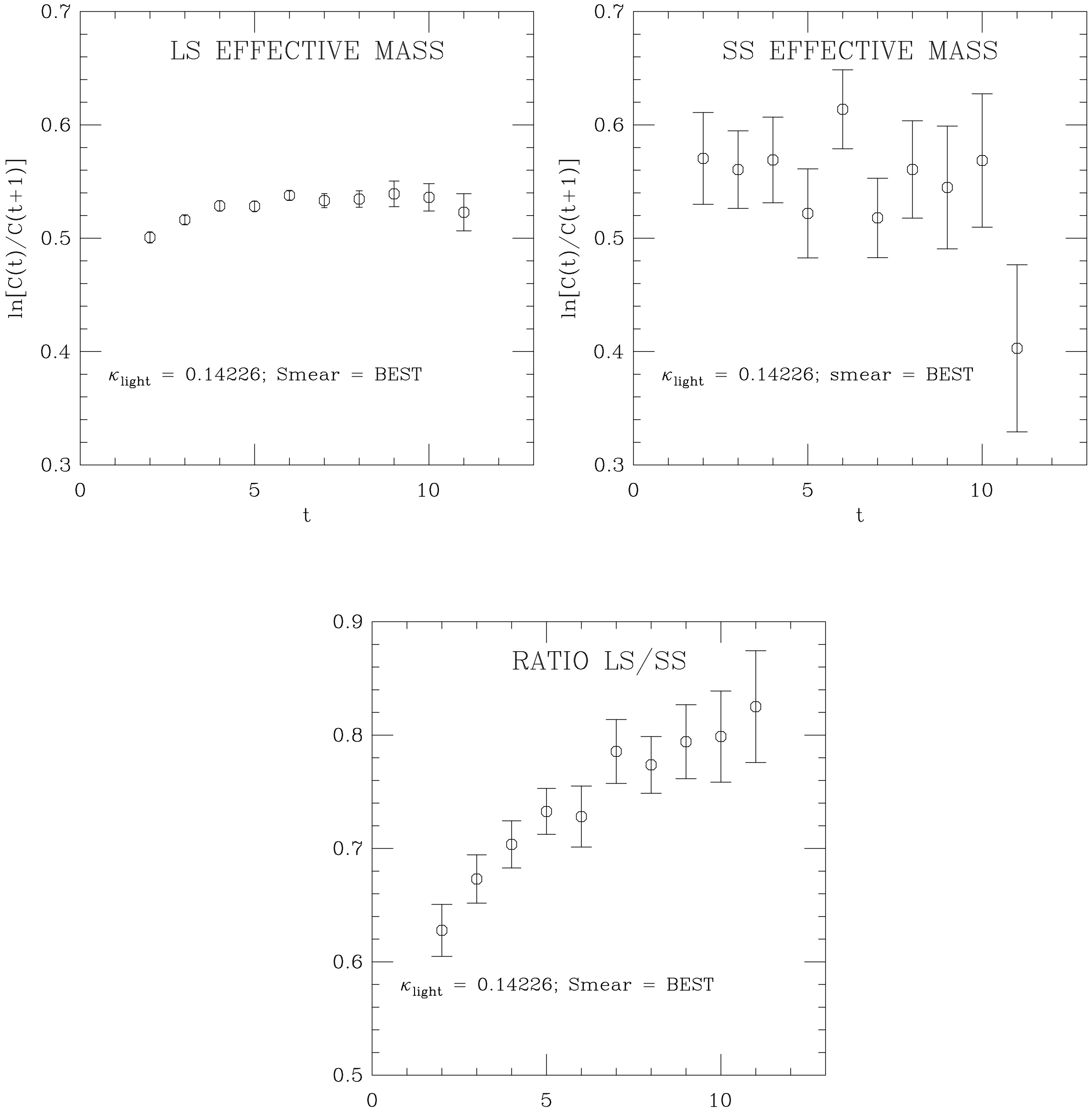

Figure 3.11: Effective mass plots and ratio $C^{\mathrm{LS}}/C^{\mathrm{SS}}$ for "Best" smearing function. This comes from the projections of the eigenvectors of the 2×2 correlator matrix constructed from EXP and EXP2S smearing functions in the Coulomb gauge. Again this is for light $\kappa = 0.14226$.

In order to salvage something from this multi-state smearing analysis, it was decided to determine a value for the mass difference between the ground and first excited states, ΔE, from the computed values, and use this as fixed in 2-state fits of the form

$$C(t) \simeq Z\,\mathrm{e}^{-E\,t}\Big\{1 + \frac{Z^*}{Z}\,\mathrm{e}^{-\Delta E t}\Big\} \tag{3.36}$$

to the LS and SS correlators for all the ground state smearing types. Z is the ground state amplitude and Z^* the first excited state amplitude. The expectation is that this should give a better and more stable fit for Z over a longer time range.

	$\Delta E(t)$		
t	0.14144	0.14226	0.14262
2	$0.21\ ^{+3}_{-3}$	$0.22\ ^{+3}_{-3}$	$0.23\ ^{+3}_{-3}$
3	$0.22\ ^{+4}_{-4}$	$0.23\ ^{+3}_{-3}$	$0.24\ ^{+3}_{-3}$
4	$0.19\ ^{+5}_{-5}$	$0.21\ ^{+5}_{-5}$	$0.24\ ^{+5}_{-5}$

Table 3.2: The energy difference between the eigenvalues of the correlator matrix calculated on the first 3 timeslices at each light κ-value.

An average value for ΔE was taken from the values at $t = 2$, as in the above table. This was used as the fixed energy difference in the 2-state fits. Similar to the exponential fits to the LS and SS correlators, a check of the sensitivity of the fit values for the ground state amplitudes from the two-state fits was undertaken. Examples of the plots from this study are shown in figures 3.12 and 3.13. The results of this reveal little more than the sensitivity tests for the exponential fits. Again INV and EXP exhibit the greatest stability. Again the fits to the SS correlators are more stable than the fits to the LS correlators. In fact it is disappointing that the 2-state fits did not perform better in removing the excited state contamination in the LS correlators. The effect of using a different value for ΔE was also investigated. This had some effect for the LS correlator fits but virtually none for the SS fits. The two-state fits proved to be quite troublesome. For some of the fit ranges the fits failed, particularly for CUB smearing and LS correlators. For some of the fits the correlation matrix became near singular, and so the reliability of the fits is questionable.

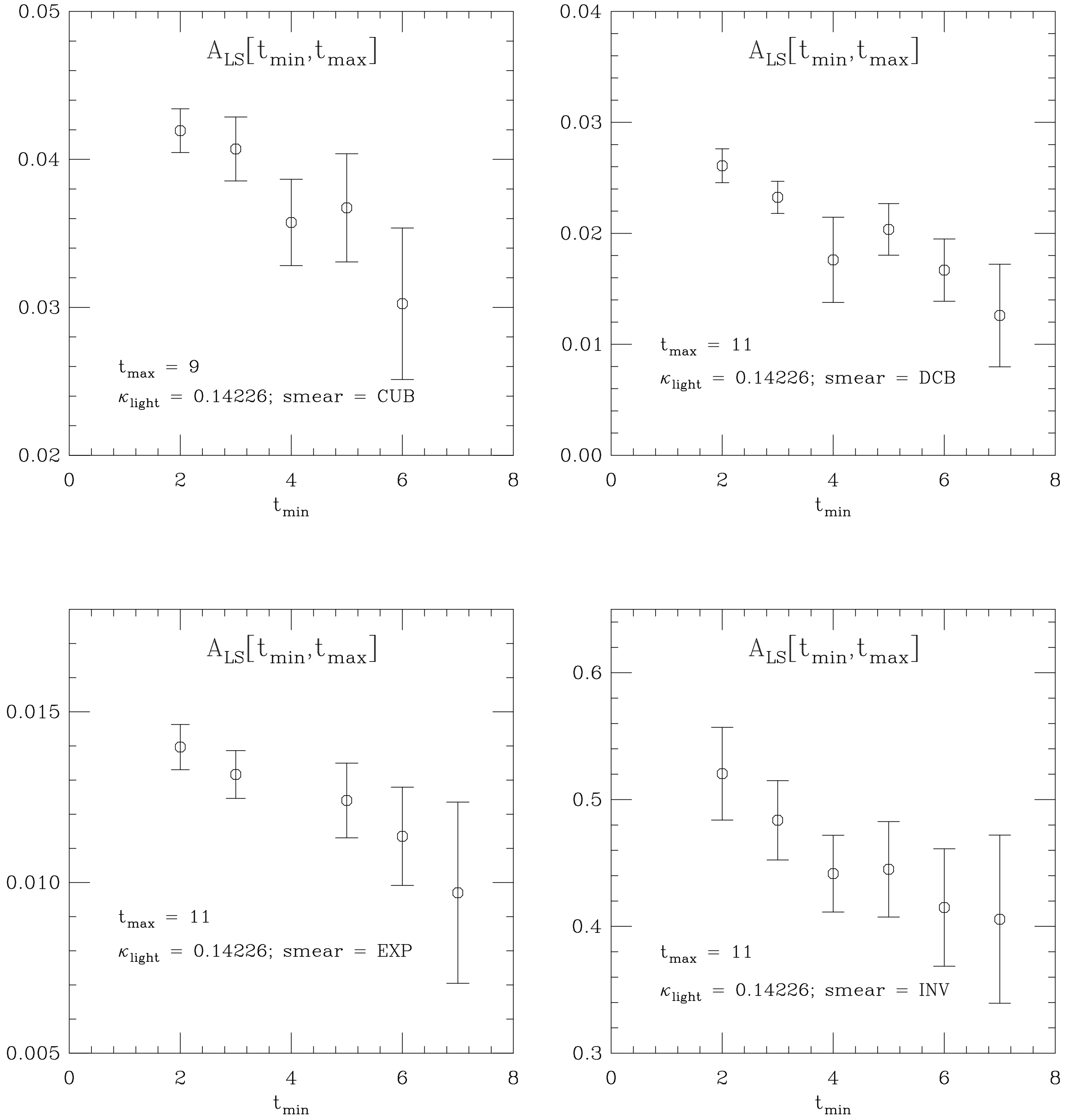

Figure 3.12: Sensitivity of the value of the ground state amplitude coming from two-state fits to the LS correlators for all smearing types. The maximum time in the fit range is fixed and the variation of the fit value with the minimum time is investigated. The point at $t_{\rm min} = 4$ for EXP smearing is not included because of the failure of the fit at this point. These fits are for light $\kappa = 0.14226$.

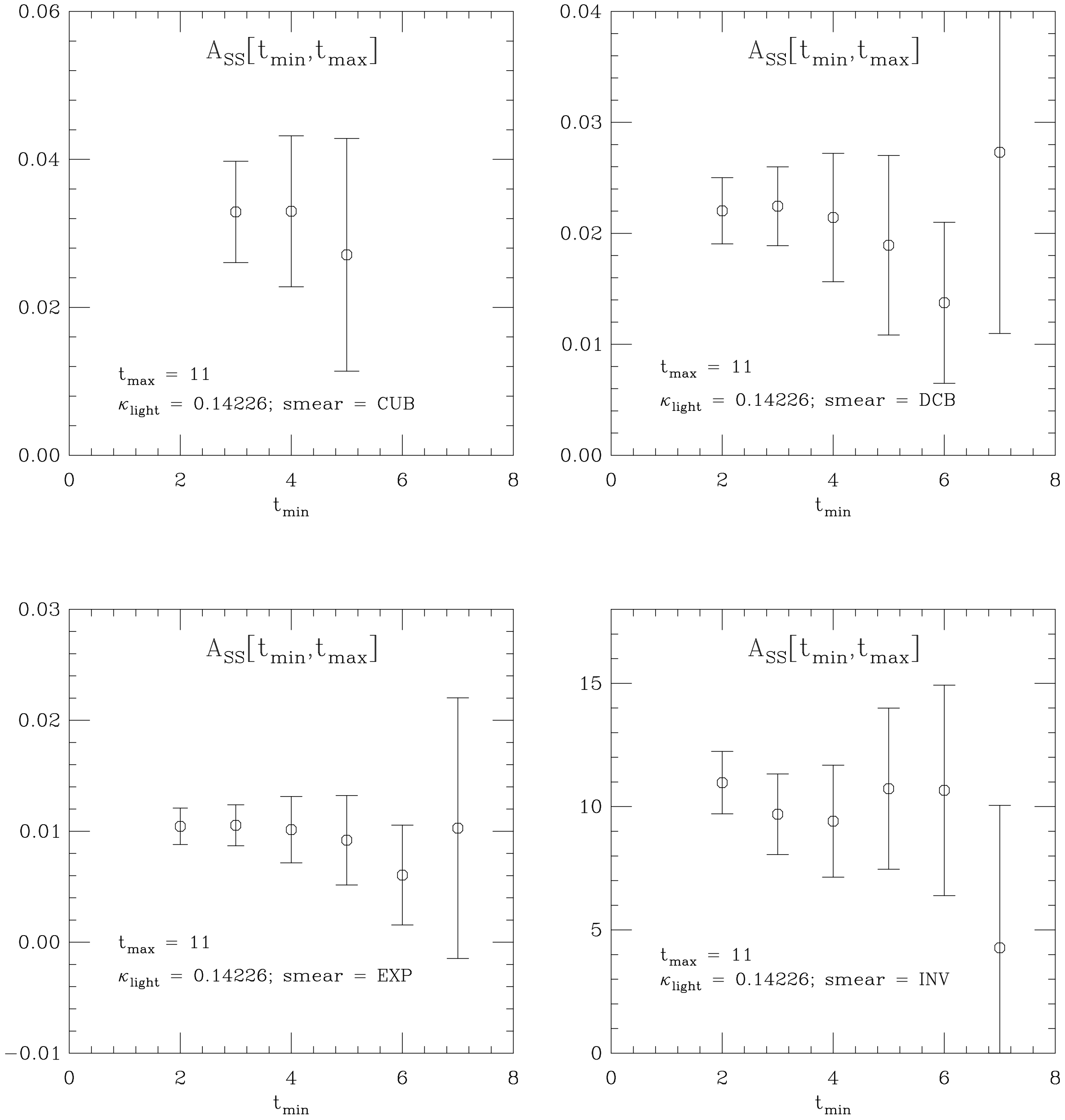

Figure 3.13: Sensitivity of the value of the ground state amplitude coming from two-state fits to the SS correlators for all smearing types. The maximum time in the fit range is fixed and the variation of the fit value with the minimum time is investigated. In the case of CUB smearing the fit for $t_{\min} = 2$ was very badly behaved and fits failed for $t_{\min}$ beyond 5. These fits are for light $\kappa = 0.14226$.

Having investigated the behaviour of different fitting methods to the various correlators I now finally present results using the chosen best fit ranges. In the tables below, fitting method I is referred to as "1-state SS" and similarly, method II as "1-state LS". "2-state SS" signifies method I was used to extract Z_L but where Z_S and the fit mass are extracted from a two-state fit to the SS correlator.

Smearing		INV	EXP	CUB	DCB
Ranges		[8,11]	[7,11]	[7,9]	[8,11]
0.14144	R	$0.0410\ ^{+7}_{-6}$	$1.30\ ^{+2}_{-2}$	$0.700\ ^{+11}_{-11}$	$0.912\ ^{+13}_{-13}$
	χ^2/dof	0.64/3	0.85/4	0.02/2	0.67/3
0.14226	R	$0.0391\ ^{+7}_{-7}$	$1.23\ ^{+3}_{-3}$	$0.676\ ^{+10}_{-11}$	$0.873\ ^{+14}_{-16}$
	χ^2/dof	1.14/3	0.74/4	0.02/2	0.83/3
0.14262	$\mathcal{E}$	$0.0383\ ^{+8}_{-8}$	$1.20\ ^{+3}_{-3}$	$0.666\ ^{+10}_{-11}$	$0.855\ ^{+13}_{-17}$
	χ^2/dof	1.75/3	0.86/4	0.20/2	0.51/3

Table 3.3: Fits to the ratio $R = C^{\mathrm{LS}}(t)/C^{\mathrm{SS}}(t)$ at each light κ-value for each smearing. The same fit ranges are used at each κ-value.

The values for the binding energy at each κ-value are given in table 3.4 with the chiral extrapolated values given in table 3.5. This also contains the computed vales in MeV of the splitting $M_{B_s} - M_{B_d}$. Table 3.6 contains the calculated values of Z_L at each of the light κ-values along with the chiral extrapolated results, using both correlated and uncorrelated chiral fits. This table also shows results for f_{B_s}/f_{B_d}.

The chiral extrapolations are performed assuming a linear chiral behaviour. An example of the chiral extrapolations is given in figure 3.14. This is for Z_L calculated using 1-state SS and correlated chiral fits. As one can see the chiral extrapolations are well behaved and differ little from their uncorrelated counterparts. This behaviour is much the same for the other two methods and also for chiral extrapolations of the binding energy. Finally, note that the chiral extrapolations are plotted against $a^2 m_\pi^2(\kappa_q)$, the calculated pion mass squared in lattice units at each light κ-value. This is entirely equivalent to plotting against $(1/\kappa - 1/\kappa_{\mathrm{crit}})$. It may be useful to note that the value at the strange quark mass is $a^2 m_\pi^2(\kappa_s) = 0.06843$.

κ		Smearing			
0.14144		INV	EXP	CUB	DCB
1-state LS	$\mathcal{E}$	$0.562\ ^{+3}_{-3}$	$0.563\ ^{+4}_{-3}$	$0.572\ ^{+4}_{-4}$	$0.569\ ^{+5}_{-5}$
	χ^2/dof	0.95/3	1.56/3	1.14/1	0.99/2
1-state SS	$\mathcal{E}$	$0.570\ ^{+6}_{-5}$	$0.570\ ^{+8}_{-6}$	$0.566\ ^{+9}_{-10}$	$0.563\ ^{+10}_{-8}$
	χ^2/dof	0.64/5	3.04/5	1.14/3	0.49/3
2-state SS	$\mathcal{E}$	$0.574\ ^{+10}_{-10}$	$0.567\ ^{+13}_{-14}$	$0.566\ ^{+15}_{-19}$	$0.564\ ^{+12}_{-11}$
	χ^2/dof	2.87/7	3.19/7	3.59/6	3.47/7
0.14226		INV	EXP	CUB	DCB
1-state LS	$\mathcal{E}$	$0.546\ ^{+3}_{-4}$	$0.546\ ^{+4}_{-3}$	$0.558\ ^{+4}_{-5}$	$0.550\ ^{+5}_{-5}$
	χ^2/dof	1.37/3	2.57/3	1.82/1	1.05/2
1-state SS	$\mathcal{E}$	$0.550\ ^{+7}_{-6}$	$0.551\ ^{+8}_{-7}$	$0.547\ ^{+10}_{-10}$	$0.543\ ^{+11}_{-9}$
	χ^2/dof	1.48/5	2.77/5	1.37/3	0.29/3
2-state SS	$\mathcal{E}$	$0.553\ ^{+12}_{-12}$	$0.548\ ^{+15}_{-15}$	$0.535\ ^{+16}_{-20}$	$0.543\ ^{+13}_{-14}$
	χ^2/dof	3.89/7	2.70/7	3.35/6	2.81/7
0.14262		INV	EXP	CUB	DCB
1-state LS	$\mathcal{E}$	$0.540\ ^{+4}_{-4}$	$0.539\ ^{+4}_{-4}$	$0.551\ ^{+5}_{-6}$	$0.541\ ^{+6}_{-6}$
	χ^2/dof	0.92/3	2.73/3	1.92/1	1.13/2
1-state SS	$\mathcal{E}$	$0.543\ ^{+7}_{-6}$	$0.543\ ^{+9}_{-9}$	$0.539\ ^{+11}_{-11}$	$0.534\ ^{+12}_{-9}$
	χ^2/dof	2.06/5	2.68/5	1.17/3	0.28/3
2-state SS	$\mathcal{E}$	$0.545\ ^{+12}_{-13}$	$0.541\ ^{+16}_{-20}$	$0.526\ ^{+20}_{-22}$	$0.535\ ^{+14}_{-15}$
	χ^2/dof	4.73/7	2.70/7	3.35/6	2.81/7
Ranges		INV	EXP	CUB	DCB
1-state LS		[7,11]	[7,11]	[7,9]	[8,11]
1-state SS		[5,11]	[5,11]	[7,11]	[7,11]
2-state SS		[2,11]	[2,11]	[3,11]	[2,11]

Table 3.4: Values for the binding energy, $\mathcal{E}$ (in lattice units), at each light κ-value and for each smearing, extracted from exponential (1-state) fits to both LS and SS correlators and from 2-state fits to the SS correlators. The same ranges are used at each κ-value.

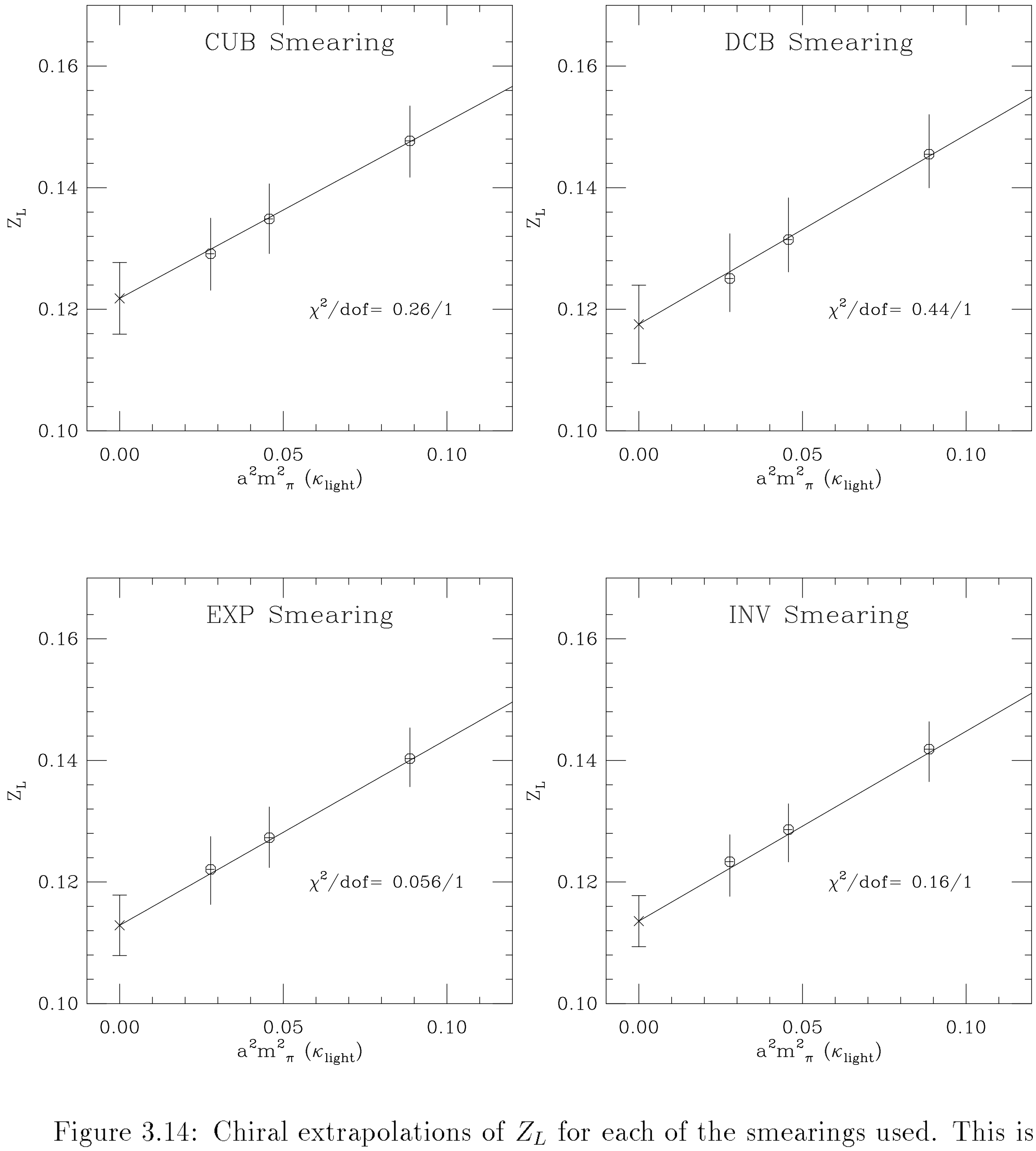

Figure 3.14: Chiral extrapolations of Z_L for each of the smearings used. This is for Z_L calculated using method I using 1-state fits to the SS correlators.

	Method	INV	EXP	CUB	DCB
Binding Energy, $\mathcal{E}$, at κ_{crit}					
COR	1-state LS	$0.529\ ^{+4}_{-4}$	$0.528\ ^{+5}_{-4}$	$0.543\ ^{+6}_{-5}$	$0.531\ ^{+6}_{-6}$
	1-state SS	$0.529\ ^{+8}_{-6}$	$0.529\ ^{+11}_{-7}$	$0.528\ ^{+5}_{-4}$	$0.520\ ^{+15}_{-9}$
	2-state SS	$0.531\ ^{+13}_{-14}$	$0.529\ ^{+18}_{-21}$	$0.512\ ^{+23}_{-24}$	$0.512\ ^{+16}_{-17}$
UNC	1-state LS	$0.529\ ^{+4}_{-4}$	$0.528\ ^{+5}_{-4}$	$0.542\ ^{+5}_{-7}$	$0.529\ ^{+7}_{-6}$
	1-state SS	$0.530\ ^{+8}_{-7}$	$0.531\ ^{+11}_{-10}$	$0.527\ ^{+12}_{-13}$	$0.521\ ^{+15}_{-9}$
	2-State SS	$0.532\ ^{+14}_{-14}$	$0.529\ ^{+18}_{-21}$	$0.512\ ^{+23}_{-23}$	$0.522\ ^{+16}_{-17}$
Mass Splitting $M_{B_s} - M_{B_d}$ (MeV)					
COR	1-state LS	$74\ ^{+4}_{-5}$	$79\ ^{+4}_{-5}$	$67\ ^{+4}_{-4}$	$85\ ^{+5}_{-6}$
	1-state SS	$91\ ^{+6}_{-7}$	$90\ ^{+8}_{-11}$	$85\ ^{+9}_{-11}$	$92\ ^{+8}_{-13}$
	2-State SS	$102\ ^{+9}_{-12}$	$94\ ^{+13}_{-21}$	$98\ ^{+26}_{-22}$	$98\ ^{+9}_{-15}$
UNC	1-state LS	$75\ ^{+6}_{-5}$	$80\ ^{+6}_{-6}$	$67\ ^{+7}_{-5}$	$89\ ^{+7}_{-10}$
	1-state SS	$87\ ^{+10}_{-10}$	$88\ ^{+16}_{-11}$	$87\ ^{+16}_{-14}$	$96\ ^{+12}_{-18}$
	2-state SS	$95\ ^{+16}_{-16}$	$84\ ^{+28}_{-25}$	$98\ ^{+31}_{-26}$	$92\ ^{+20}_{-21}$

Table 3.5: Chiral extrapolated values for the binding energy in lattice units, for both correlated (COR) and uncorrelated (UNC) fits. Also given are the corresponding values for the mass splitting $M_{B_s} - M_{B_d}$. The χ^2/dof are not given – they are all less than 1.0.

κ	Method	INV	EXP	CUB	DCB
0.14144	1-state LS	$0.137\ ^{+3}_{-3}$	$0.137\ ^{+3}_{-3}$	$0.152\ ^{+3}_{-3}$	$0.148\ ^{+4}_{-4}$
	1-state SS	$0.142\ ^{+5}_{-5}$	$0.140\ ^{+5}_{-5}$	$0.147\ ^{+6}_{-6}$	$0.145\ ^{+7}_{-6}$
	2-state SS	$0.144\ ^{+9}_{-9}$	$0.138\ ^{+9}_{-10}$	$0.137\ ^{+12}_{-12}$	$0.144\ ^{+9}_{-9}$
0.14226	1-state LS	$0.126\ ^{+3}_{-3}$	$0.126\ ^{+3}_{-3}$	$0.140\ ^{+3}_{-3}$	$0.135\ ^{+3}_{-3}$
	1-state SS	$0.129\ ^{+4}_{-5}$	$0.127\ ^{+5}_{-5}$	$0.134\ ^{+6}_{-6}$	$0.131\ ^{+7}_{-5}$
	2-State SS	$0.129\ ^{+8}_{-9}$	$0.125\ ^{+8}_{-10}$	$0.123\ ^{+12}_{-13}$	$0.129\ ^{+8}_{-9}$
0.14262	1-state LS	$0.122\ ^{+3}_{-4}$	$0.121\ ^{+2}_{-3}$	$0.135\ ^{+3}_{-4}$	$0.128\ ^{+4}_{-3}$
	1-state SS	$0.123\ ^{+4}_{-6}$	$0.122\ ^{+5}_{-6}$	$0.129\ ^{+6}_{-6}$	$0.125\ ^{+7}_{-5}$
	2-State SS	$0.124\ ^{+8}_{-10}$	$0.121\ ^{+9}_{-12}$	$0.117\ ^{+13}_{-14}$	$0.123\ ^{+9}_{-10}$
Correlated Chiral Extrapolation					
$\kappa_{\rm crit}$	1-state LS	$0.115\ ^{+4}_{-3}$	$0.113\ ^{+3}_{-3}$	$0.127\ ^{+4}_{-4}$	$0.122\ ^{+4}_{-4}$
	1-state SS	$0.114\ ^{+5}_{-5}$	$0.113\ ^{+6}_{-5}$	$0.122\ ^{+6}_{-6}$	$0.118\ ^{+8}_{-6}$
	2-state SS	$0.111\ ^{+9}_{-8}$	$0.109\ ^{+10}_{-9}$	$0.108\ ^{+13}_{-14}$	$0.113\ ^{+10}_{-8}$
f_{B_s}/f_{B_d}	1-state LS	$1.14\ ^{+1}_{-1}$	$1.15\ ^{+1}_{-1}$	$1.12\ ^{+1}_{-1}$	$1.17\ ^{+1}_{-2}$
	1-state SS	$1.18\ ^{+2}_{-2}$	$1.17\ ^{+2}_{-2}$	$1.15\ ^{+2}_{-2}$	$1.17\ ^{+2}_{-3}$
	2-state SS	$1.21\ ^{+3}_{-3}$	$1.18\ ^{+4}_{-5}$	$1.20\ ^{+7}_{-5}$	$1.20\ ^{+3}_{-4}$
Uncorrelated Chiral Extrapolation					
$\kappa_{\rm crit}$	1-state LS	$0.115\ ^{+3}_{-3}$	$0.113\ ^{+2}_{-3}$	$0.128\ ^{+3}_{-4}$	$0.120\ ^{+4}_{-4}$
	1-state SS	$0.115\ ^{+5}_{-6}$	$0.114\ ^{+6}_{-6}$	$0.121\ ^{+6}_{-6}$	$0.116\ ^{+8}_{-5}$
	2-state SS	$0.115\ ^{+8}_{-10}$	$0.113\ ^{+9}_{-12}$	$0.108\ ^{+14}_{-14}$	$0.115\ ^{+10}_{-11}$
f_{B_s}/f_{B_d}	1-state LS	$1.14\ ^{+1}_{-1}$	$1.15\ ^{+1}_{-1}$	$1.13\ ^{+1}_{-1}$	$1.17\ ^{+2}_{-2}$
	1-state SS	$1.17\ ^{+2}_{-2}$	$1.17\ ^{+3}_{-2}$	$1.16\ ^{+2}_{-2}$	$1.19\ ^{+3}_{-4}$
	2-state SS	$1.19\ ^{+4}_{-4}$	$1.16\ ^{+7}_{-5}$	$1.20\ ^{+8}_{-7}$	$1.19\ ^{+5}_{-5}$

Table 3.6: Values for Z_L calculated using various methods at each κ-value and each smearing. The correlated and uncorrelated values for the chiral extrapolated values are also given, along with the corresponding values for f_{B_s}/f_{B_d}.

The results for INV and EXP smearing show good consistency across the various fitting methods, with the results for CUB and DCB smearing showing a lot greater variability. However, given the very disparate types of smearing function used, the agreement within one or two sigma across all smearing types is quite remarkable.

Results using 1-state LS have the smallest statistical errors. They also give the lowest values for $M_{B_s} - M_{B_d}$ and f_{B_s}/f_{B_d}. This method for extracting Z_L suffers from the fact that the plateau in LS effective mass plots is approached from below and thus it is harder to isolate unambiguously. So, even though the noise in SS correlators is always greater, using method I (or 1-state SS) is often preferred. The statistical errors are by far the greatest using the 2-state fits to SS. These also show a slightly greater variation between correlated and uncorrelated chiral extrapolations. The good agreement between the 1-state and 2-state fits to the SS correlators gives one confidence that the ground state has been properly isolated in these correlators, particularly for EXP and INV smearing.

In quoting final values I take the results from the 1-state SS fits to the EXP smeared correlators, and from the correlated chiral extrapolations. EXP smearing also shows the longest plateau in the ratio plots. I only quote a statistical error on these results, except for dimensionful quantities where I take the systematic error from the error in the scale. At any rate, the statistical errors in these values encompasses the values from varying the fitting methods and smearing used. This gives

$$Z_L = 0.113 \ {}^{+\ 6}_{-\ 5} \tag{3.37}$$

with

$$f_B^{\mathrm{static}} = 268 \ {}^{+14}_{-11}(\mathrm{stat}) \ {}^{+28}_{-27}(\mathrm{syst}) \ \mathrm{MeV}\,. \tag{3.38}$$

The value of Z_L is in good agreement with the value $Z_L = 0.111(6)$ quoted by the APE group in [75]. They also work at $\beta = 6.2$ and with the SW-clover fermion action for the light quarks. In fact one of the light κ-values they simulate at is $\kappa = 0.14144$ at which they quote $Z_L = 0.135(2)$ which is also in good agreement with the results presented above.

Corresponding to this choice of central value for Z_L is the ratio

$$\frac{f_{B_s}}{f_{B_d}} = 1.17 \ {}^{+\,2}_{-\,2} \tag{3.39}$$

and a value for the mass splitting

$$M_{B_s} - M_{B_d} = 90 \ {}^{+\ 8}_{-11}(\text{stat}) \ {}^{+16}_{-17}(\text{syst}) \ \text{MeV}\,. \tag{3.40}$$

In this case I also add to the systematic error an error from the spread over different results. This is in good agreement with the value $86 \ {}^{+12}_{-12} \ {}^{+7}_{-9}$ from the FermiLab calculation in the static limit [76] – this is in fact quoted as their continuum result. This result can also be compared to results using propagating heavy quarks calculated on this configuration set [50]. Extrapolating those results in $1/M_P$ to $M_P = M_B$ or $M_P = \infty$ one finds

$$\begin{aligned}
M_{B_s} - M_{B_d} &= 84 \ {}^{+14}_{-12} \ {}^{+6}_{-6} \ \text{MeV} \qquad M_P = \infty & (3.41)\\
M_{B_s} - M_{B_d} &= 93 \ {}^{+12}_{-12} \ {}^{+6}_{-7} \ \text{MeV} \qquad M_P = M_{B_d} & (3.42)\\
M_{D_s} - M_{D_d} &= 107 \ {}^{+12}_{-12} \ {}^{+8}_{-6} \ \text{MeV} \qquad M_P = M_{D_d}\,. & (3.43)
\end{aligned}$$

The experimental value at $M_P = M_B$ is 96 ± 6 MeV [5]. The result from this work is in good agreement with all these values.

Many groups have already performed calculations of f_B^{static}, using a wide variety of smearing techniques. The APE group [75] use Cube and Double Cube smearing functions but have more statistics than this work. Others have used the variational approach described earlier. The FermiLab group [76] construct their variational basis using smearing functions obtained from a relativistic quark model while Draper and McNeile [77, 78] construct a large basis from all the possible distinct separations allowed by the cubic point group. Given these many and widely varied approaches it is important to compare the results presented here with other published work.

Comparing actual values of $f_B^{\rm static}$ isn't useful as the comparison is clouded by other systematic differences such as ambiguities over the scale or the perturbative matching. Allton [79] suggests plotting $\log Z_L$ as a function of β. This presumes a scaling behaviour $\log Z_L \sim \log a$ and assuming $g_0^{-2} \sim \log a$. In figure 3.15 the results using Wilson light quarks [80, 76, 81, 82, 77, 51, 83], and using SW-Clover light quarks, [82, 80] are plotted in this way. Allton claims that for $\beta \geq 6.0$ the linearity in this graph is evidence for scaling. The result of this work certainly fits in well with this behaviour.

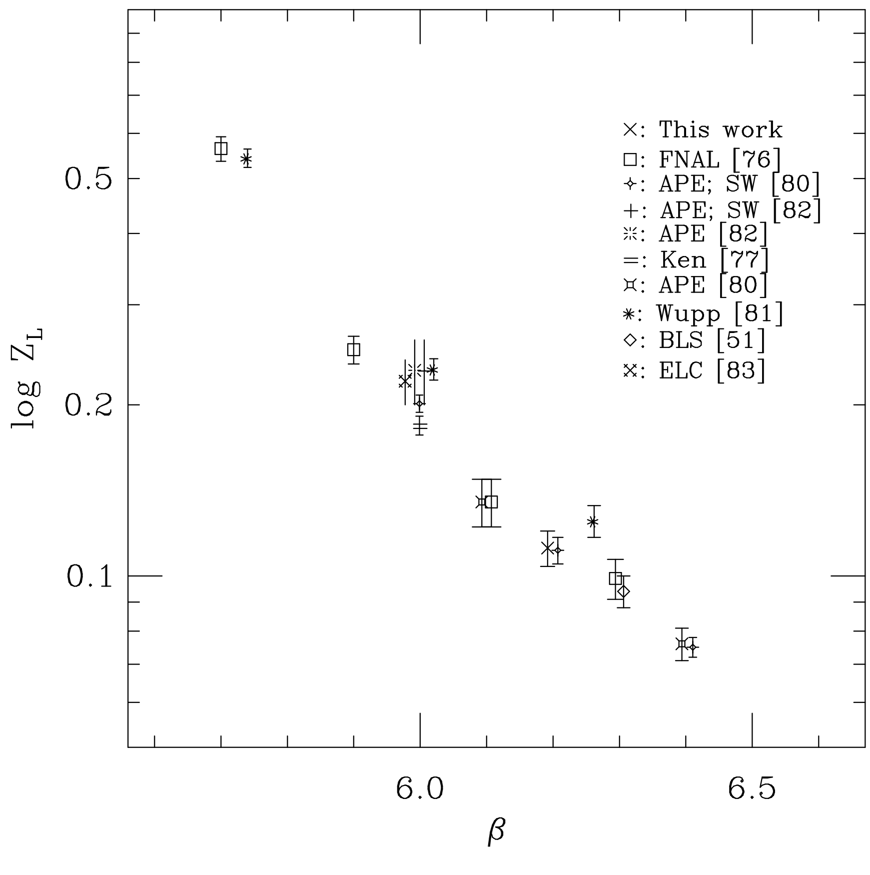

Figure 3.15: Z^L plotted logarithmically versus β using data from several simulations obtained using both the Wilson and the SW-clover action.

Perhaps the most interesting point to note concerns the fact that the values of Z_L for both Wilson and SW-clover light quarks are more or less the same. This is hardly surprising since the improvement is only for the light quarks where the effects on static-light matrix elements is expected to be small. However, the perturbative matching factor, Z_A, is substantially, different in both cases, with the value of Z_A increased for the SW-Clover case over that of the Wilson case, by up to 15% [64, 66] in the range of β-values currently being used for SW-clover simulations.

In summary, in this chapter I have presented results of a calculation of f_B, f_{B_s}/f_{B_d} and $M_{B_s} - M_{B_d}$ in the static approximation. For static-light matrix elements the main difficulty in extracting values from the lattice calculation is ensuring that the ground state has been correctly isolated. In order to achieve this one technique is to use smeared interpolating operators. A major aspect of the study in this chapter has been the comparison of a wide variety of smearing functions used to isolate the ground state. The results show reasonable consistency between the various smearing techniques. In particular, the results from exponential smearing in the Coulomb gauge and gauge invariant Jacobi smearing show very good consistency and stability over fitting ranges and fitting methods. The good agreement between 1-state and 2-state fits for the SS correlators show that the ground state is well isolated in these correlators using INV and EXP smearing. The study also suggests that a cube is not a particularly good choice for a smearing function, although with a judicious choice of fitting ranges the results with cube smearing are in reasonable agreement with those using the more reliable methods. Double cube smearing certainly seems to be a better choice than cube smearing, though the plateau in the ratio and effective mass plots and the stability of the fits show that it is not quite as good as exponential and gauge invariant smearing.

Any improvement on these results requires a greater configuration set. Firstly, this would allow a better determination of the correct smearing radius with the probable use of different radii at the different light-κ values. Secondly, one would hope to get better results from using the multi-state smearing technique.

Chapter 4

Calculation of B_B in the Static Limit

In this chapter I present results of a calculation of B_B in the static approximation. The calculation was performed on the same data set as that described at the start of the last chapter. In the first section I present the details of how B_B can be calculated on the lattice and in the remaining section I present and discuss the results.

4.1 The Calculation

4.1.1 $\bar{B}^0 - B^0$ Mixing in the Static Limit on the Lattice

The purpose of the calculation is to extract the renormalisation group invariant "bag" parameter,

$$B_B = [\alpha_{\overline{MS}}(\mu)]^{-2/\beta_0}\, B_B(\mu) \tag{4.1}$$

where

$$B_B(\mu) = \frac{\left\langle \bar{B}^0 \right| \mathcal{O}_L(\mu) \left| B^0 \right\rangle}{\frac{8}{3} f_B^2\, M_B^2} \tag{4.2}$$

and where

$$O_L = [\bar{b}\gamma_\mu(1-\gamma_5)d][\bar{b}\gamma^\mu(1-\gamma_5)d]\,. \tag{4.3}$$

This definition of $B_B(\mu)$ is for the matrix element of O_L calculated in full QCD in some continuum scheme, here the $\overline{MS}$ scheme. So, in order to extract B_B from a lattice calculation in the static approximation requires a two stage matching procedure similar to the situation with f_B^{static}. However, the situation is more complicated here in that new operators get introduced at both stages of the matching process.

The one-loop matching between the continuum full theory and the continuum static theory at the scale $\mu < m_b$ is given by [66, 84]

$$O_L^{\rm full}(m_b) = \left\{1 + \frac{\alpha_{\overline{MS}}(\mu)}{4\pi}\left[4\ln(m_b^2/\mu^2) + C_L\right]\right\} O_L^{\rm stat}(\mu) + \frac{\alpha_{\overline{MS}}(\mu)}{4\pi} C_S\, O_S^{\rm stat}(\mu) \tag{4.4}$$

with $C_L = -14$ and $C_S = -8$. The operator O_S is defined through

$$O_S = [\bar{b}(1-\gamma_5)d][\bar{b}(1-\gamma_5)d]\,. \tag{4.5}$$

Its origin is the same as the term proportional to v_μ in the matching of the axial current between the full and effective theories, equation (1.69). The matching quoted here differs slightly from that in [66, 84]. They match for $O_L^{\rm full}(\mu)$ at the heavy scale $\mu = a^{-1} < m_b$. This requires the factor $\ln(m_b^2/\mu^2)$ to be multiplied by $6 = 4 - (-2)$, which is the difference of the anomalous dimensions of O_L in the continuum full and static theories.

The next step is to match these continuum static operators to their lattice counterparts. The operator O_L is a purely left-handed operator, so because of the Wilson term there is nothing protecting it from mixing with operators of different chiralities when renormalised in the lattice scheme. In fact two extra operators are introduced in this matching step. The one-loop matching at the scale $\mu = a^{-1}$ can be written as [66, 84]

$$\begin{aligned} O_L^{\rm stat}(a^{-1}) &= \left\{1 + \frac{\alpha_{\rm latt}(a^{-1})}{4\pi}[D_L + D_L^I]\right\} O_L^{\rm latt} \\ &+ \frac{\alpha_{\rm latt}(a^{-1})}{4\pi}[D_R + D_R^I]\, O_R^{\rm latt} + \frac{\alpha_{\rm latt}(a^{-1})}{4\pi}[D_N + D_N^I]\, O_N^{\rm latt} \end{aligned} \tag{4.6}$$

where the two new operators are defined through

$$\begin{aligned} O_N &= [\bar{b}\gamma_\mu(1-\gamma_5)d][\bar{b}\gamma_\mu(1+\gamma_5)d] + [\bar{b}\gamma_\mu(1+\gamma_5)d][\bar{b}\gamma_\mu(1-\gamma_5)d] \\ &+ 2[\bar{b}(1-\gamma_5)d][\bar{b}(1+\gamma_5)d] + 2[\bar{b}(1+\gamma_5)d][\bar{b}(1-\gamma_5)d] \\ O_R &= [\bar{b}\gamma_\mu(1+\gamma_5)d][\bar{b}\gamma_\mu(1+\gamma_5)d]\,. \end{aligned} \tag{4.7}$$

The coefficients D_L, D_R and D_N come from just the Wilson action and were calculated in [84]. The coefficients for the SW improved action, D_L^I, D_R^I and D_N^I were calculated in [66]. These values are listed below.

D_L	D_L^I	D_R	D_R^I	D_N	D_N^I
-38.90	16.25	-1.61	-2.58	-14.40	0.44

Table 4.1: Coefficients used in matching the continuum static and lattice static operator O_L for the Wilson and SW-clover actions.

The value for D_L quoted here differs from [66, 84] where $D_L = -65.5$ is quoted. Calculating D_L involves using a value for the heavy quark self-energy, e, coming from the heavy quark wavefunction renormalisation on the lattice. This has been calculated to one-loop giving $e = 24.48$ [85, 65]. However, as noted in [65], the heavy quark self-energy contributes to axial current static-light correlators with a reduced value, $e^{(R)} = 4.53$ [66]. Using this reduced value in calculating D_L gives the value quoted in table 4.1. In calculating the matching factor for the static-light axial current, Z_A, this reduced value was used.

So, finally, to one-loop the matching from the continuum full theory to the lattice static theory can be written as

$$\begin{aligned} O_L^{\text{full}}(m_b) &= \left\{1 + \frac{\alpha_{\overline{MS}}(a^{-1})}{4\pi}\left[4\ln(a^2 m_b^2) - 14\right] - 22.06\,\frac{\alpha_{\text{latt}}(a^{-1})}{4\pi}\right\} O_L^{\text{latt}} \\ &- 4.19\,\frac{\alpha_{\text{latt}}(a^{-1})}{4\pi} O_R^{\text{latt}} - 13.96\,\frac{\alpha_{\text{latt}}(a^{-1})}{4\pi} O_N^{\text{latt}} - 2\,\frac{\alpha_{\overline{MS}}(a^{-1})}{\pi} O_S^{\text{latt}} \qquad (4.8) \\ &\equiv Z_L O_L^{\text{latt}} + Z_R O_R^{\text{latt}} + Z_N O_N^{\text{latt}} + Z_S O_S^{\text{latt}}\,. \qquad (4.9) \end{aligned}$$

Note that at this one-loop level it is sufficient to replace the operator O_S with its lattice counterpart. Inserting values for $\alpha_{\overline{MS}}(a^{-1})$ and the boosted $\alpha_{\text{latt}}(a^{-1})$ as in the last chapter then gives values

$$Z_L = 0.53, \qquad Z_R = -0.04, \qquad Z_N = -0.15, \qquad Z_S = -0.20\,. \qquad (4.10)$$

The matching factor for O_L is substantially different from 1, thus calling into question the applicability of one-loop matching. Equation (4.9) has been arrived at by just keeping terms at first order in α. However, if $O_L^{\mathrm{stat}}(a^{-1})$ is calculated from equation (4.6) and this is then substituted into equation (4.4) then the matching coefficients are changed to

$$Z_L = 0.59, \qquad Z_R = -0.03, \qquad Z_N = -0.11, \qquad Z_S = -0.20 \tag{4.11}$$

which will lead to a different final value of B_B. Using these values amounts to including some of the $\mathcal{O}(\alpha^2)$ contribution to the matching coefficients. I predominantly use the first set of matching coefficients, but I will also quote results using the latter set. There is also some variation in the matching factors if a different value of $\Lambda^{(4)}_{\overline{MS}}$ is used[1], and also if u_0 is instead measured from the average plaquette. However, this ambiguity is much less than that coming from the two possible ways of writing the matching coefficients as given in equations (4.10) and (4.11).

4.1.2 Extracting B_B

The determination of B_B requires the extraction of the matrix elements

$$\left\langle \bar{B}^0 \right| \mathcal{O}_i^{\mathrm{latt}}(0) \left| B^0 \right\rangle \tag{4.12}$$

for each of the operators $i = L, R, S, N$. This can be done by calculating the three-point function

$$\begin{aligned} K_i^{SS}(t_x, t_y) &\equiv \sum_{\vec{x},\vec{y}} \left\langle 0 \left| A_4^{\dagger S}(\vec{x}, t_x)\, O_i^{\mathrm{latt}}(0)\, A_4^{\dagger S}(\vec{y}, t_y) \right| 0 \right\rangle \\ &\longrightarrow \frac{(Z^S)^2}{2\, M_B}\, \mathrm{e}^{-E\,(t_x - t_y)} \left\langle \bar{B}^0 \left| O_i^{\mathrm{latt}} \right| B^0 \right\rangle , \end{aligned} \tag{4.13}$$

where it is assumed $t_y < 0 < t_x$ and the asymptotic behaviour is reached for $t_y \ll 0 \ll t_x$. A_4^S is the smeared axial current as in the last chapter. Using the axial current rather than the interpolating operator $\chi_B^\dagger$ is irrelevant in the static

[1] In fact the numbers in equation (4.10) differ slightly from those in [63] as I use $\Lambda^{(4)}_{\overline{MS}} = 250$ MeV here throughout.

approximation. The expansion of this three-point function in terms of the quark fields and the subsequent Wick-contractions is described in detail in Appendix B.

The contributions from Z^S and the exponentials in equation (4.13) can be cancelled out by calculating the ratio

$$R_i(t_x, t_y) = \frac{K_i^{SS}(t_x, t_y)}{\frac{8}{3}\, C^{SL}(t_x)\, C^{SL}(t_y)}\,. \tag{4.14}$$

$B_B(m_b)$ can then be extracted from this in the asymptotic regime through

$$Z_A^{-2} \sum_i Z_i\, R_i(t_x, t_y) \longrightarrow B_B(m_b), \qquad i = L,\ R,\ S,\ N \tag{4.15}$$

with the Z_i's given in equation (4.10) or (4.11) and Z_A is the matching factor for the static-light axial current given in the last chapter. The matrix elements must be of local operators. Hence, with the operators only inserted at the source this means that only smearing at the sink can be implemented to help improve the ground state domination in the three-point correlators. This is a problem in that it is known that SL static-light two-point correlators give poor signals.

Time-reversal symmetry on the lattice can be used to improve the signal for the correlator. In this work the "folded" ratio

$$R_i(t_x, t_y) = \frac{[K_i^{SS}(t_x, t_y) + K_i^{SS}(T - t_y, T - t_x)]}{\frac{4}{3}\, [C^{SL}(t_x) + C^{SL}(T - t_x)]\, [C^{SL}(t_y) + C^{SL}(T - t_y)]} \tag{4.16}$$

is calculated. As with the calculations in the previous chapter, the correlators were calculated only over the timeslices $2 \le t_x \le 12$ and $36 \le t_y \le 46$. The same ground state smearing functions were used as in the last chapter, namely gauge invariant (INV), exponential (EXP), cube (CUB) and double cube (DCB), the latter three in the Coulomb gauge. Another smearing function was also used in the Coulomb gauge for this calculation which was not used for the f_b calculation. This was

$$\text{Gaussian (GAU)}: \quad f(\vec{x}, \vec{y}) = \exp\left\{-|\vec{x} - \vec{y}|^2 / r_0^2\right\}\,. \tag{4.17}$$

4.2 Results

Two separate methods are used to extract $B_B(m_b)$ as in equation (4.15).

Method (a): Fit to the ratios $R_i(t_x, t_y)$ individually in the asymptotic region giving fit values R_i. The B parameter is then obtained through

$$B_B(m_b) = Z_A^{-2} \sum_i Z_i \, R_i \,. \tag{4.18}$$

Method (b): Define $\widetilde{B}_B(m_b; t_x, t_y)$ as

$$\widetilde{B}_B(m_b; t_x, t_y) = Z_A^{-2} \sum_i Z_i \, R_i(t_x, t_y), \tag{4.19}$$

and fit $\widetilde{B}_B(m_b; t_x, t_y)$ to a constant in the asymptotic region.

The easiest way of identifying the asymptotic region in which to fit to either the $R_i(t_x, t_y)$ or $\widetilde{B}_B(m_b; t_x, t_y)$ is to fix one of the times, $t_y = t_f$ say, and look for a plateau in the plots of $R_i(t_x, t_f)$ versus t_x, and equivalently for $\widetilde{B}_B$. The variation of the signal for $R_L(t_x, t_f)$ with t_f is illustrated in figure 4.1, for EXP smearing. As can be seen, the signal gets noisier with increasing $|t_f|$, as is expected. The optimal signal seems to be for[2] $t_f = -3$. This general behaviour is also observed for the other R_i and $\widetilde{B}_B$, and across all smearing types. Also there is little variation in the quality of the signal across the light κ-values.

In the analysis that follows $B_B(m_b)$ is extracted for all smearing types using both methods and using fixed times $t_f = -2, -3, -4$. Beyond $t_f = -4$ the signal gets too noisy to have any confidence that a plateau is being fit to. All the fits to R_i and $\widetilde{B}_B$ take correlations across timeslices into account. In order to obtain $B_{B_d}(m_b)$ the results are extrapolated to the chiral limit assuming a linear chiral behaviour. $B_{B_s}(m_b)$ is also determined in these chiral extrapolations by finding the value at κ_s. Fits taking into account correlations between kappa values are performed as well as fits where these correlations are ignored.

[2]Note that I use the notation $t_f = -3$ rather than $t_f = 45$. This is just a personal preference.

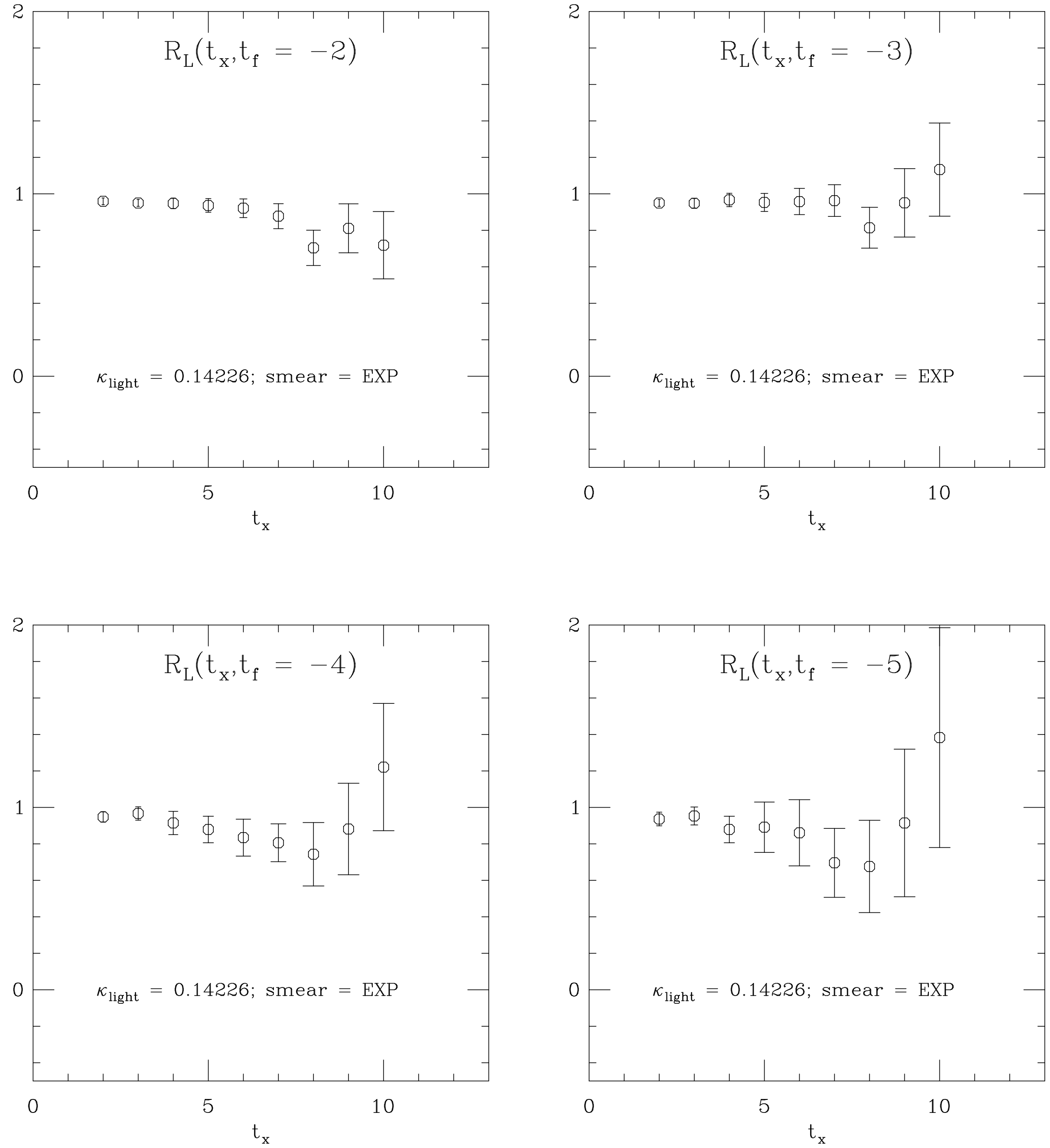

Figure 4.1: Variation of the signal for $R_L(t_x, t_f)$ with t_f for EXP smearing at light $\kappa = 0.14226$.

Tables 4.3, 4.4 and 4.5 give the results of fits to the individual $R_i(t_x, t_f)$ for values of $t_f = -2, -3, -4$ respectively. The values for $B_B(m_b)$ calculated using method (a) and using the Z_i from equation (4.10) are also given. The ranges used in these fits are given in the table below. Figures 4.2, 4.3 and 4.4 are included to

Operator	t_f	EXP	GAU	CUB	DCB	INV
	2	[3,6]	[3,6]	[3,6]	[3,6]	[3,6]
R_L	3	[3,7]	[3,7]	[3,7]	[3,7]	[3,7]
	4	[5,7]	[5,7]	[5,7]	[5,7]	[5,7]
	2	[3,7]	[3,7]	[3,7]	[3,7]	[3,7]
R_R	3	[3,7]	[3,7]	[3,7]	[3,7]	[3,7]
	4	[4,7]	[4,7]	[4,7]	[4,7]	[4,7]
	2	[3,7]	[3,7]	[3,7]	[3,7]	[4,6]
R_N	3	[3,7]	[3,7]	[3,7]	[3,7]	[3,6]
	4	[3,5]	[3,5]	[3,5]	[3,5]	[3,6]
	2	[3,5]	[3,5]	[3,5]	[3,5]	[3,5]
R_S	3	[3,5]	[3,5]	[3,5]	[3,5]	[3,5]
	4	[3,5]	[3,5]	[3,5]	[3,5]	[3,5]

Table 4.2: Fit ranges for fits to ratios R_i, $i = L,R,N,S$, as presented in the following pages. The same ranges are used at all the light κ-values.

illustrate the quality of the fits at the different t_f. Although only the plots using a single smearing at each t_f are presented it should be stressed that the variation of the quality of the signal and fit across the different smearings was small.

The values for $B_{B_d}(m_b)$ and $B_{B_s}(m_b)$ extracted using method (a) are given in table 4.6 with plots illustrating the various chiral extrapolations leading to these results given in figures 4.5 and 4.6. As in the last chapter all the chiral extrapolations are plotted against $a^2 m_\pi^2(\kappa_q)$.

The values for $B_B(m_b)$ at each κ-value extracted using method (b) are presented in table 4.7, along with the fitting ranges used. Again the Z_i from equation (4.10) are used. Plots illustrating the quality of the signals and fits are presented in figures 4.7 and 4.8. The values for $B_{B_d}(m_b)$ and $B_{B_s}(m_b)$ extracted using this method are given in table 4.8 with plots illustrating the various chiral extrapolations leading to these results given in figures 4.9 and 4.10.

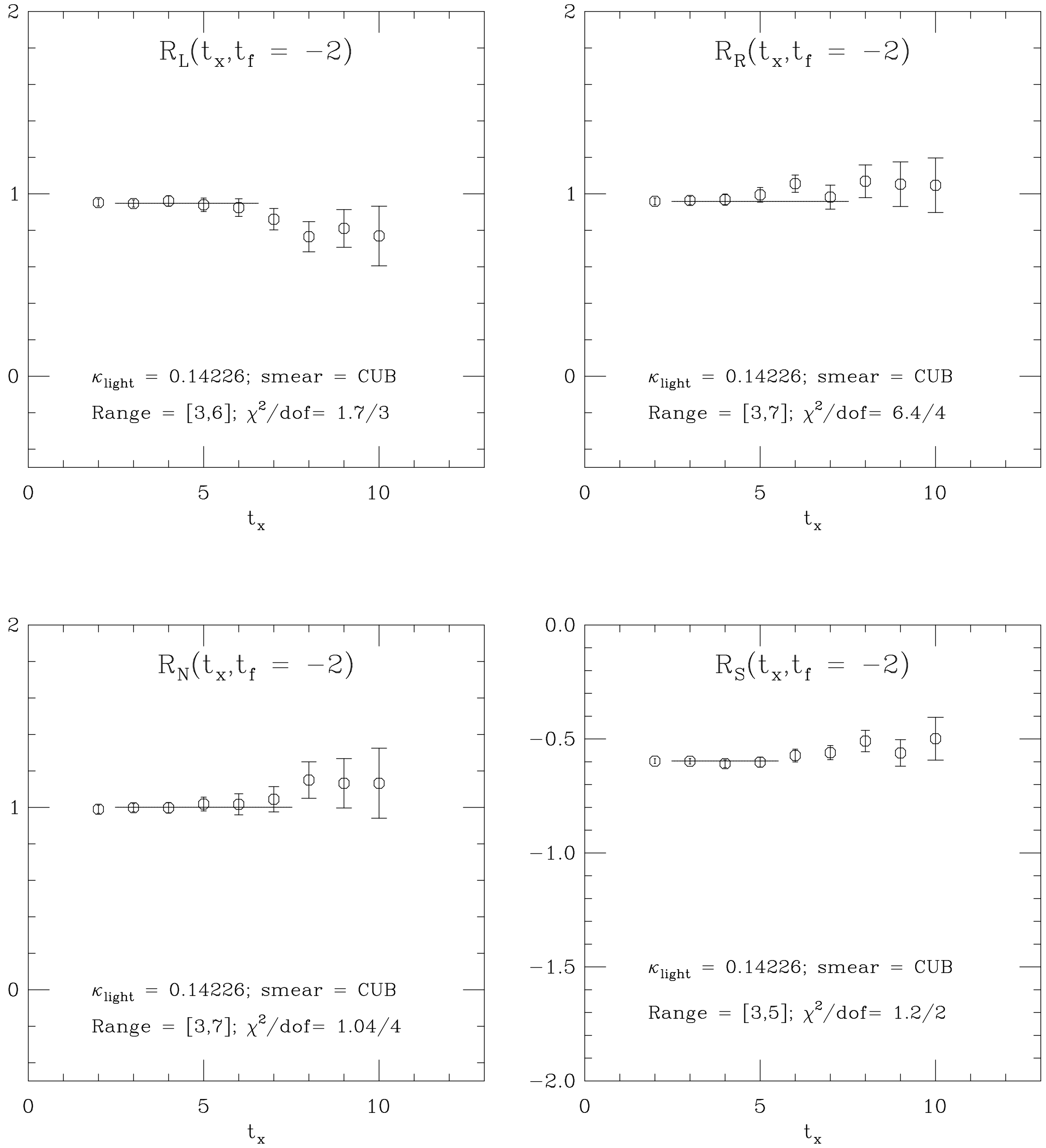

Figure 4.2: Example of fits to R_i, $i = L,R,N,S$, for $t_f = -2$, CUB smearing, and at light $\kappa = 0.14226$.

κ	Smearing				
0.14144	EXP	GAU	CUB	DCB	INV
R_L	$0.96\ ^{+1}_{-1}$	$0.97\ ^{+1}_{-1}$	$0.95\ ^{+1}_{-1}$	$0.96\ ^{+1}_{-1}$	$0.94\ ^{+2}_{-2}$
χ^2/dof	1.39/3	2.92/3	3.01/3	2.36/3	3.24/3
R_R	$0.96\ ^{+2}_{-2}$	$0.96\ ^{+2}_{-2}$	$0.96\ ^{+2}_{-2}$	$0.96\ ^{+2}_{-2}$	$0.97\ ^{+2}_{-2}$
χ^2/dof	8.42/5	6.85/4	7.80/4	7.83/4	2.72/4
R_N	$1.00\ ^{+1}_{-2}$	$0.99\ ^{+1}_{-2}$	$1.00\ ^{+2}_{-3}$	$1.00\ ^{+1}_{-2}$	$1.01\ ^{+3}_{-4}$
χ^2/dof	0.64/4	1.24/4	0.91/4	0.97/4	1.32/2
R_S	$-0.60\ ^{+1}_{-1}$	$-0.61\ ^{+1}_{-1}$	$-0.60\ ^{+1}_{-1}$	$-0.60\ ^{+1}_{-1}$	$-0.59\ ^{+1}_{-1}$
χ^2/dof	0.84/2	2.13/2	2.64/2	1.69/2	2.75/2
$B_B(m_b)$	$0.72\ ^{+2}_{-2}$	$0.73\ ^{+1}_{-1}$	$0.72\ ^{+2}_{-2}$	$0.73\ ^{+1}_{-1}$	$0.70\ ^{+2}_{-2}$
0.14226	EXP	GAU	CUB	DCB	INV
R_L	$0.95\ ^{+2}_{-2}$	$0.96\ ^{+1}_{-1}$	$0.95\ ^{+2}_{-2}$	$0.96\ ^{+2}_{-1}$	$0.94\ ^{+2}_{-3}$
χ^2/dof	0.47/3	1.63/3	1.71/3	1.11/3	2.57/3
R_R	$0.97\ ^{+2}_{-2}$	$0.97\ ^{+2}_{-2}$	$0.96\ ^{+3}_{-2}$	$0.97\ ^{+2}_{-2}$	$0.99\ ^{+3}_{-2}$
χ^2/dof	5.95/4	5.81/4	6.43/4	6.34/4	2.77/4
R_N	$1.00\ ^{+1}_{-2}$	$1.00\ ^{+1}_{-2}$	$1.00\ ^{+2}_{-3}$	$1.00\ ^{+2}_{-2}$	$1.01\ ^{+3}_{-4}$
χ^2/dof	0.49/4	1.31/4	1.04/4	1.00/4	1.73/4
R_S	$-0.60\ ^{+1}_{-1}$	$-0.60\ ^{+1}_{-1}$	$-0.60\ ^{+1}_{-1}$	$-0.60\ ^{+1}_{-1}$	$-0.59\ ^{+1}_{-1}$
χ^2/dof	0.01/2	0.90/2	1.20/2	0.44/2	1.91/2
$B_B(m_b)$	$0.72\ ^{+2}_{-2}$	$0.73\ ^{+2}_{-1}$	$0.71\ ^{+2}_{-2}$	$0.72\ ^{+2}_{-1}$	$0.70\ ^{+3}_{-3}$
0.14262	EXP	GAU	CUB	DCB	INV
R_L	$0.95\ ^{+2}_{-2}$	$0.96\ ^{+2}_{-1}$	$0.94\ ^{+2}_{-2}$	$0.96\ ^{+2}_{-2}$	$0.93\ ^{+3}_{-3}$
χ^2/dof	0.82/3	0.78/3	0.72/3	0.56/3	1.76/3
R_R	$0.98\ ^{+2}_{-2}$	$0.97\ ^{+2}_{-1}$	$0.97\ ^{+3}_{-2}$	$0.97\ ^{+2}_{-2}$	$0.99\ ^{+3}_{-3}$
χ^2/dof	4.80/4	5.26/4	5.38/4	5.37/4	3.14/4
R_N	$1.00\ ^{+1}_{-2}$	$1.00\ ^{+1}_{-2}$	$1.00\ ^{+2}_{-3}$	$0.99\ ^{+1}_{-2}$	$1.01\ ^{+3}_{-4}$
χ^2/dof	0.99/4	1.62/4	1.48/4	1.40/4	2.43/4
R_S	$-0.60\ ^{+1}_{-1}$	$-0.60\ ^{+1}_{-1}$	$-0.59\ ^{+1}_{-1}$	$-0.60\ ^{+1}_{-1}$	$-0.58\ ^{+1}_{-2}$
χ^2/dof	0.27/2	0.24/2	0.35/2	0.04/2	1.31/2
$B_B(m_b)$	$0.71\ ^{+2}_{-2}$	$0.72\ ^{+2}_{-1}$	$0.70\ ^{+2}_{-2}$	$0.72\ ^{+2}_{-2}$	$0.69\ ^{+4}_{-3}$

Table 4.3: Values for fits to the ratios R_i, $i = L,R,N,S$, for $t_f = -2$ and all smearing types.

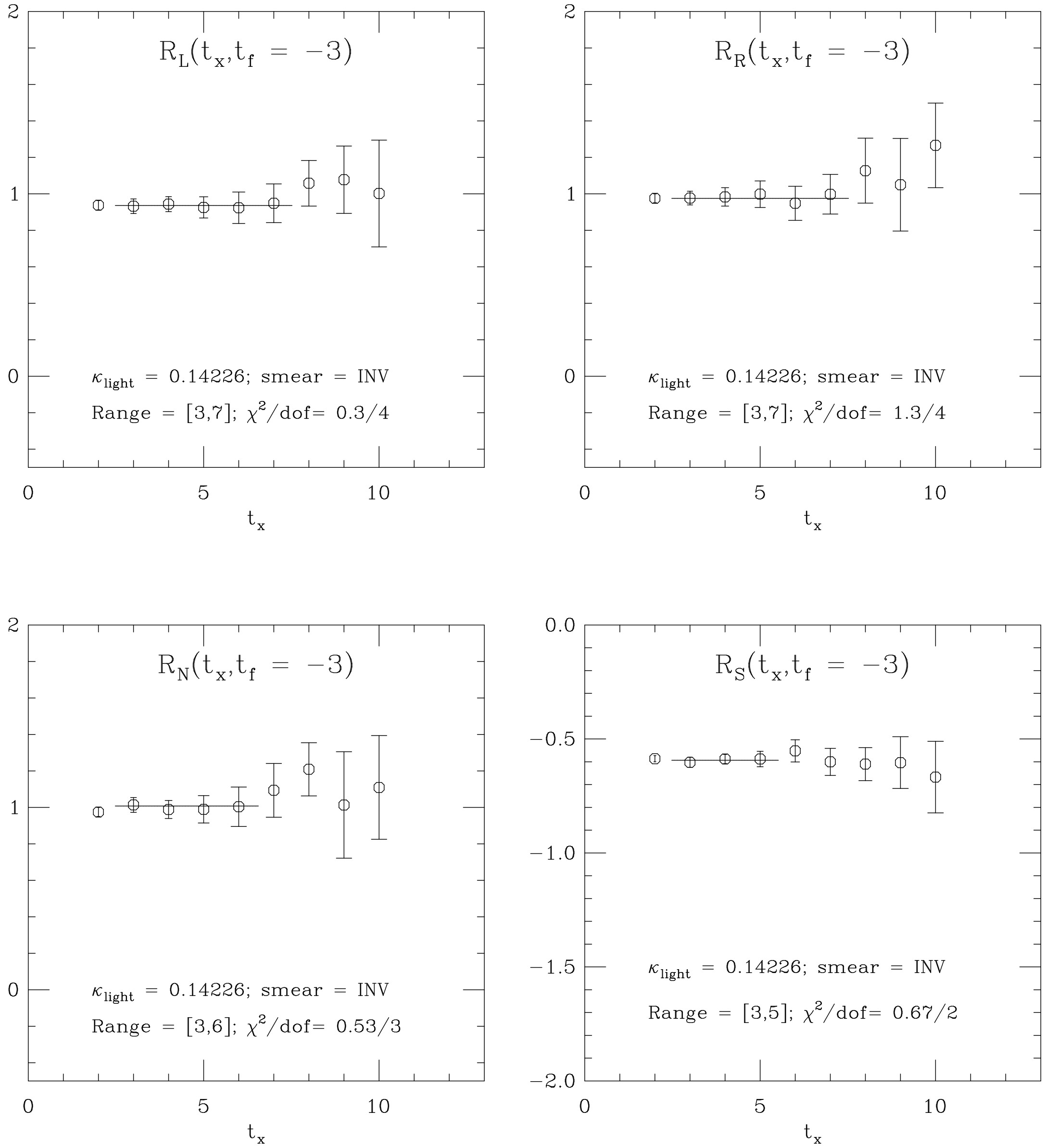

Figure 4.3: Example of fits to R_i, $i = L,R,N,S$, for $t_f = -3$, INV smearing, and at light $\kappa = 0.14226$.

κ	Smearing				
0.14144	EXP	GAU	CUB	DCB	INV
R_L	$0.96\ ^{+2}_{-2}$	$0.97\ ^{+2}_{-3}$	$0.96\ ^{+3}_{-3}$	$0.97\ ^{+2}_{-2}$	$0.95\ ^{+3}_{-4}$
χ^2/dof	1.09/4	1.75/4	2.31/4	1.52/4	0.32/4
R_R	$0.98\ ^{+2}_{-3}$	$0.97\ ^{+2}_{-3}$	$0.97\ ^{+2}_{-3}$	$0.97\ ^{+2}_{-3}$	$0.96\ ^{+3}_{-4}$
χ^2/dof	1.37/4	1.77/4	1.61/4	1.49/4	0.65/4
R_N	$1.02\ ^{+2}_{-4}$	$1.01\ ^{+2}_{-4}$	$1.02\ ^{+3}_{-4}$	$1.02\ ^{+2}_{-3}$	$1.01\ ^{+3}_{-3}$
χ^2/dof	1.98/4	2.24/4	2.05/4	2.17/4	0.46/3
R_S	$-0.61\ ^{+1}_{-1}$	$-0.61\ ^{+1}_{-1}$	$-0.61\ ^{+1}_{-1}$	$-0.61\ ^{+1}_{-1}$	$-0.60\ ^{+1}_{-1}$
χ^2/dof	1.84/2	1.99/2	2.15/2	2.05/2	0.42/2
$B_B(m_b)$	$0.72\ ^{+3}_{-2}$	$0.74\ ^{+2}_{-2}$	$0.72\ ^{+3}_{-3}$	$0.73\ ^{+2}_{-2}$	$0.71\ ^{+3}_{-3}$
0.14226	EXP	GAU	CUB	DCB	INV
R_L	$0.95\ ^{+3}_{-3}$	$0.97\ ^{+3}_{-3}$	$0.95\ ^{+3}_{-3}$	$0.96\ ^{+3}_{-3}$	$0.94\ ^{+3}_{-4}$
χ^2/dof	0.66/4	1.55/4	2.20/4	1.15/4	0.30/4
R_R	$1.00\ ^{+2}_{-3}$	$0.98\ ^{+2}_{-3}$	$0.98\ ^{+2}_{-3}$	$0.99\ ^{+2}_{-3}$	$0.98\ ^{+3}_{-4}$
χ^2/dof	1.72/4	2.02/4	1.86/4	1.80/4	1.28/4
R_N	$1.02\ ^{+2}_{-4}$	$1.01\ ^{+2}_{-4}$	$1.02\ ^{+3}_{-4}$	$1.02\ ^{+2}_{-3}$	$1.01\ ^{+3}_{-4}$
χ^2/dof	2.01/4	2.30/4	2.07/4	2.24/4	0.53/3
R_S	$-0.61\ ^{+2}_{-2}$	$-0.61\ ^{+1}_{-1}$	$-0.61\ ^{+2}_{-2}$	$-0.61\ ^{+2}_{-2}$	$-0.59\ ^{+2}_{-2}$
χ^2/dof	1.32/2	1.56/2	1.59/2	1.51/2	0.67/2
$B_B(m_b)$	$0.71\ ^{+3}_{-3}$	$0.73\ ^{+3}_{-2}$	$0.71\ ^{+4}_{-3}$	$0.72\ ^{+3}_{-3}$	$0.70\ ^{+4}_{-4}$
0.14262	EXP	GAU	CUB	DCB	INV
R_L	$0.93\ ^{+3}_{-3}$	$0.96\ ^{+3}_{-3}$	$0.94\ ^{+4}_{-4}$	$0.95\ ^{+3}_{-3}$	$0.93\ ^{+4}_{-5}$
χ^2/dof	0.41/4	1.20/4	1.74/4	0.68/4	0.26/4
R_R	$1.02\ ^{+3}_{-4}$	$0.99\ ^{+2}_{-1}$	$1.00\ ^{+3}_{-4}$	$1.00\ ^{+3}_{-4}$	$0.99\ ^{+3}_{-3}$
χ^2/dof	2.28/4	2.71/4	2.45/4	2.45/4	2.05/4
R_N	$1.02\ ^{+2}_{-4}$	$1.01\ ^{+2}_{-3}$	$1.02\ ^{+3}_{-4}$	$1.02\ ^{+2}_{-3}$	$1.00\ ^{+3}_{-4}$
χ^2/dof	1.90/4	2.33/4	2.11/4	2.26/4	0.92/4
R_S	$-0.60\ ^{+2}_{-2}$	$-0.61\ ^{+2}_{-1}$	$-0.60\ ^{+2}_{-2}$	$-0.61\ ^{+2}_{-2}$	$-0.59\ ^{+3}_{-2}$
χ^2/dof	1.66/2	1.49/2	1.35/2	1.54/2	0.92/2
$B_B(m_b)$	$0.69\ ^{+3}_{-3}$	$0.72\ ^{+3}_{-3}$	$0.70\ ^{+4}_{-3}$	$0.71\ ^{+3}_{-3}$	$0.69\ ^{+5}_{-5}$

Table 4.4: Values for fits to the ratios R_i, $i = L,R,N,S$, for $t_f = -3$ and all smearing types.

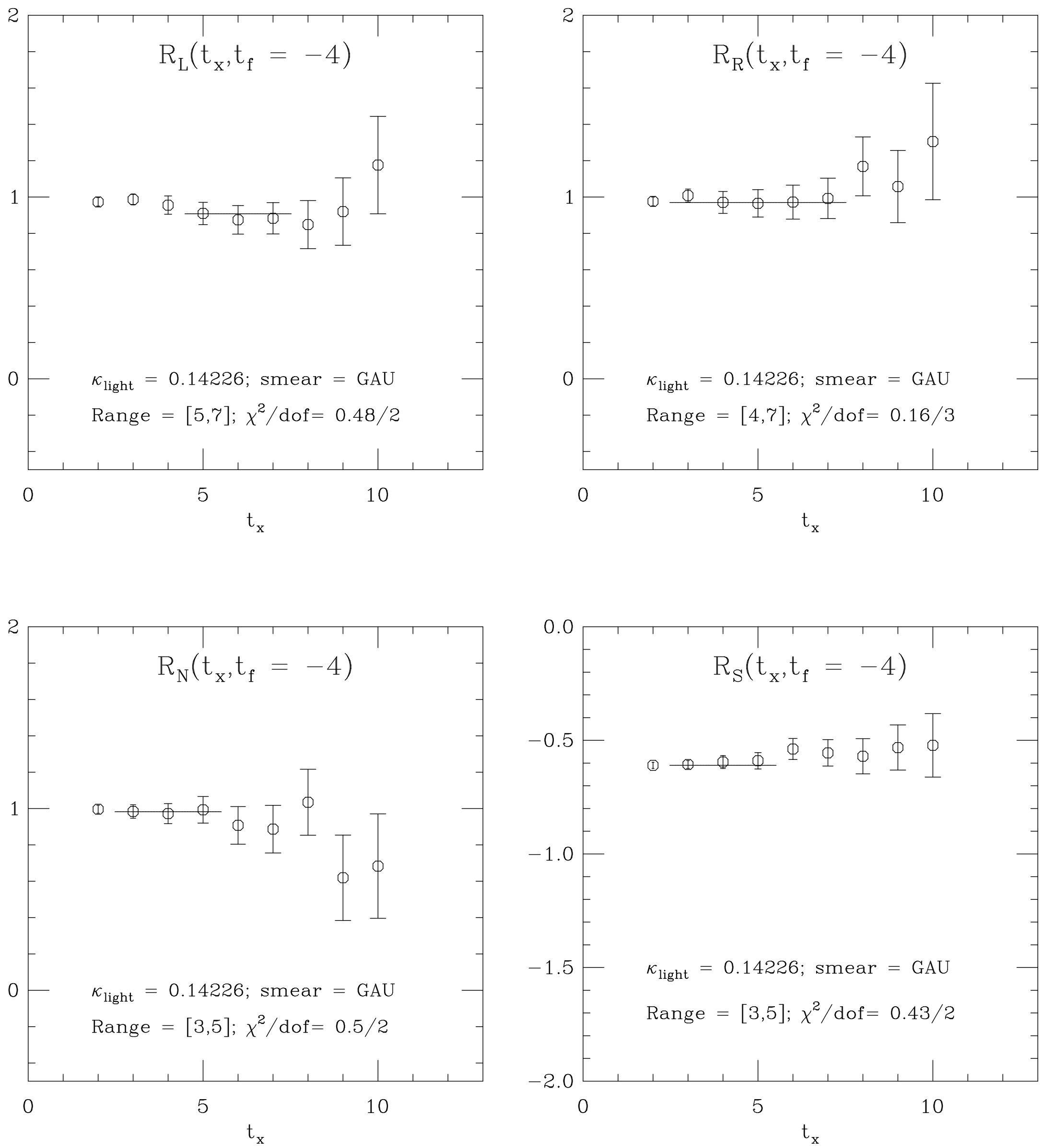

Figure 4.4: Example of fits to R_i, $i = L,R,N,S$, for $t_f = -4$, GAU smearing, and at light $\kappa = 0.14226$.

κ	Smearing				
0.14144	EXP	GAU	CUB	DCB	INV
R_L	$0.90\ ^{+4}_{-6}$	$0.92\ ^{+4}_{-5}$	$0.90\ ^{+5}_{-6}$	$0.91\ ^{+4}_{-5}$	$0.91\ ^{+7}_{-7}$
χ^2/dof	1.18/2	0.68/2	0.71/2	0.90/2	0.90/2
R_R	$0.94\ ^{+7}_{-6}$	$0.95\ ^{+6}_{-5}$	$0.93\ ^{+7}_{-7}$	$0.94\ ^{+6}_{-6}$	$0.92\ ^{+7}_{-8}$
χ^2/dof	0.11/3	0.065/3	0.01/3	0.06/3	0.84/3
R_N	$0.99\ ^{+4}_{-5}$	$0.99\ ^{+3}_{-4}$	$0.99\ ^{+4}_{-5}$	$0.99\ ^{+4}_{-4}$	$1.00\ ^{+4}_{-5}$
χ^2/dof	0.37/2	0.57/2	0.39/2	0.39/2	1.92/3
R_S	$-0.61\ ^{+2}_{-1}$	$-0.61\ ^{+2}_{-1}$	$-0.61\ ^{+2}_{-2}$	$-0.61\ ^{+2}_{-1}$	$-0.60\ ^{+2}_{-1}$
χ^2/dof	0.16/2	0.41/2	0.35/2	0.27/2	0.46/2
$B_B(m_b)$	$0.68\ ^{+6}_{-6}$	$0.70\ ^{+5}_{-5}$	$0.68\ ^{+7}_{-7}$	$0.69\ ^{+6}_{-6}$	$0.68\ ^{+7}_{-6}$
0.14226	EXP	GAU	CUB	DCB	INV
R_L	$0.87\ ^{+8}_{-8}$	$0.91\ ^{+7}_{-7}$	$0.88\ ^{+8}_{-8}$	$0.89\ ^{+7}_{-8}$	$0.90\ ^{+8}_{-7}$
χ^2/dof	0.89/2	0.48/2	0.54/2	0.75/2	0.98/2
R_R	$0.98\ ^{+6}_{-8}$	$0.96\ ^{+6}_{-6}$	$0.95\ ^{+7}_{-8}$	$0.97\ ^{+7}_{-7}$	$0.95\ ^{+8}_{-9}$
χ^2/dof	0.16/3	0.15/3	0.08/3	0.9/3	1.11/3
R_N	$0.98\ ^{+4}_{-5}$	$0.98\ ^{+3}_{-4}$	$0.99\ ^{+5}_{-5}$	$0.98\ ^{+4}_{-4}$	$0.99\ ^{+4}_{-5}$
χ^2/dof	0.25/2	0.50/2	0.28/2	0.29/2	1.22/2
R_S	$-0.60\ ^{+2}_{-2}$	$-0.61\ ^{+2}_{-1}$	$-0.61\ ^{+2}_{-2}$	$-0.61\ ^{+2}_{-2}$	$-0.59\ ^{+2}_{-2}$
χ^2/dof	0.31/2	0.42/2	0.32/2	0.30/2	0.47/2
$B_B(m_b)$	$0.65\ ^{+7}_{-7}$	$0.69\ ^{+6}_{-6}$	$0.66\ ^{+8}_{-8}$	$0.67\ ^{+7}_{-7}$	$0.67\ ^{+8}_{-7}$
0.14262	EXP	GAU	CUB	DCB	INV
R_L	$0.84\ ^{+9}_{-10}$	$0.89\ ^{+8}_{-8}$	$0.85\ ^{+10}_{-9}$	$0.87\ ^{+9}_{-9}$	$0.88\ ^{+10}_{-9}$
χ^2/dof	0.87/2	0.36/2	0.51/2	0.74/2	0.82/2
R_R	$1.03\ ^{+7}_{-10}$	$1.00\ ^{+6}_{-7}$	$0.99\ ^{+8}_{-10}$	$1.01\ ^{+7}_{-8}$	$1.00\ ^{+8}_{-11}$
χ^2/dof	0.18/3	0.22/3	0.12/3	0.10/3	1.45/3
R_N	$0.98\ ^{+4}_{-5}$	$0.98\ ^{+3}_{-4}$	$0.99\ ^{+4}_{-6}$	$0.98\ ^{+4}_{-5}$	$0.98\ ^{+4}_{-5}$
χ^2/dof	0.25/2	0.67/2	0.39/2	0.39/2	1.11/3
R_S	$-0.59\ ^{+3}_{-2}$	$-0.60\ ^{+2}_{-2}$	$-0.60\ ^{+3}_{-2}$	$-0.60\ ^{+2}_{-2}$	$-0.58\ ^{+2}_{-2}$
χ^2/dof	0.75/2	0.61/2	0.45/2	0.56/2	0.54/2
$B_B(m_b)$	$0.62\ ^{+9}_{-8}$	$0.66\ ^{+8}_{-7}$	$0.63\ ^{+10}_{-9}$	$0.65\ ^{+9}_{-8}$	$0.65\ ^{+10}_{-9}$

Table 4.5: Values for fits to the ratios R_i, $i = L,R,N,S$, for $t_f = -4$ and all smearing types.

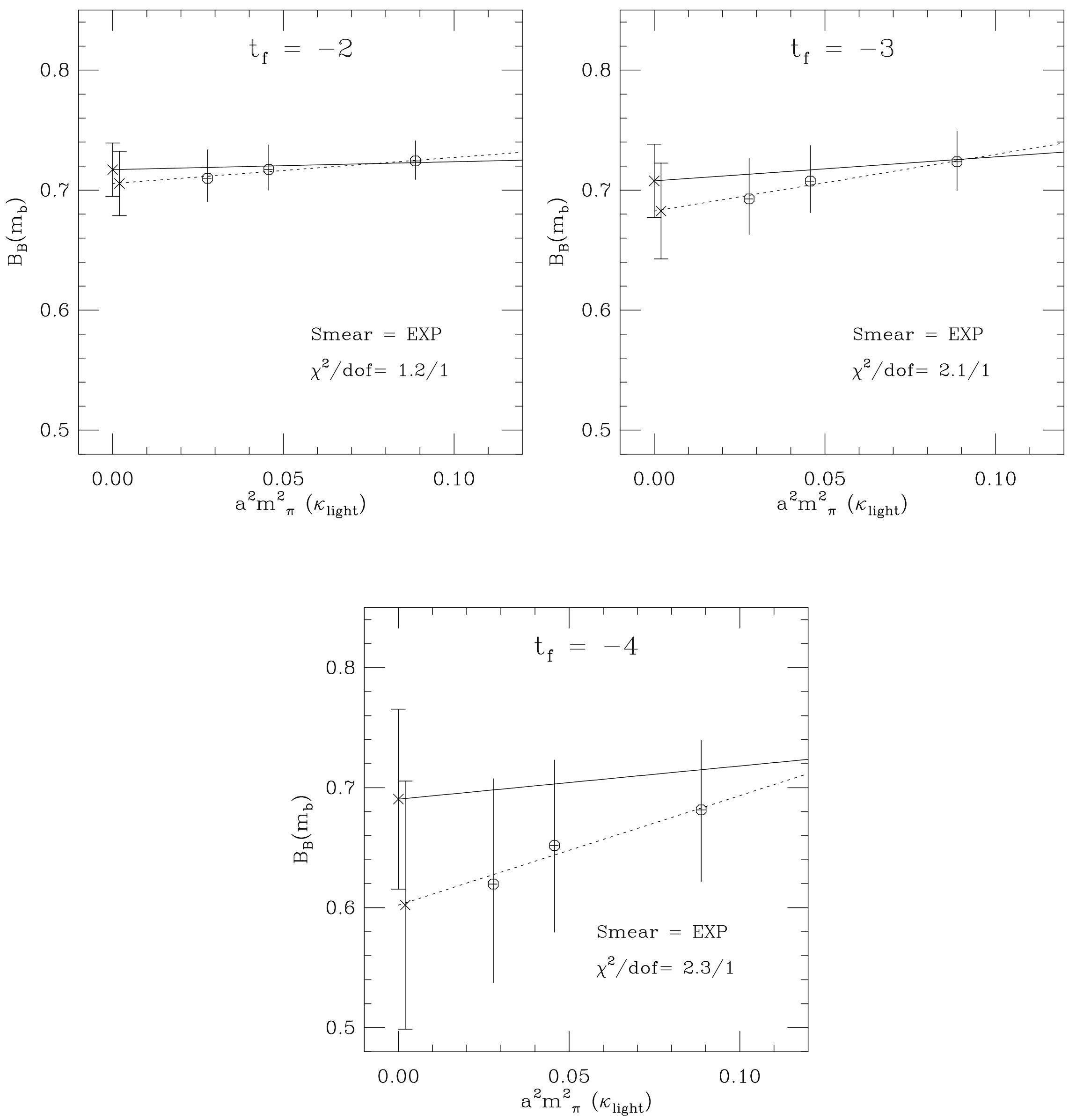

Figure 4.5: Chiral fits for $B_B(m_b)$ from method (a) using EXP smearing at $t_f = -2, -3, -4$. Solid lines are correlated fits and dashed lines are uncorrelated fits. The uncorrelated chiral extrapolated results are slightly shifted in $a^2m_\pi^2$ for clarity. The χ^2/dof is for the correlated fit.

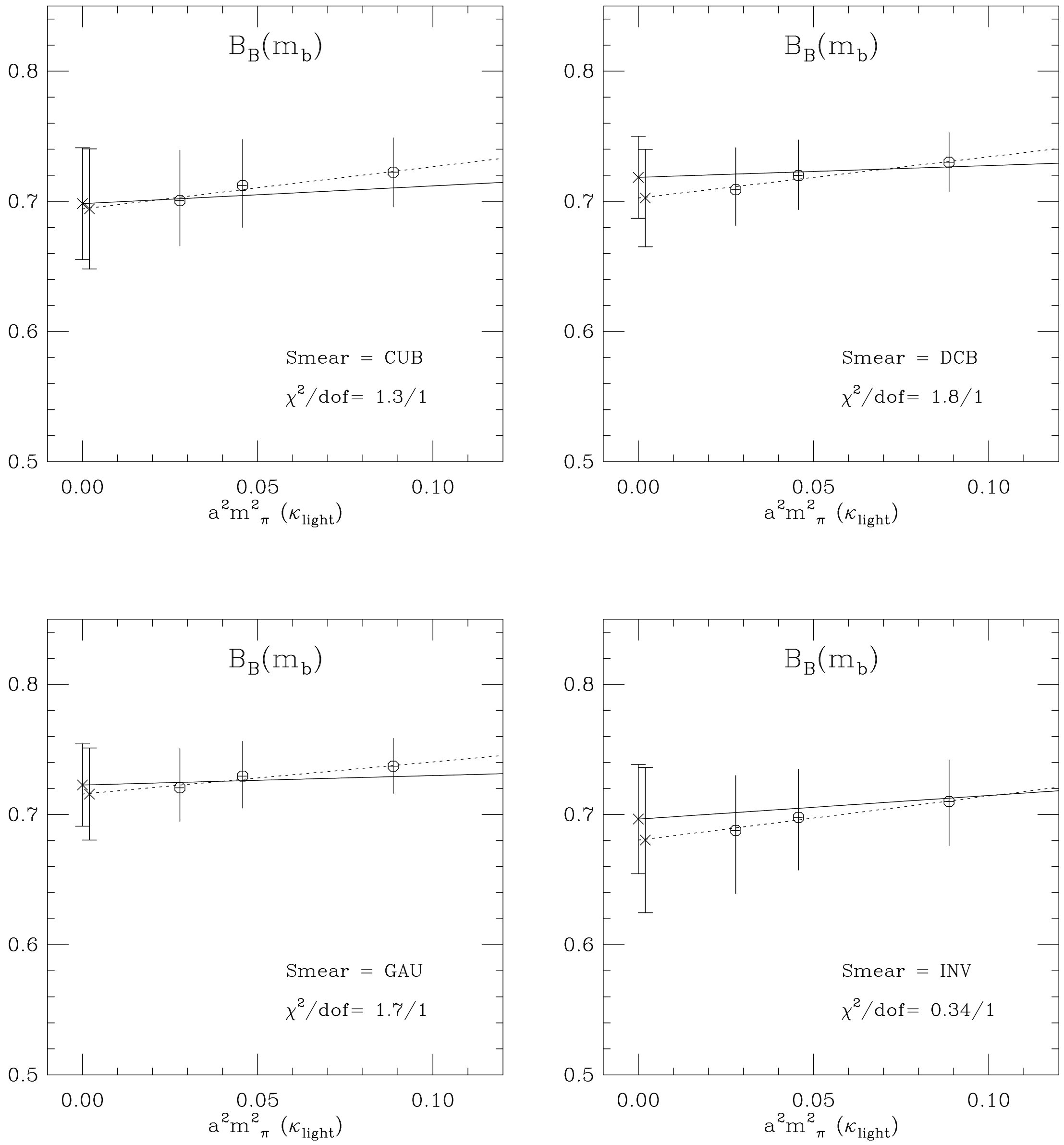

Figure 4.6: Chiral fits for $B_B(m_b)$ from method (a) using CUB, DCB, GAU and INV smearing at $t_f = -3$. Solid lines are correlated fits and dashed lines are uncorrelated fits. The uncorrelated chiral extrapolated results are slightly shifted in $a^2m_\pi^2$ for clarity. The χ^2/dof is for the correlated fit.

	UNCORRELATED			CORRELATED		
$t_f = -2$	κ_s	$\kappa_{\rm crit}$	$\chi^2/{\rm dof}$	κ_s	$\kappa_{\rm crit}$	$\chi^2/{\rm dof}$
EXP	$0.72\ ^{+2}_{-2}$	$0.71\ ^{+3}_{-2}$	0.02/1	$0.72\ ^{+2}_{-2}$	$0.72\ ^{+2}_{-2}$	1.22/1
GAU	$0.73\ ^{+1}_{-1}$	$0.72\ ^{+2}_{-1}$	0.02/1	$0.73\ ^{+2}_{-1}$	$0.73\ ^{+2}_{-2}$	1.67/1
CUB	$0.71\ ^{+2}_{-2}$	$0.70\ ^{+3}_{-3}$	0.02/1	$0.72\ ^{+2}_{-2}$	$0.72\ ^{+2}_{-2}$	1.51/1
DCB	$0.72\ ^{+2}_{-1}$	$0.72\ ^{+2}_{-2}$	0.01/1	$0.73\ ^{+2}_{-2}$	$0.73\ ^{+2}_{-2}$	1.17/1
INV	$0.70\ ^{+3}_{-3}$	$0.68\ ^{+4}_{-4}$	0.02/1	$0.70\ ^{+2}_{-3}$	$0.68\ ^{+3}_{-3}$	1.80/1
$t_f = -3$	κ_s	$\kappa_{\rm crit}$	$\chi^2/{\rm dof}$	κ_s	$\kappa_{\rm crit}$	$\chi^2/{\rm dof}$
EXP	$0.71\ ^{+3}_{-3}$	$0.68\ ^{+4}_{-3}$	0.02/1	$0.72\ ^{+3}_{-2}$	$0.71\ ^{+4}_{-3}$	2.12/1
GAU	$0.73\ ^{+2}_{-2}$	$0.72\ ^{+3}_{-3}$	0.01/1	$0.73\ ^{+3}_{-2}$	$0.72\ ^{+3}_{-3}$	1.70/1
CUB	$0.72\ ^{+3}_{-3}$	$0.69\ ^{+5}_{-4}$	0.01/1	$0.71\ ^{+3}_{-3}$	$0.70\ ^{+4}_{-4}$	1.30/1
DCB	$0.72\ ^{+3}_{-2}$	$0.70\ ^{+4}_{-3}$	0.02/1	$0.72\ ^{+3}_{-2}$	$0.72\ ^{+3}_{-3}$	1.84/1
INV	$0.70\ ^{+4}_{-4}$	$0.68\ ^{+5}_{-5}$	0.004/1	$0.71\ ^{+3}_{-4}$	$0.70\ ^{+4}_{-4}$	0.34/1
$t_f = -4$	κ_s	$\kappa_{\rm crit}$	$\chi^2/{\rm dof}$	κ_s	$\kappa_{\rm crit}$	$\chi^2/{\rm dof}$
EXP	$0.66\ ^{+6}_{-7}$	$0.60\ ^{+10}_{-10}$	0.02/1	$0.71\ ^{+6}_{-6}$	$0.69\ ^{+7}_{-8}$	2.34/1
GAU	$0.69\ ^{+6}_{-6}$	$0.66\ ^{+9}_{-8}$	0.01/1	$0.74\ ^{+5}_{-6}$	$0.73\ ^{+5}_{-7}$	1.85/1
CUB	$0.66\ ^{+8}_{-7}$	$0.62\ ^{+11}_{-9}$	0.01/1	$0.71\ ^{+6}_{-7}$	$0.71\ ^{+7}_{-9}$	2.16/1
DCB	$0.68\ ^{+7}_{-7}$	$0.63\ ^{+10}_{-9}$	0.01/1	$0.72\ ^{+5}_{-6}$	$0.72\ ^{+8}_{-6}$	2.03/1
INV	$0.67\ ^{+8}_{-7}$	$0.64\ ^{+10}_{-9}$	0.01/1	$0.69\ ^{+7}_{-7}$	$0.70\ ^{+8}_{-9}$	1.42/1

Table 4.6: Chiral extrapolated results for $B_B(m_b)$ from method (a) for both correlated and uncorrelated chiral extrapolations.

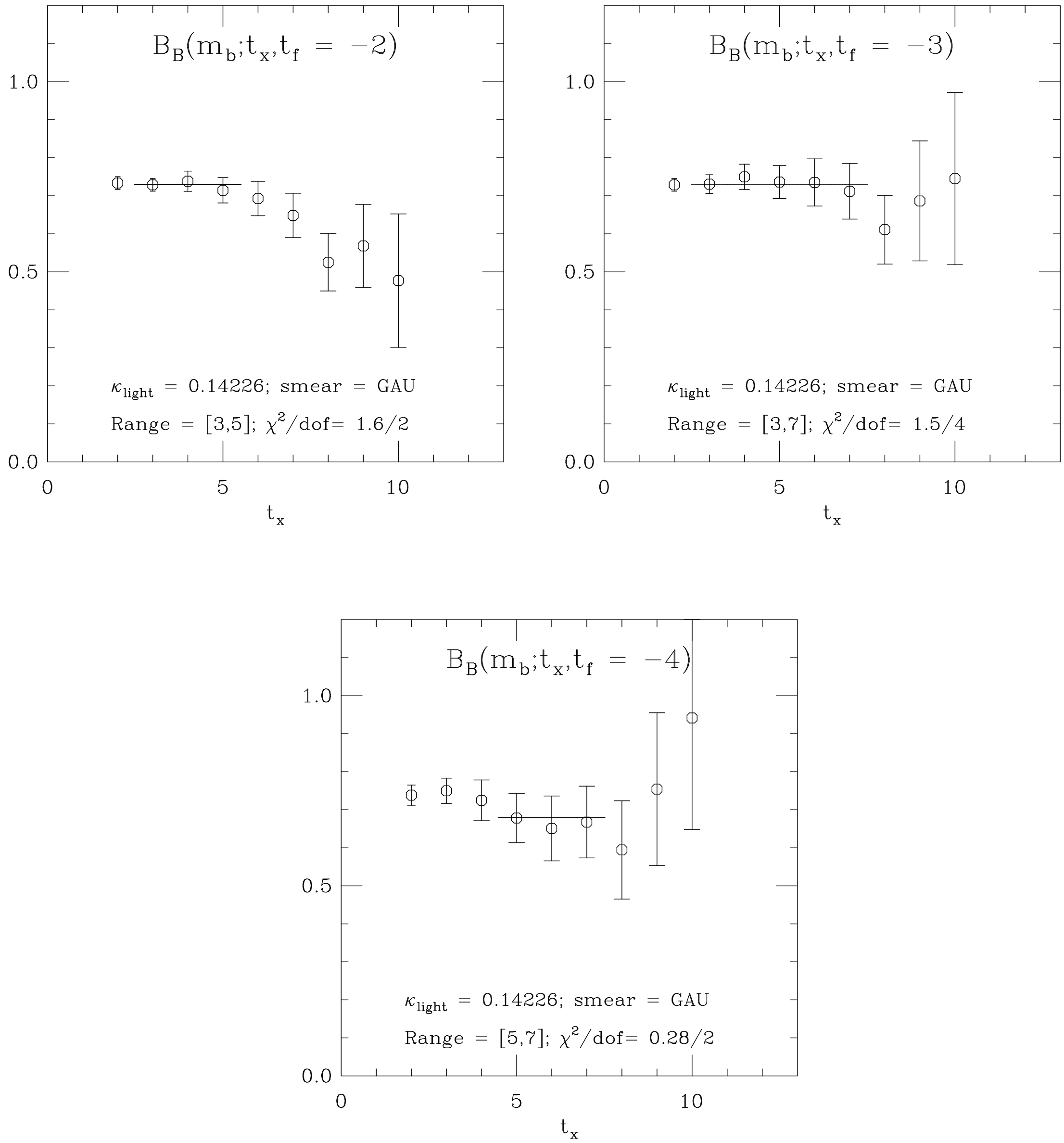

Figure 4.7: Example of fits to $\widetilde{B}_B(m_b; t_x, t_f)$ at $t_f = -2$, -3, -4 using GAU smearing.

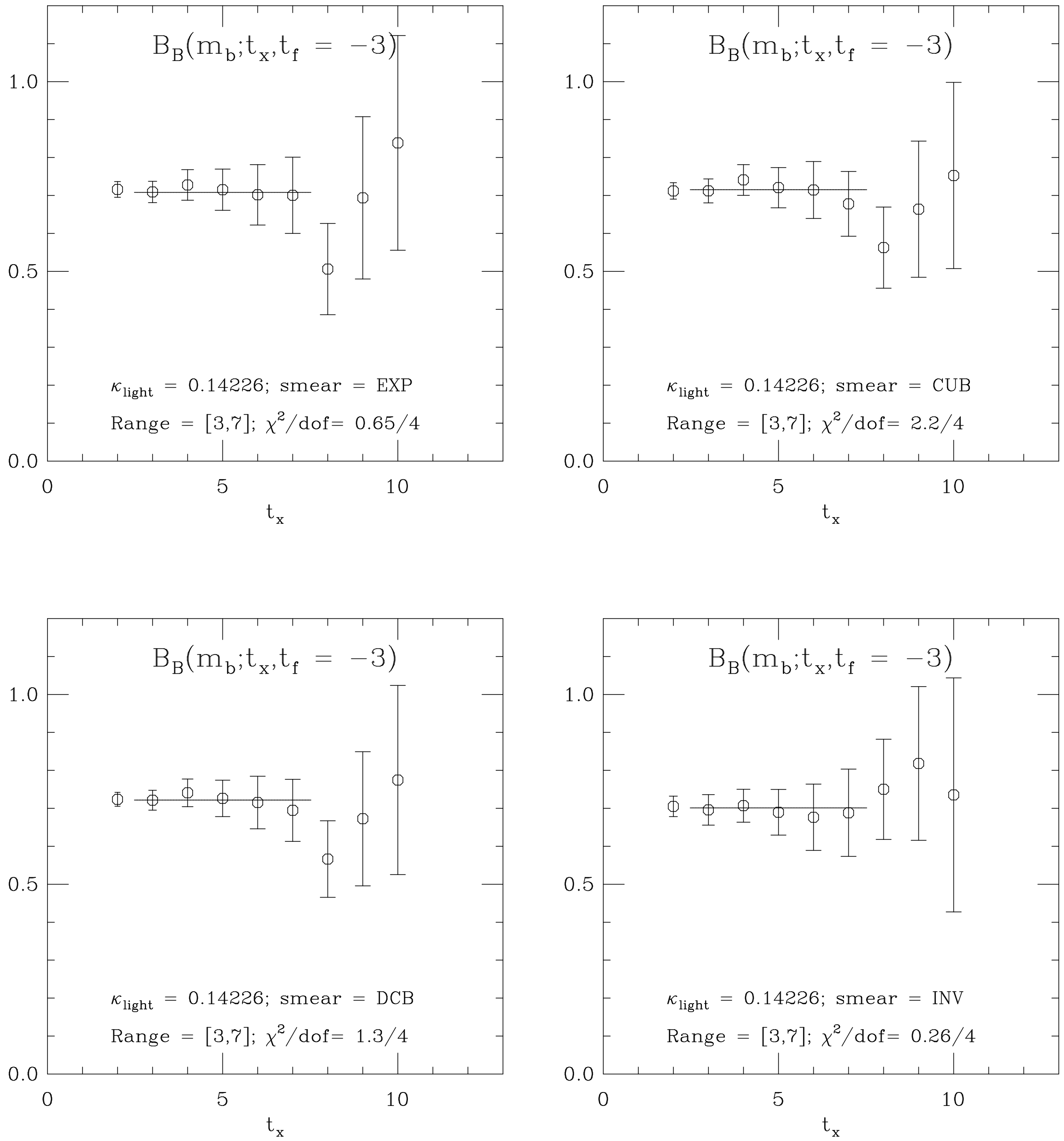

Figure 4.8: Example of fits to $\widetilde{B}_B(m_b; t_x, t_f)$ at $t_f = -3$ for smearing types EXP, CUB, DCB and INV.

	Smearing				
$t_f = -2$	EXP	GAU	CUB	DCB	INV
Ranges	[3–5]	[3–5]	[3–5]	[3–5]	[3–5]
0.14144	$0.72\ ^{+1}_{-2}$	$0.73\ ^{+1}_{-1}$	$0.72\ ^{+2}_{-2}$	$0.73\ ^{+1}_{-1}$	$0.70\ ^{+2}_{-2}$
χ^2/dof	0.99/2	2.64/2	1.24/2	1.98/2	1.45/2
0.14226	$0.72\ ^{+2}_{-2}$	$0.73\ ^{+1}_{-1}$	$0.71\ ^{+2}_{-2}$	$0.73\ ^{+2}_{-2}$	$0.70\ ^{+2}_{-3}$
χ^2/dof	0.34/2	1.60/2	1.62/2	0.95/2	0.76/2
0.14262	$0.71\ ^{+2}_{-2}$	$0.73\ ^{+2}_{-1}$	$0.71\ ^{+2}_{-2}$	$0.72\ ^{+2}_{-2}$	$0.69\ ^{+3}_{-3}$
χ^2/dof	0.92/2	1.10/2	0.88/2	0.68/2	0.30/2
$t_f = -3$	EXP	GAU	CUB	DCB	INV
Ranges	[3–7]	[3–7]	[3–7]	[3–7]	[3–7]
0.14144	$0.73\ ^{+3}_{-2}$	$0.74\ ^{+2}_{-2}$	$0.73\ ^{+3}_{-3}$	$0.73\ ^{+2}_{-3}$	$0.71\ ^{+3}_{-4}$
χ^2/dof	1.37/4	1.86/4	2.49/4	1.79/4	0.27/4
0.14226	$0.71\ ^{+3}_{-2}$	$0.73\ ^{+3}_{-3}$	$0.72\ ^{+4}_{-3}$	$0.72\ ^{+3}_{-3}$	$0.70\ ^{+4}_{-4}$
χ^2/dof	0.65/4	1.50/4	2.23/4	1.30/4	0.26/4
0.14262	$0.69\ ^{+4}_{-3}$	$0.72\ ^{+3}_{-3}$	$0.70\ ^{+2}_{-2}$	$0.71\ ^{+4}_{-3}$	$0.69\ ^{+4}_{-5}$
χ^2/dof	0.18/4	1.10/4	1.77/4	0.70/4	0.33/4
$t_f = -4$	EXP	GAU	CUB	DCB	INV
Ranges	[5–7]	[5–7]	[5–7]	[5–7]	[5–7]
0.14144	$0.67\ ^{+7}_{-7}$	$0.70\ ^{+6}_{-6}$	$0.67\ ^{+7}_{-7}$	$0.66\ ^{+6}_{-6}$	$0.67\ ^{+8}_{-8}$
χ^2/dof	0.29/2	0.38/2	0.32/2	0.39/2	0.87/2
0.14226	$0.65\ ^{+8}_{-8}$	$0.68\ ^{+7}_{-7}$	$0.65\ ^{+8}_{-9}$	$0.66\ ^{+8}_{-8}$	$0.66\ ^{+10}_{-9}$
χ^2/dof	0.1/2	0.28/2	0.20/2	0.27/2	1.00/2
0.14262	$0.62\ ^{+10}_{-10}$	$0.66\ ^{+8}_{-8}$	$0.63\ ^{+10}_{-10}$	$0.64\ ^{+10}_{-9}$	$0.63\ ^{+11}_{-9}$
χ^2/dof	0.07/2	0.14/2	0.18/2	0.22/2	0.85/2

Table 4.7: Values for fits to $\widetilde{B}_B(m_b; t_x, t_f)$, for $t_f = -2, -3, -4$.

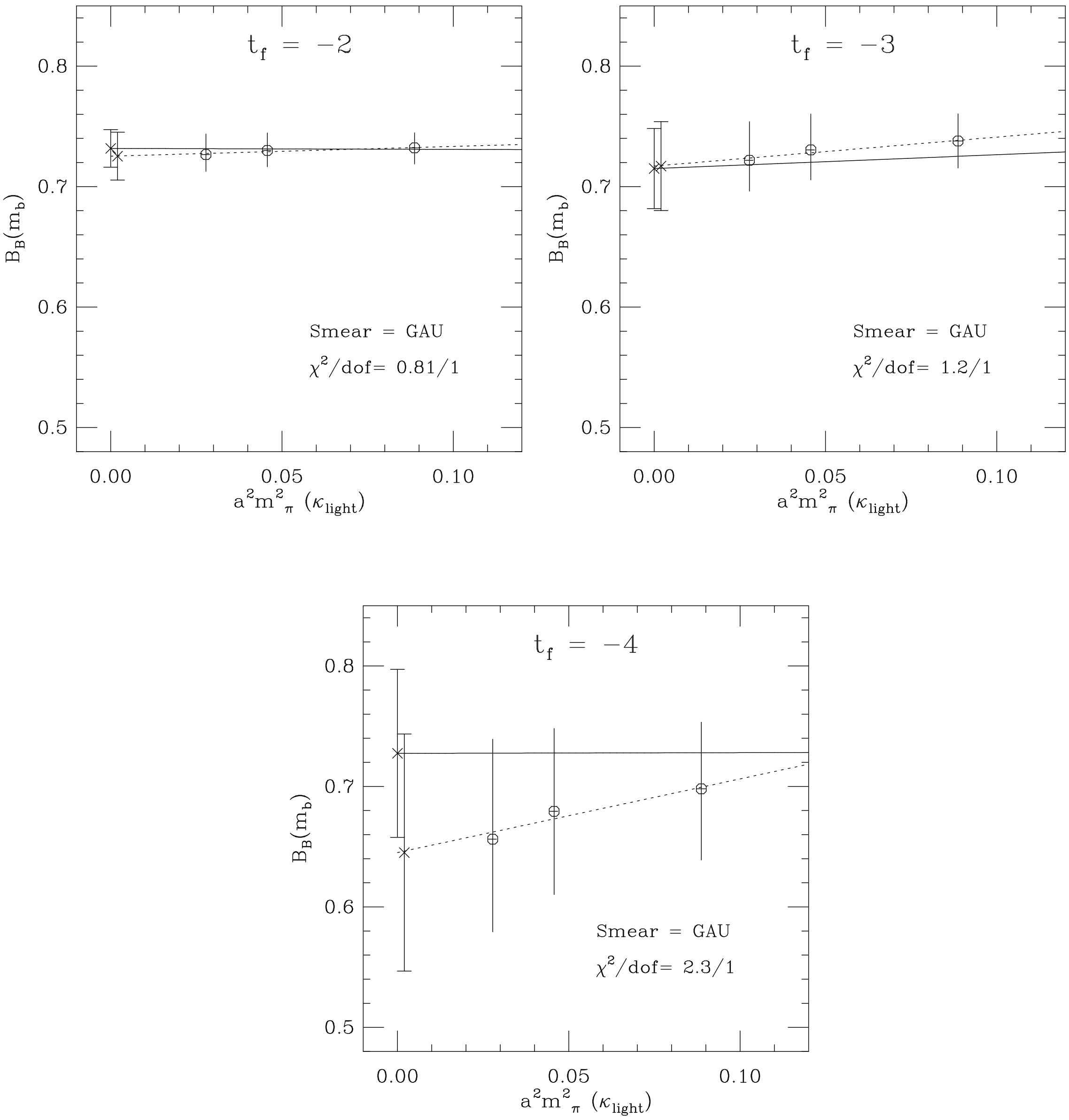

Figure 4.9: Chiral fits for $B_B(m_b)$ from method (b) using GAU smearing at $t_f = -2, -3, -4$. Solid lines are correlated fits and dashed lines are uncorrelated fits. The uncorrelated chiral extrapolated results are slightly shifted in $a^2m_\pi^2$ for clarity. The χ^2/dof is for the correlated fit.

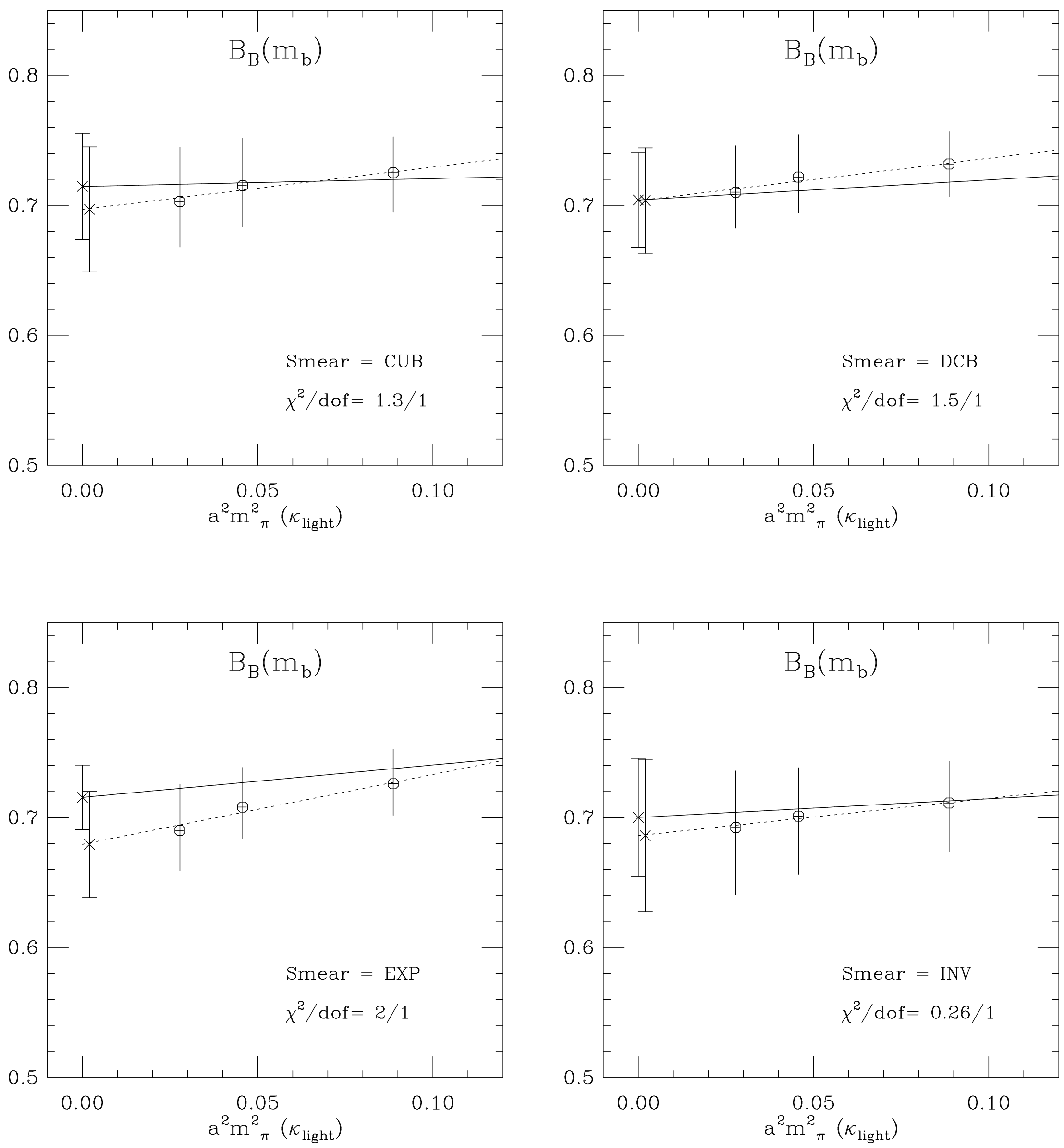

Figure 4.10: Chiral fits for $B_B(m_b)$ from method (a) using CUB, DCB, EXP and INV smearing at $t_f = -3$. Solid lines are correlated fits and dashed lines are uncorrelated fits. The uncorrelated chiral extrapolated results are slightly shifted in $a^2m_\pi^2$ for clarity. The χ^2/dof is for the correlated fit.

	UNCORRELATED			CORRELATED		
$t_f = -2$	κ_s	$\kappa_{\rm crit}$	$\chi^2/{\rm dof}$	κ_s	$\kappa_{\rm crit}$	$\chi^2/{\rm dof}$
EXP	$0.72\ ^{+2}_{-2}$	$0.71\ ^{+2}_{-2}$	0.008/1	$0.72\ ^{+2}_{-2}$	$0.71\ ^{+2}_{-2}$	0.63/1
GAU	$0.73\ ^{+1}_{-1}$	$0.73\ ^{+2}_{-1}$	0.009/1	$0.73\ ^{+1}_{-1}$	$0.73\ ^{+1}_{-2}$	0.80/1
CUB	$0.71\ ^{+2}_{-2}$	$0.70\ ^{+2}_{-2}$	0.01/1	$0.72\ ^{+2}_{-2}$	$0.72\ ^{+2}_{-2}$	1.22/1
DCB	$0.73\ ^{+1}_{-2}$	$0.72\ ^{+2}_{-2}$	0.006/1	$0.73\ ^{+2}_{-1}$	$0.72\ ^{+2}_{-2}$	0.51/1
INV	$0.70\ ^{+2}_{-3}$	$0.69\ ^{+3}_{-4}$	0.01/1	$0.72\ ^{+2}_{-2}$	$0.71\ ^{+2}_{-3}$	0.98/1
$t_f = -3$	κ_s	$\kappa_{\rm crit}$	$\chi^2/{\rm dof}$	κ_s	$\kappa_{\rm crit}$	$\chi^2/{\rm dof}$
EXP	$0.72\ ^{+3}_{-2}$	$0.68\ ^{+4}_{-3}$	0.04/1	$0.73\ ^{+3}_{-2}$	$0.72\ ^{+4}_{-3}$	1.96/1
GAU	$0.73\ ^{+3}_{-2}$	$0.72\ ^{+4}_{-3}$	0.03/1	$0.72\ ^{+3}_{-2}$	$0.71\ ^{+4}_{-4}$	1.25/1
CUB	$0.72\ ^{+3}_{-3}$	$0.70\ ^{+5}_{-4}$	0.02/1	$0.72\ ^{+3}_{-3}$	$0.71\ ^{+4}_{-4}$	1.31/1
DCB	$0.73\ ^{+3}_{-3}$	$0.70\ ^{+4}_{-3}$	0.02/1	$0.71\ ^{+3}_{-3}$	$0.70\ ^{+4}_{-3}$	1.50/1
INV	$0.71\ ^{+3}_{-4}$	$0.69\ ^{+5}_{-6}$	0.003/1	$0.71\ ^{+3}_{-4}$	$0.70\ ^{+4}_{-4}$	0.26/1
$t_f = -4$	κ_s	$\kappa_{\rm crit}$	$\chi^2/{\rm dof}$	κ_s	$\kappa_{\rm crit}$	$\chi^2/{\rm dof}$
EXP	$0.66\ ^{+7}_{-7}$	$0.60\ ^{+10}_{-10}$	0.01/1	$0.70\ ^{+6}_{-6}$	$0.68\ ^{+8}_{-9}$	1.03/1
GAU	$0.69\ ^{+6}_{-6}$	$0.65\ ^{+9}_{-8}$	0.01/1	$0.73\ ^{+5}_{-6}$	$0.73\ ^{+6}_{-7}$	2.25/1
CUB	$0.66\ ^{+8}_{-8}$	$0.61\ ^{+12}_{-10}$	0.01/1	$0.72\ ^{+6}_{-7}$	$0.72\ ^{+7}_{-9}$	1.45/1
DCB	$0.67\ ^{+7}_{-7}$	$0.63\ ^{+10}_{-10}$	0.01/1	$0.71\ ^{+6}_{-6}$	$0.71\ ^{+7}_{-8}$	1.86/1
INV	$0.66\ ^{+9}_{-8}$	$0.63\ ^{+12}_{-10}$	0.008/1	$0.67\ ^{+8}_{-8}$	$0.67\ ^{+9}_{-10}$	0.88/1

Table 4.8: Chiral extrapolated results for $B_B(m_b)$ from method (b) for both correlated and uncorrelated chiral extrapolations.

The plateaux in $R_i(t_x, t_f)$ are longest and most stable for $t_f = -3$. However, fits to the plateaux at $t_f = -2, -4$ are statistically consistent with those at $t_f = -3$. The data and fit values at $t_f = -2$ have smaller errors but the fits generally have a higher χ^2/dof. In particular, R_R, which is fit over the same range for all t_f, has a χ^2/dof much higher for $t_f = -2$ than at $t_f = -3$. Going to $t_f = -4$ the data and fit values have larger errors than at $t_f = -3$, and are slightly shifted to lower values. This is particularly noticeable for R_L. This is mainly because the fit range has been moved to higher values in t_x compared to the cases of $t_f = -2, -3$. Fitting R_L with the same fit ranges as at $t_f = -2, -3$ gave slightly more consistent results, but the plateaux were not as flat and the χ^2/dof was higher.

The case is much the same for $\widetilde{B}_B(m_b; t_x, t_f)$, though the plots in this case seem to show more unambiguously that $t_f = -3$ gives the best results. There is excellent consistency between the values of $B_B(m_b)$ at each κ-value extracted using both methods (a) and (b). However, method (a) is preferable. It allows one greater flexibility to fit the individual R_i in their correct plateau regions. Also the plateaux at $t_f = -2, -4$ for $\widetilde{B}_B$ are shorter than the plateaux for some of the individual R_i at the same fixed times.

There is remarkable consistency in the results across the different smearings used. This gives one good confidence that the ground state has been correctly isolated in these plateaux.

The chiral extrapolations for $t_f = -2, -3$ show greater consistency between correlated and uncorrelated fits than for $t_f = -4$. This is true for all smearings and fitting methods. Some of the correlated chiral extrapolations have a negative slope, albeit small. In fact the chiral extrapolations show the behaviour of $B_B(m_b)$ with light κ-value to be consistent with $B_B(m_b)$ being independent of the light quark mass.

At $t_f = -3$ the chiral extrapolations for all smearings give statistically compatible results, though INV smearing gives the lowest χ^2/dof for the correlated fits. Hence in quoting a best result for $B_{B_d}(m_b)$ I take the value extracted using method (a) for INV smearing. This gives

$$B_{B_d}(m_b) = 0.70 \ {}^{+4}_{-4}(\mathrm{stat}) \ {}^{+3}_{-7}(\mathrm{syst}) \tag{4.20}$$

$$B_{B_s}(m_b) = 0.71 \ {}^{+3}_{-4}(\mathrm{stat}) \ {}^{+3}_{-5}(\mathrm{syst}) \tag{4.21}$$

where the systematic error quoted is estimated from the spread of values over different smearings, differences between correlated and uncorrelated chiral extrapolations, different fitting methods and different fixed times, t_f. The RG invariant bag parameter is given by

$$B_B = [\alpha_{\overline{MS}}(m_b)]^{-2/23} B_B(m_b) \simeq 1.43 B_B(m_b) \tag{4.22}$$

for five active quark flavours and using $\Lambda^{(4)}_{\overline{MS}} = 250$ MeV and $m_b = 5$ GeV. So,

$$B_{B_d} = 1.00 \ {}^{+6}_{-6}(\mathrm{stat}) \ {}^{+5}_{-10}(\mathrm{syst}) \tag{4.23}$$

$$B_{B_s} = 1.02 \ {}^{+5}_{-6}(\mathrm{stat}) \ {}^{+5}_{-7}(\mathrm{syst}). \tag{4.24}$$

This calculated value of B_B is consistent with the vacuum saturation approximation. Indeed, the lattice matrix elements of O_L, O_R and O_N also give values consistent with 1.0.

However, these results are changed if the set of values for the matching factors as in equation (4.11) is used. This gives

$$B_{B_d}(m_b) = 0.87 \ {}^{+4}_{-5}(\mathrm{stat}) \ {}^{+3}_{-7}(\mathrm{syst}) \tag{4.25}$$

$$B_{B_s}(m_b) = 0.88 \ {}^{+3}_{-4}(\mathrm{stat}) \ {}^{+3}_{-5}(\mathrm{syst}) \tag{4.26}$$

again with the central value taken for INV smearing at $t_f = -3$, with the RG invariant parameters

$$B_{B_d} = 1.25 \ {}^{+6}_{-7}(\mathrm{stat}) \ {}^{+6}_{-11}(\mathrm{syst}) \tag{4.27}$$

$$B_{B_s} = 1.27 \ {}^{+5}_{-6}(\text{stat}) \ {}^{+6}_{-8}(\text{syst}). \tag{4.28}$$

This is a sizeable change $\sim 25\%$. It should also be noted that some uncertainty arises in the values of the Z_i due to various possible choices of $\alpha_{\overline{MS}}(a^{-1})$ and $\alpha_{\text{latt}}(a^{-1})$, but these induce changes in the final values for B_B less than the statistical errors.

So it would appear the greatest uncertainty in extracting a value for B_B is the use of one-loop perturbative matching. The systematics of performing the calculation seem to be under control, given the good agreement across fit ranges and smearings used. It would certainly be desirable if these matching factors were determined to higher order in perturbation theory, or better still, from a non-perturbative method as described in [86].

Finally, B_B has also been calculated at $\beta = 6.4$ using propagating heavy Wilson quarks [87]. Their simulation was performed with heavy quarks around the mass of the c quark and extrapolating their result to the mass of the b quark they find a value $B_B = 1.16 \pm 0.07$. Given the large uncertainty induced by the ambiguity in the matching factors this result is not incompatible with the result in this work.

Chapter 5

Conclusions

I conclude with a brief summary of the main findings of this work. The ultimate aim of lattice calculations is the extraction of parameters of importance for high energy phenomenology. To this end I also briefly discuss the phenomenological implications of the results presented in this work.

5.1 Summary of Results

In chapters 3 and 4 I presented calculations of the leptonic decay constant of the B meson, f_B, and the "bag" parameter of $\bar{B}^0 - B^0$ mixing, B_B, with the heavy quark constituent of the B meson treated in the static approximation. The main numerical results are

$$
\begin{aligned}
f_B^{\mathrm{static}} &= 268 \; {}^{+14}_{-11}(\mathrm{stat}) \; {}^{+28}_{-27}(\mathrm{syst}) \;\; \mathrm{MeV} && (5.1)\\
\frac{f_{B_s}}{f_{B_d}} &= 1.17 \; {}^{+2}_{-2}(\mathrm{stat}) && (5.2)\\
B_{B_d} &= 1.00 \; {}^{+6}_{-6}(\mathrm{stat}) \; {}^{+5}_{-10}(\mathrm{syst}) && (5.3)\\
B_{B_s} &= 1.02 \; {}^{+5}_{-6}(\mathrm{stat}) \; {}^{+5}_{-7}(\mathrm{syst}) && (5.4)\\
M_{B_s} - M_{B_d} &= 90 \; {}^{+8}_{-11}(\mathrm{stat}) \; {}^{+16}_{-17}(\mathrm{syst}) \;\; \mathrm{MeV}\,. && (5.5)
\end{aligned}
$$

The value of f_B^{static} comes from a value for the lattice matrix element of

$$Z_L = 0.113 \; {}^{+6}_{-5}. \tag{5.6}$$

and using $Z_A = 0.78$ and $a^{-1} = 2.9(2) GeV$.

These final results can be combined to give the parameters

$$f_{B_d}\sqrt{B_{B_d}} = 268 \ {}^{+15}_{-13}(\text{stat}) \ {}^{+28}_{-27}(\text{syst}) \ \text{MeV} \tag{5.7}$$

$$\frac{f^2_{B_s}B_{B_s}}{f^2_{B_d}B_{B_d}} = 1.34 \ {}^{+\ 4}_{-\ 4}(\text{stat}) \ {}^{+\ 5}_{-\ 4}(\text{syst}), \tag{5.8}$$

those which are relevant to the phenomenology of $\bar{B}^0 - B^0$ mixing.

As has been stressed throughout this thesis, the main problem in calculating static-light matrix elements is accurately isolating the ground state in the large time behaviour of correlators. The only way to do this is to use some technique to enhance the overlap of operators with the ground state. One such technique is smearing. One of the purposes of this study was to investigate the effectiveness of different smearing methods in isolating the ground state. It is important to show that one can construct smearing functions that do this job properly and also that there is consistency between different smearing methods – smearing, after all, is only a trick, the effects of which should not be seen in the final results. The results in chapter 3 satisfy both these aims. There is good agreement across all the smearing types used, particularly between exponential smearing in the Coulomb gauge and gauge invariant Jacobi smearing. This consistency between using a gauge fixed and a gauge covariant smearing function is quite encouraging.

Comparing the results of this work and those of other groups (see figure 3.15) it would appear that the systematic errors in the determination of the lattice matrix element, Z_L, are now under reasonable control. Also, some of these groups use very different smearing methods from those presented in this work. The greatest uncertainty in extracting a value for f_B^{static} now seems to lie with the value of Z_A and the choice of scale, a^{-1}. It is particularly important that any ambiguities in the matching factor, Z_A, be sorted out if static results are to be properly compared with those determined using the heavy quark treated according to Wilson/SW-clover fermions or NRQCD.

The calculation of B_B in chapter 4 is one of the few lattice calculations of this quantity. This study shows that the systematics of performing the lattice calculation again seem to be under control. There is good agreement between the different smearing methods and across the different fitting ranges. Again the main uncertainty in extracting a value for B_B lies in the matching of the lattice and continuum theories. In this case the uncertainty is quite large, with two different ways of implementing the same one-loop matching giving rise to a $\sim 25\%$ change in the final results. The quoted final result agrees with the vacuum saturation hypothesis. However, there can be no real confidence about this result until such time as improved matching factors are calculated, be it to higher loops or, preferably, non-perturbatively.

5.2 Phenomenological Implications

It is not really feasible to use the result for $f_B\sqrt{B_B}$ for phenomenology. Firstly, the calculated result suffers from the uncertainties discussed in the last section, namely ambiguities in the perturbative matching coefficients and errors in the scale. More importantly the result is only valid in the static approximation. It is well known from many lattice simulations that the scaling law for $f_P\sqrt{M_P}$ is broken by $1/M_P$ corrections $\sim 10\%$ at the mass of the B meson [50]. The only direct usefulness for the quoted result is in combination with results using Wilson/SW-clover heavy quarks or NRQCD, allowing one to interpolate between these results and the static point, finally giving a value at M_B. Even at that there are still further systematic uncertainties that need to be taken into account, such as the need to extrapolate the result to infinite volume and zero lattice spacing, and, of course, the effects of quenching.

However, it is expected that many of these systematic uncertainties will cancel in ratios, such as $f_{B_s}^2 B_{B_s}/f_{B_d}^2 B_{B_d}$. It is this ratio which is important when comparing $\bar{B}_d^0 - B_d^0$ and $\bar{B}_s^0 - B_s^0$ mixing. Recall from chapter 1 the relation

$$\frac{x_s}{x_d} = \frac{\tau_{B_s} f_{B_s}^2 B_{B_s} M_{B_s}^2}{\tau_{B_d} f_{B_d}^2 B_{B_d} M_{B_d}^2}\left|\frac{V_{ts}}{V_{td}}\right|^2 . \tag{5.9}$$

Using the results quoted above this gives

$$\frac{x_s}{x_d} = (1.38 \pm 0.16) \left|\frac{V_{ts}}{V_{td}}\right|^2 \tag{5.10}$$

where $\tau_{B_d} = 1.53 \pm 0.09\,\text{ps}$ and $\tau_{B_s} = 1.54 \pm 0.14\,\text{ps}$ [12] have been used. The mixing parameter x_d has been measured by several groups, with a world average

$$x_d = 0.78 \pm 0.05 \tag{5.11}$$

and so given a measurement of x_s then an estimate of $|V_{ts}/V_{td}|^2$ is possible. However, x_s has not been reliably measured yet. Conversely, given an estimate of $|V_{ts}/V_{td}|^2$ a prediction of the expected x_s can be made.

Making an estimate of $|V_{ts}/V_{td}|^2$ requires several experimental and theoretical inputs. Amongst these are the experimental value for ϵ_K, the CP violating parameter in the K-system (see chapter 1), an estimate of the bag parameter of $\bar{K} - K$ mixing, B_K, and a value for the product $f_B\sqrt{B_B}$. Ali and London [12] have recently performed a study of the dependence of the Wolfenstein parameters ρ and η with a variation in the input values of B_K and $f_B\sqrt{B_B}$, for a given experimental value of $|\epsilon_K|$. Note that $|V_{ts}/V_{td}|^2$ is related to ρ and η through

$$\left|\frac{V_{td}}{V_{ts}}\right|^2 = \lambda^2(1 - 2\rho + \rho^2 + \eta^2) \tag{5.12}$$

where $\lambda \equiv |V_{us}| = 0.2205 \pm 0.0018$ [5]. The results of their study show that there is still a great uncertainty in the location of the apex of the unitarity triangle (ρ, η) due to uncertainties in the given values of B_K and $f_B\sqrt{B_B}$. From their fits they quote best values

$$(\rho, \eta) = (-0.12, 0.34) \tag{5.13}$$

corresponding to $B_K = 0.8$ and $f_B\sqrt{B_B} = 180$ MeV. This gives a value

$$\left|\frac{V_{td}}{V_{ts}}\right| = 0.26\,. \tag{5.14}$$

Putting this into equation (5.10) this gives the rather high value

$$\frac{x_s}{x_d} = 20.2 \pm 2.4\,. \tag{5.15}$$

The effect on this result of varying the value of $f_B\sqrt{B_B}$ can also be investigated. This is shown in figure 5.1 where B_K has been fixed to the "best" value used by Ali and London, $B_K = 0.8 \pm 0.2$. This value is in good agreement with recent estimates from lattice calculations [88].

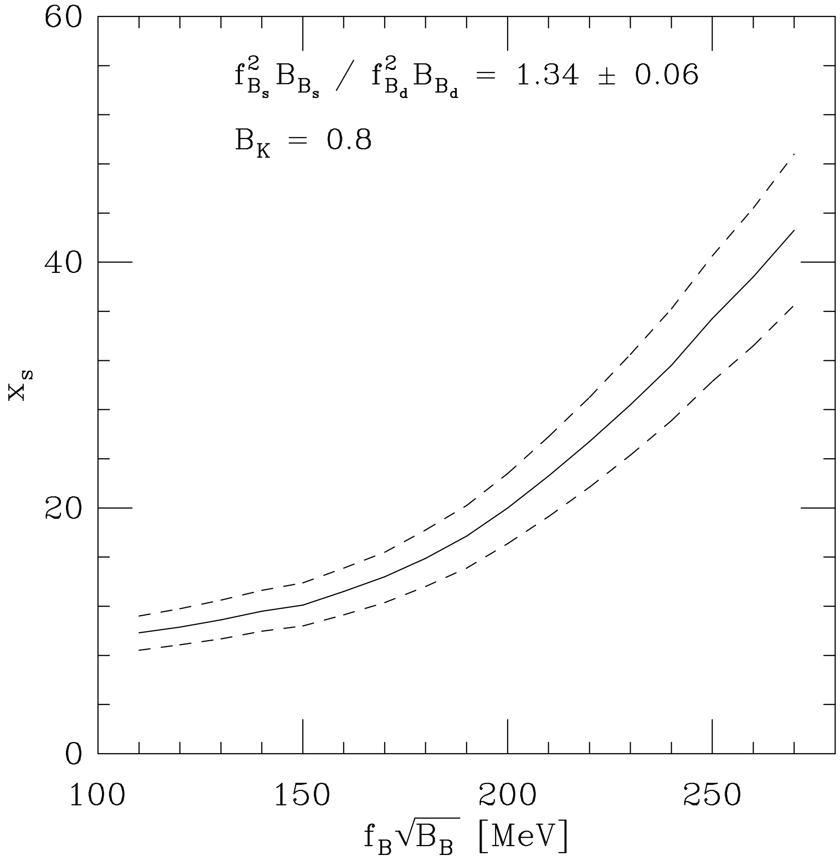

Figure 5.1: The mixing parameter x_s as a function of $f_B\sqrt{B_B}$ for $B_K = 0.8$ and with the value quoted in equation (5.10). The dashed line represents the errors at the 68% confidence level.

This plot shows that higher values of $f_B\sqrt{B_B}$ result in unmeasurably large values of x_s. The results of the study in [12] also suggest that $f_B\sqrt{B_B} = 270$ MeV is the maximum allowed value at $B_K = 0.8$. It should be noted that these results are quite sensitive to the value of B_K used.

In conclusion, the lattice is a useful tool in extracting phenomenologically important parameters in B physics. There are still many uncertainties in the final lattice values but it is hoped that these uncertainties will be understood and brought under control in the next few years. Only then can the lattice set firm constraints on the elements of the CKM matrix and perhaps point us in the direction of new physics beyond the Standard Model.

Appendix A

Statistical Fitting

Consider a two-point function $C(t)$. The lattice simulation yields data $C_k(t_i)$ for $k = 1, \cdots, N$ and $i = 1, \cdots, T$ where N is the number of configurations and T is the temporal extent of the lattice. At each timeslice, t_i, the configuration average is

$$\bar{C}(t_i) = \frac{1}{N} \sum_{k=1}^{N} C_k(t_i) \tag{A.16}$$

with variance

$$\sigma_C^2(t_i) = \frac{1}{N(N-1)} \sum_{k=1}^{N} \Big(C_k(t_i) - \bar{C}(t_i) \Big)^2 \tag{A.17}$$

Normally one wants to fit this two-point function to some functional form, $f(t) = a \exp(-b\,t)$ for example. A general way to do this is to minimize the χ^2-function

$$\chi^2 = \sum_{t_i} \left(\frac{f(t_i) - \bar{C}(t_i)}{\sigma_C(t_i)} \right)^2 \tag{A.18}$$

to obtained the best-fit parameters a and b. The sum is over the number of timeslices being used in the fit. An estimate of how good the fit of this functional form is to the data is given by $\chi^2_{\rm min}$/d.o.f where d.o.f is the number of degrees of freedom in the fit; d.o.f $= q - r$ where q is the number of timeslices in the fit and r is the number of free parameters in the fit function. A value $\chi^2_{\rm min}$/d.o.f ~ 1 indicates a good fit. In this work the Marquardt-Levenberg algorithm is used to perform the minimum χ^2 fitting [89].

There are two things to note about the above. Firstly, the form of the χ^2 given ignores any possible correlations between the $C(t_i)$ calculated on different timeslices. Usually these will be correlated, so uncorrelated fitting may give an erroneous fit. Secondly, what are the errors on the best-fit parameters ? In principle, one should repeat the measurements and subsequent fits on different configuration samples. This would give a spread of values for the fit parameters from which a variance could be calculated.

The first issue can be resolved by using a correlated χ^2-function, defined as

$$\chi^2 = \sum_{t_i,t_j} \left[f(t_i) - \bar{C}(t_i)\right] \sigma_C^{-1}(t_i,t_j) \left[f(t_j) - \bar{C}(t_j)\right] \tag{A.19}$$

where the covariance matrix is

$$\sigma_C(t_i,t_j) = \frac{1}{N(N-1)} \sum_{k=1}^{N} \left(C_k(t_i) - \bar{C}(t_i)\right) \left(C_k(t_j) - \bar{C}(t_j)\right) . \tag{A.20}$$

For highly correlated data this covariance matrix may become singular. Equally well it will become singular as its dimension approaches the size of the data set, N. In either of these cases one must be careful using correlated χ^2 fits as this may lead to spurious results [90, 91, 92].

It is not feasible to generate distinct samples of configurations, so the errors on fit parameters are estimated from the given configuration set by using bootstrap resampling. The procedure is straightforward. A "fictional" configuration sample of size N, called a bootstrap sample, is generated by randomly sampling from the original configuration set, allowing for repetitions and omissions. Generating a set of bootstrap samples and performing the fits on each of these samples then gives a distribution of fit parameters from which an error on the best-fit parameters can be estimated.

Often one wants to fit to a secondary quantity such as the ratio of two correlators, $A(t)$ and $B(t)$ say. If both $\langle A(t)\rangle$ and $\langle B(t)\rangle$ are the configuration average (observables) then the configuration average of the ratio is

$$\langle R(t)\rangle = \frac{\langle A(t)\rangle}{\langle B(t)\rangle} \neq \left\langle \frac{A(t)}{B(t)} \right\rangle . \tag{A.21}$$

If the measurements $A(t)$ and $B(t)$ are independent then the fractional error in the ratio is easily estimated from quadrature of the individual fractional errors in $A(t)$ and $B(t)$. However measurements on a given timeslice like these are likely to be highly correlated. So, although $A(t)$ and $B(t)$ may separately have large statistical errors, the statistical error on the ratio may be much smaller because of these correlations.

So how is the error, or more importantly the covariance matrix, for a secondary quantity estimated ? In this work the jackknife method is used. It is similar to the bootstrap method. The idea is to create a configuration sample of "pseudo-measurements" for the ratio $R(t)$ and use this sample to determine the covariance matrix. It works as follows. For each of the configurations, n, calculate the configuration average for the ratio on the other $N-1$ configurations with this n-th configuration omitted,

$$R^{(n)}(t) = \frac{\langle A^{(n)}(t)\rangle}{\langle B^{(n)}(t)\rangle} \tag{A.22}$$

where

$$\langle A^{(n)}(t)\rangle = \frac{1}{N-1}\sum_{k\neq n}^{N-1} A_k(t) \tag{A.23}$$

and similarly for $B^{(n)}(t)$. The covariance matrix for R is then

$$\sigma_R(t_i,t_j) = \frac{1}{N(N-1)}\sum_{n=1}^{N}\left(R^{(n)}(t_i)-\bar{R}(t_i)\right)\left(R^{(n)}(t_j)-\bar{R}(t_j)\right) \tag{A.24}$$

and this can be used in subsequent χ^2-fits and bootstrap resampling. $\bar{R}(t)$ is determined as the average over the jackknife set $\{R^{(n)}(t)\}$ and so $\bar{R}(t) \neq \langle R(t)\rangle$ in general. The use of $\bar{R}(t)$ in the above ensures that the covariance matrix has the correct behaviour for a perfect Gaussian distribution. Naturally this procedure generalises to any secondary quantity one wishes to fit to.

Finally, in this work error estimates are given at the 68% confidence level and 250 bootstrap samples are used for estimating the errors on fit parameters.

Appendix B

Three-Point Functions

In this appendix I detail the Wick contractions for the three-point functions used in chapter 4.

B.1 General Case

The generic object of interest is

$$C_{3\mathrm{pt}}(t_x, t_y) = \sum_{\vec{x},\vec{y}} \langle 0|\, \chi^\dagger(\vec{x}, t_x)\, O(\vec{0}, 0)\, \chi^\dagger(\vec{y}, t_y)\, |0\rangle \tag{B.25}$$

with $\chi^\dagger = \bar{q}\,\Gamma_P\, b$ and

$$O = \bar{b}\Gamma_A q \bar{b}\Gamma_B q \ . \tag{B.26}$$

$\Gamma_P = \gamma_5$ for the pseudoscalar meson. Γ_A and Γ_B are the combinations of γ-matrices given in chapter 4. So, the term under the sum is

$$\langle 0|\ \bar{q}(\vec{x}, t_x)\, \Gamma_P\, b(\vec{x}, t_x)\, \bar{b}(\vec{0}, 0)\, \Gamma_A\, q(\vec{0}, 0)\bar{b}(\vec{0}, 0)\, \Gamma_B\, q(\vec{0}, 0)\, \bar{q}(\vec{y}, t_y)\, \Gamma_P\, b(\vec{y}, t_y)\ |0\rangle \ . \tag{B.27}$$

The spinor and colour indices have been suppressed for convenience. However, it is important for what follows to note that $\chi^\dagger$ is a spinor-colour singlet operator and each of the bilinears $\bar{b}\,\Gamma_{A,B}\, q$ in O are also spinor-colour singlets. Only spinor-colour singlets can be moved around inside this product without spoiling the matrix structure.

The Wick contraction can be performed in two ways: (1) $b(\vec{x}, t_x)$ with left-most $\bar{b}(\vec{0}, 0)$, and (2) $b(\vec{x}, t_x)$ with right-most $\bar{b}(\vec{0}, 0)$. Both ways give identical answers so I restrict attention to the first case. Proceeding thus gives

$$\bar{q}(\vec{x},t_x)\Gamma_P\ G_{(b)}(\vec{x},t_x;\vec{0},0)\,\Gamma_A\,q(\vec{0},0)\,\bar{q}(\vec{y},t_y)\Gamma_P\,G_{(b)}(\vec{y},t_y;\vec{0},0)\,\Gamma_B q(\vec{0},0)\ . \quad \text{(B.28)}$$

There are a further two ways of contracting the q fields: (a) $\bar{q}(\vec{x},t_x)$ with left-most $q(\vec{0},0)$ to give

$$\mathsf{Tr}\left[G_{(q)}(\vec{0},0;\vec{x},t_x)\,\Gamma_P\,G_{(b)}(\vec{x},t_x;\vec{0},0)\Gamma_A\right]\ \times\ \mathsf{Tr}\left[G_{(q)}(\vec{0},0;\vec{y},t_y)\,\Gamma_P\,G_{(b)}(\vec{y},t_y;\vec{0},0)\Gamma_B\right] \quad \text{(B.29)}$$

and (b) $\bar{q}(\vec{x},t_x)$ with right-most $q(\vec{0},0)$ giving

$$-\mathsf{Tr}\left[G_{(q)}(\vec{0},0;\vec{x},t_x)\,\Gamma_P\,G_{(b)}(\vec{x},t_x;\vec{0},0)\Gamma_A G_{(q)}(\vec{0},0;\vec{y},t_y)\,\Gamma_P\,G_{(b)}(\vec{y},t_y;\vec{0},0)\Gamma_B\right]\ . \quad \text{(B.30)}$$

The traces (Tr) are over the spinor-colour indices.

Now, using the hermiticity relation $G(0,x)=\gamma_5 G^\dagger(x,0)\gamma_5$, bringing the loose γ_5's to the ends of the traces and substituting $\Gamma_P=\gamma_5$ gives

$$\begin{aligned}
&\text{(a)}\quad \mathsf{Tr}\left[{G_{(q)}}^\dagger(\vec{x},t_x;\vec{0},0)\,G_{(b)}(\vec{x},t_x;\vec{0},0)\Gamma_A\gamma_5\right]\\
&\qquad\qquad\qquad\times\mathsf{Tr}\left[{G_{(q)}}^\dagger(\vec{y},t_y;\vec{0},0)\,G_{(b)}(\vec{y},t_y;\vec{0},0)\Gamma_B\gamma_5\right]\\
&\text{(b)}\quad -\mathsf{Tr}\left[{G_{(q)}}^\dagger(\vec{x},t_x;\vec{0},0)\,G_{(b)}(\vec{x},t_x;\vec{0},0)\Gamma_A\gamma_5{G_{(q)}}^\dagger(\vec{y},t_y;\vec{0},0)\,G_{(b)}(\vec{y},t_y;\vec{0},0)\Gamma_B\gamma_5\right]
\end{aligned}$$

respectively. The sums over $\vec{x}$ and $\vec{y}$ can be done independently. Hence it can be seen that the fundamental object to be calculated on the lattice is

$$A^{bd}_{\beta\delta}(t_x)=\sum_{\vec{x}}{G^{ab}_{(q)}}^{*}_{\alpha\beta}(\vec{x},t_x;\vec{0},0)\,{G^{ad}_{(b)}}_{\alpha\delta}(\vec{x},t_x;\vec{0},0) \quad \text{(B.31)}$$

– in other words with the *source* indices untraced[1]. Note that sink indices are to the left in the propagators. The full traces in cases (a) and (b), and hence the full correlator $C_{3\text{pt}}(t_x,t_y)$, can then be reconstructed from these matrices A.

[1]Greek letters are used for spinor indices and Roman for colour.

B.2 Static Case

There are some modifications to the above in the case where the b quark is treated in the static approximation. The reason is that the quark and antiquark fields are independent in the static limit. I use the same notation as before,

- b – 2 component column vector, annihilates quark.
- $b^\dagger$ – 2 component row vector, creates quark.
- $\tilde{b}$ – 2 component row vector, annihilates antiquark.
- $\tilde{b}^\dagger$ – 2 component column vector, creates antiquark.

for these separate fields. In the correlator only b and $b^\dagger$, or $\tilde{b}$ and $\tilde{b}^\dagger$, can be contracted with each other. These contractions give the usual propagators

$$\begin{aligned} H(\vec{x},t_x;\vec{0},0) &= \langle 0|\, b(\vec{x},t_x) b^\dagger(\vec{0},0)\,|0\rangle = \langle 0|\, \tilde{b}^\dagger(\vec{x},t_x)\tilde{b}(\vec{0},0)\,|0\rangle \\ &= \left(\frac{1+\gamma_4}{2}\right) P_{\vec{0}}(t_x,0)\delta^3(\vec{x}) \qquad t_x > 0 \qquad \text{(B.32)} \\ &= \left(\frac{1-\gamma_4}{2}\right) P_{\vec{0}}(t_x,0)\delta^3(\vec{x}) \qquad t_x < 0 \qquad \text{(B.33)} \end{aligned}$$

where $P_{\vec{0}}(t_x,0)$ is as in chapter 2.

In terms of these fields the operators in the three-point function are replaced as

$$\begin{aligned} \chi^\dagger(\vec{y},t_y)\,|0\rangle &\rightarrow \bar{q}(\vec{y},t_y)\,\Gamma_P\,\tilde{b}^\dagger(\vec{y},t_y)\,|0\rangle \qquad \text{(B.34)} \\ \langle 0|\,\chi^\dagger(\vec{x},t_x) &\rightarrow \langle 0|\,\bar{q}(\vec{x},t_x)\,\Gamma_P\,b(\vec{x},t_x) \qquad \text{(B.35)} \\ O(\vec{0},0) &\rightarrow b^\dagger(\vec{0},0)\,\Gamma_A\,q(\vec{0},0)\,\tilde{b}(\vec{0},0)\,\Gamma_B\,q(\vec{0},0)\ . \qquad \text{(B.36)} \end{aligned}$$

This gives the un-summed correlator as

$$\langle 0|\ \bar{q}(\vec{x},t_x)\,\Gamma_P\,b(\vec{x},t_x)\,b^\dagger(\vec{0},0)\,\Gamma_A\,q(\vec{0},0)\tilde{b}(\vec{0},0)\,\Gamma_B\,q(\vec{0},0)\,\bar{q}(\vec{y},t_y)\,\Gamma_P\,\tilde{b}^\dagger(\vec{y},t_y)\ |0\rangle\ . \qquad \text{(B.37)}$$

Unlike the general case, only one contraction of the b-quark fields is possible. So there is a factor two difference between the general and static case that one must take care of. Doing the b contractions, one is still left with the two possible contractions of the q fields as before. Hence the final traces are similar to before,

$$\begin{aligned}
&\text{(a)} \quad \mathsf{Tr}\left[{G_{(q)}}^{\dagger}(\vec{x},t_x;\vec{0},0)\, H(\vec{x},t_x;\vec{0},0)\Gamma_A\gamma_5\right] \\
&\qquad\qquad \times \mathsf{Tr}\left[{G_{(q)}}^{\dagger}(\vec{y},t_y;\vec{0},0)\, H(\vec{y},t_y;\vec{0},0)\Gamma_B\gamma_5\right] \\
&\text{(b)} \quad -\mathsf{Tr}\left[{G_{(q)}}^{\dagger}(\vec{x},t_x;\vec{0},0)\, H(\vec{x},t_x;\vec{0},0)\Gamma_A\gamma_5 {G_{(q)}}^{\dagger}(\vec{y},t_y;\vec{0},0)\, H(\vec{y},t_y;\vec{0},0)\Gamma_B\gamma_5\right] \; .
\end{aligned}$$

The operator at the source must be local so smearing can only be done at the sink. The smeared-at-sink static props are

$$\begin{aligned}
H^{SL}(\vec{x},t_x;\vec{0},0) &= \left(\frac{1\pm\gamma_4}{2}\right) f(\vec{x},0)P_{\vec{0}}(t_x,0) \\
&= \left(\frac{1\pm\gamma_4}{2}\right) P^{SL}_{\vec{x}}(t_x,0)
\end{aligned} \tag{B.38}$$

where f is the appropriate smearing function. Again the sum over $\vec{x}$ and $\vec{y}$ can be done independently so for this static case the fundamental object to calculate is the matrix

$$A^{\beta\delta}_{bd}(t_x) = \sum_{\vec{x}} G^{\alpha\beta *}_{(q)ab}(\vec{x},t_x;\vec{0},0) \left(\frac{1\pm\gamma_4}{2}\right)^{\alpha\delta} {P^{SL}_{\vec{x}}}_{ad}(t_x,0)\,. \tag{B.39}$$

Note that the second (first) two columns of the spinor matrix $A^{\beta\delta}$ are zero because of the $(1\pm\gamma_4)/2$ factor. Again the full three-point correlator can be reconstructed from this.

Appendix C

Choosing the Smearing Radius

Ideally the study presented in chapters 3 and 4 should have been completed at a variety of smearing radii for all the smearing types. This would have given a wider choice in the optimisation of the signal for each correlator and at each κ-value. In practice this was not possible, principally due to the limitations of time and the computing facilities available. However, to justify the smearing radii used, a subsidiary study on a subset of the configurations using a variety of smearing radii was performed. In this study just the LS and SS axial current correlators (as used for f_B) were calculated.

For the Coulomb gauge smearing functions the simulation was performed on 29 of the configurations using $r_0 = 4, 5, 6$. The first criterion used in choosing the "optimum" smearing radius is the existence and persistence of a plateau in the effective mass plots. Figures C.2, C.3 C.4 show the SS correlators at a single light kappa value using radii $r_0 = 4, 5, 6$ for each of the three types of Coulomb gauge smearing function, CUB, DCB and EXP respectively. The plots show that the signal for $r_0 = 5$ persists longer than for $r_0 = 4, 6$. The behaviour is similar in the LS correlators. These have a higher signal-to-noise ratio but generally approach the plateau region from below – these are not shown here. Finally, there is no appreciable difference in the behaviour of the effective mass plots at $\kappa = 0.14144, 0.14262$. Hence $r_0 = 5$ was chosen as the smearing radius for all Coulomb gauge smearing types and at all light κ values for the study on the full 60 configurations.

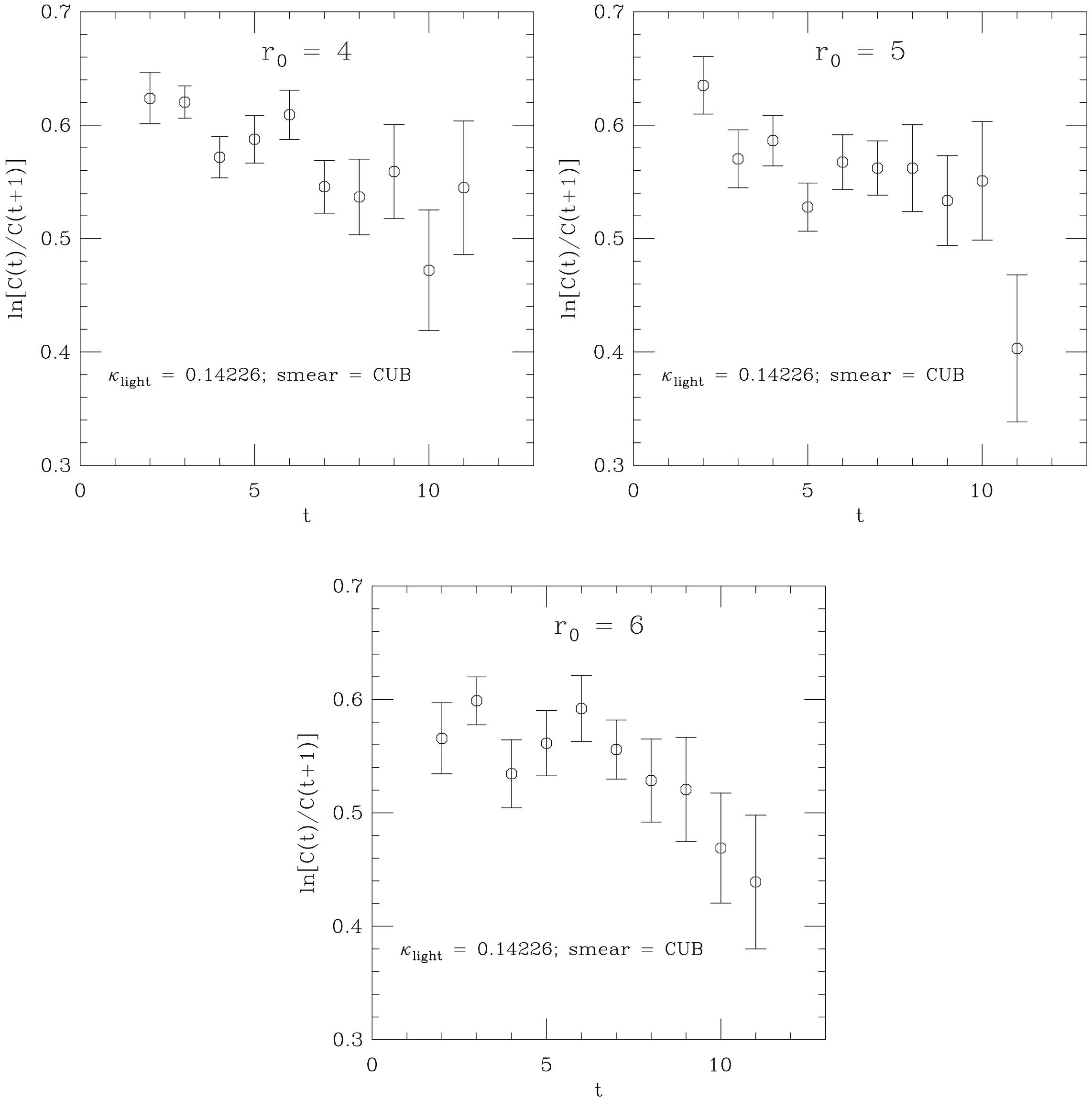

Figure C.2: Effective mass plots, $\ln[C(t)/C(t+1)]$ versus t, for SS correlators at light $\kappa = 0.14226$ using CUB smearing for each of the radii $r_0 = 4, 5, 6$ on a subset of 29 configurations.

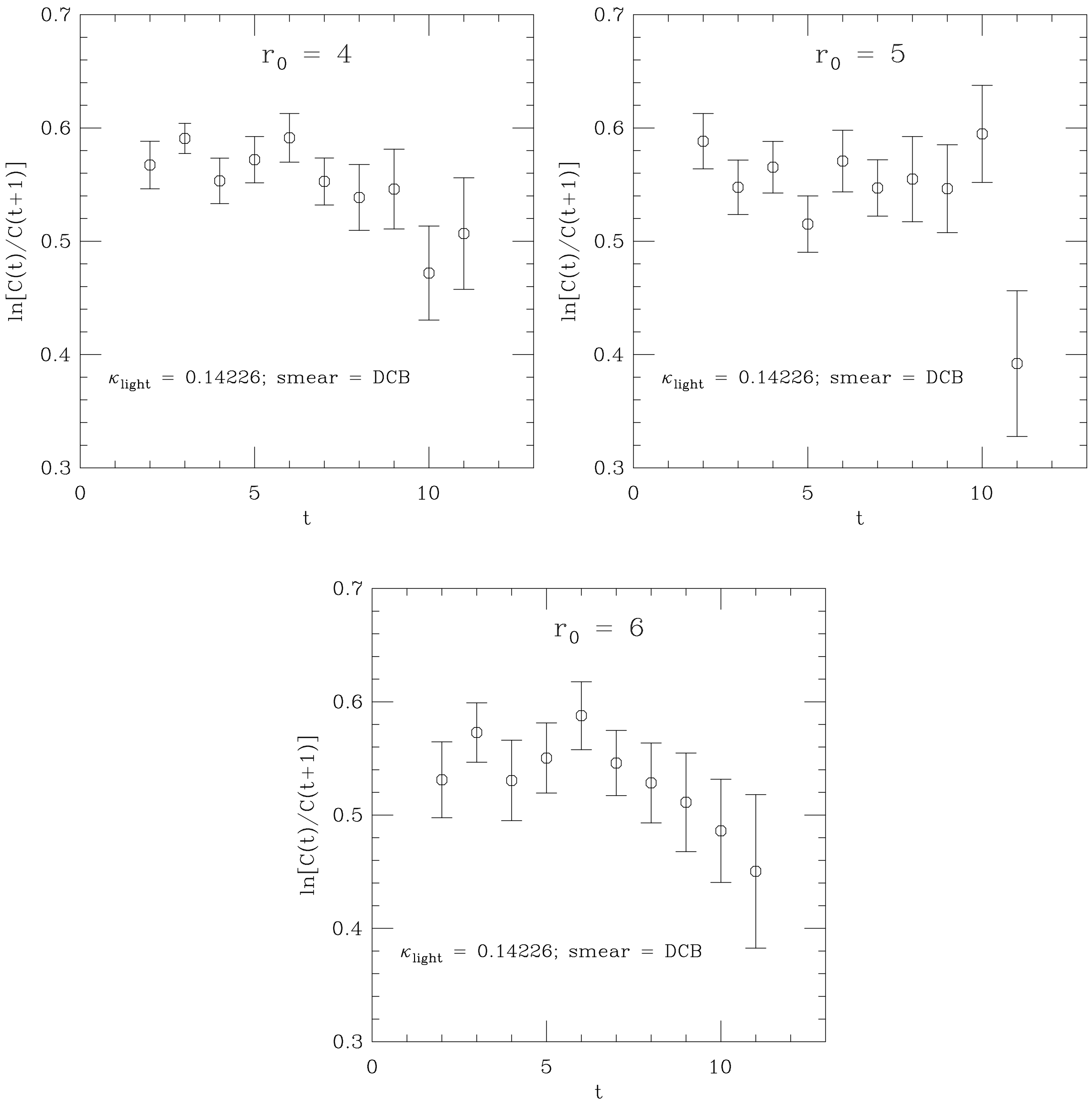

Figure C.3: Effective mass plots, $\ln[C(t)/C(t+1)]$ versus t, for SS correlators at light $\kappa = 0.14226$ using DCB smearing for each of the radii $r_0 = 4, 5, 6$ on a subset of 29 configurations.

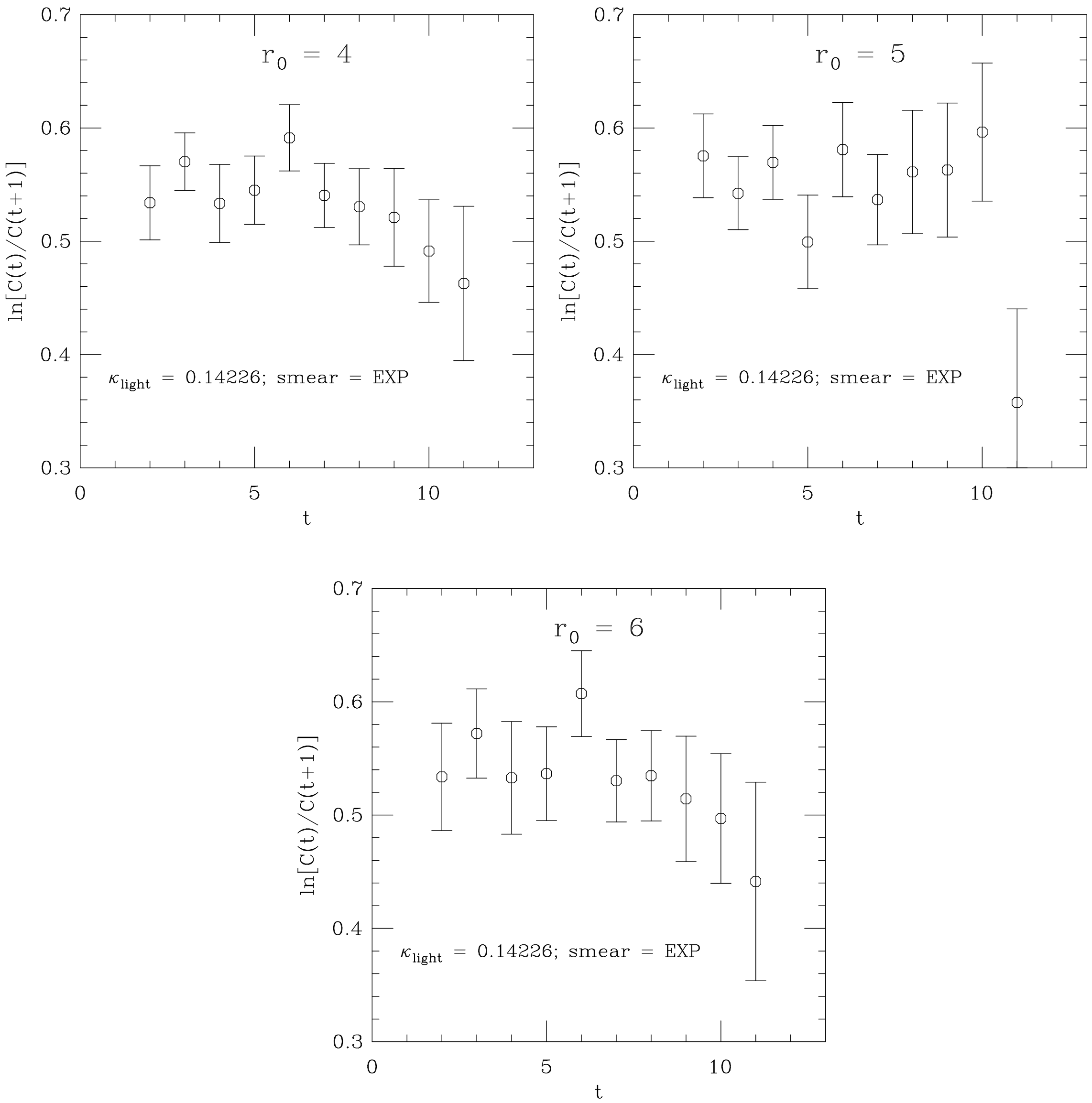

Figure C.4: Effective mass plots, $\ln[C(t)/C(t+1)]$ versus t, for SS correlator at light $\kappa = 0.14226$ using EXP smearing for each of the radii $r_0 = 4, 5, 6$ on a subset of 29 configurations.

In the case of the gauge invariant smearing technique the smearing radius is varied by changing the number of iterations of the Jacobi algorithm, N. In this study the simulation was performed on a subset of 30 of the configurations using $N = 80, 110, 140, 170, 200$.

N	R.M.S. Radius
80	5.1 ± 0.1
110	5.8 ± 0.2
140	6.5 ± 0.2
170	7.0 ± 0.3
200	7.4 ± 0.3

Table C.1: R.m.s radius for each of the iterations, N, of the Jacobi algorithm, averaged over 30 configurations – the errors are statistical.

From the effective mass plots at $\kappa = 0.14226$, figures C.5 and C.6, it is not clear which of the smearing radii is optimal. Also the fitted values for the effective mass are relatively consistent across the different radii – see table C.2. The ratios $C^{\mathrm{LS}}/C^{\mathrm{SS}}$ are also plotted[2] at $\kappa = 0.14226$, figures C.7 and C.8. The trend in these plots suggests higher values of N give worse results. The behaviour is similar at $\kappa = 0.14144, 0.14262$ (these plots are not shown), but at the higher κ value the plateaux for the higher values of N are slightly improved and vice-versa. This observation qualitatively agrees with the results of Duncan *et al.* [76]. They tune the smearing radius independently for each light κ value.

	80	110	140	170	200
Range	[6–9]	[6–9]	[6–10]	[6–10]	[6–10]
0.14144	$0.580\ ^{+11}_{-11}$	$0.574\ ^{+11}_{-11}$	$0.569\ ^{+11}_{-7}$	$0.569\ ^{+10}_{-12}$	$0.569\ ^{+10}_{-14}$
0.14226	$0.561\ ^{+11}_{-11}$	$0.554\ ^{+11}_{-11}$	$0.555\ ^{+11}_{-11}$	$0.544\ ^{+11}_{-13}$	$0.544\ ^{+12}_{-14}$
0.14262	$0.553\ ^{+11}_{-11}$	$0.545\ ^{+12}_{-12}$	$0.551\ ^{+12}_{-9}$	$0.532\ ^{+12}_{-14}$	$0.531\ ^{+13}_{-15}$
κ_{crit}	$0.540\ ^{+12}_{-12}$	$0.533\ ^{+12}_{-12}$	$0.534\ ^{+12}_{-12}$	$0.522\ ^{+11}_{-12}$	$0.519\ ^{+11}_{-13}$

Table C.2: The SS effective mass in lattice units at each of the light κ values along with the chiral extrapolated value. All the χ^2/dof are less than one.

[2]The scales in these ratio plots should not be compared.

The data seems to favour using $N = 110, 140$ over the others. The higher values of Z_L and effective mass using $N = 80$ suggests smearing using this radius hasn't clearly isolated the ground state. Similarly, the behaviour of ratio $C^{\mathrm{LS}}/C^{\mathrm{SS}}$ for $N = 170, 200$ suggests against the use of these radii. At any rate, it was decided to use $N = 140$ at all values of κ for the study on the full set of 60 configurations. This is a convenient choice in that it is consistent with previously published work using a subset of these configurations [50]. However, I believe this study really needs to be done on a larger configuration set to correctly sort out this issue of "optimal" smearing radius.

Finally, the chiral extrapolations of Z_L using fitting method I (see chapter 3) are also presented – figures C.9, C.10 and table C.3. The results using fitting method II are entirely consistent. The results for the correlated fits for $N = 140$ seem to be better behaved than for the other values of N. This is also true when the fitting ranges are varied.

		80	110	140	170	200
Range	R	[8–10]	[8–10]	[8–11]	[8–11]	[9–11]
	SS	[6–10]	[6–10]	[6–11]	[6–11]	[6–11]
0.14144		0.159^{+10}_{-10}	0.149^{+10}_{-10}	0.140^{+6}_{-6}	0.139^{+9}_{-12}	0.138^{+9}_{-13}
0.14226		0.144^{+9}_{-8}	0.135^{+9}_{-8}	0.128^{+7}_{-6}	0.123^{+9}_{-11}	0.121^{+8}_{-12}
0.14262		0.138^{+9}_{-8}	0.128^{+9}_{-9}	0.125^{+7}_{-6}	0.116^{+9}_{-10}	0.114^{+8}_{-12}
κ_{crit}	COR	0.130^{+9}_{-8}	0.121^{+8}_{-7}	0.117^{+7}_{-6}	0.105^{+9}_{-9}	0.106^{+7}_{-11}
	UNC	0.128^{+9}_{-8}	0.119^{+9}_{-8}	0.118^{+8}_{-7}	0.105^{+9}_{-9}	0.103^{+9}_{-11}
f_{B_s}/f_{B_d}	COR	1.17^{+2}_{-2}	1.19^{+2}_{-2}	1.15^{+2}_{-3}	1.22^{+2}_{-4}	1.23^{+3}_{-4}
	UNC	1.18^{+3}_{-3}	1.19^{+3}_{-3}	1.14^{+4}_{-4}	1.24^{+3}_{-5}	1.25^{+4}_{-5}

Table C.3: Z_L at each of the light κ values determined using fitting method I (see chapter 3), with the correlated (COR) and uncorrelated (UNC) chiral extrapolated values. The values for f_{B_s}/f_{B_d} are also quoted. The fit ranges are for the ratio (R) and the SS correlator. The same ranges are used at all κ values. Again all the χ^2/dof are less than one.

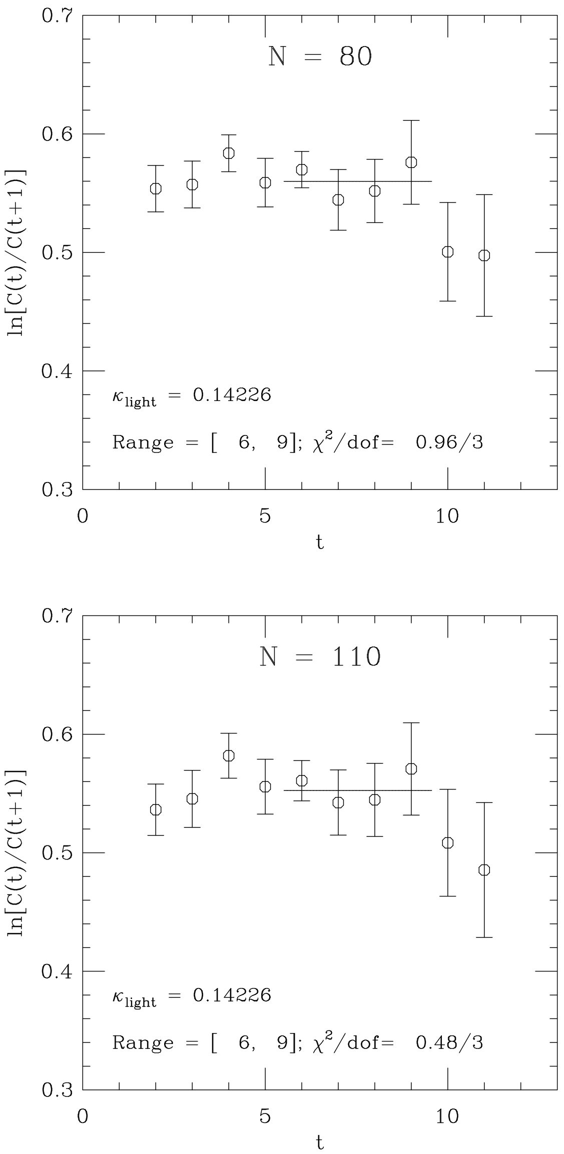

Figure C.5: Effective mass plots, $\ln[C(t)/C(t+1)]$ versus t, for SS correlators at light $\kappa = 0.14226$ using INV smearing for iterations of the Jacobi algorithm $N = 80, 110$ on a subset of 30 configurations.

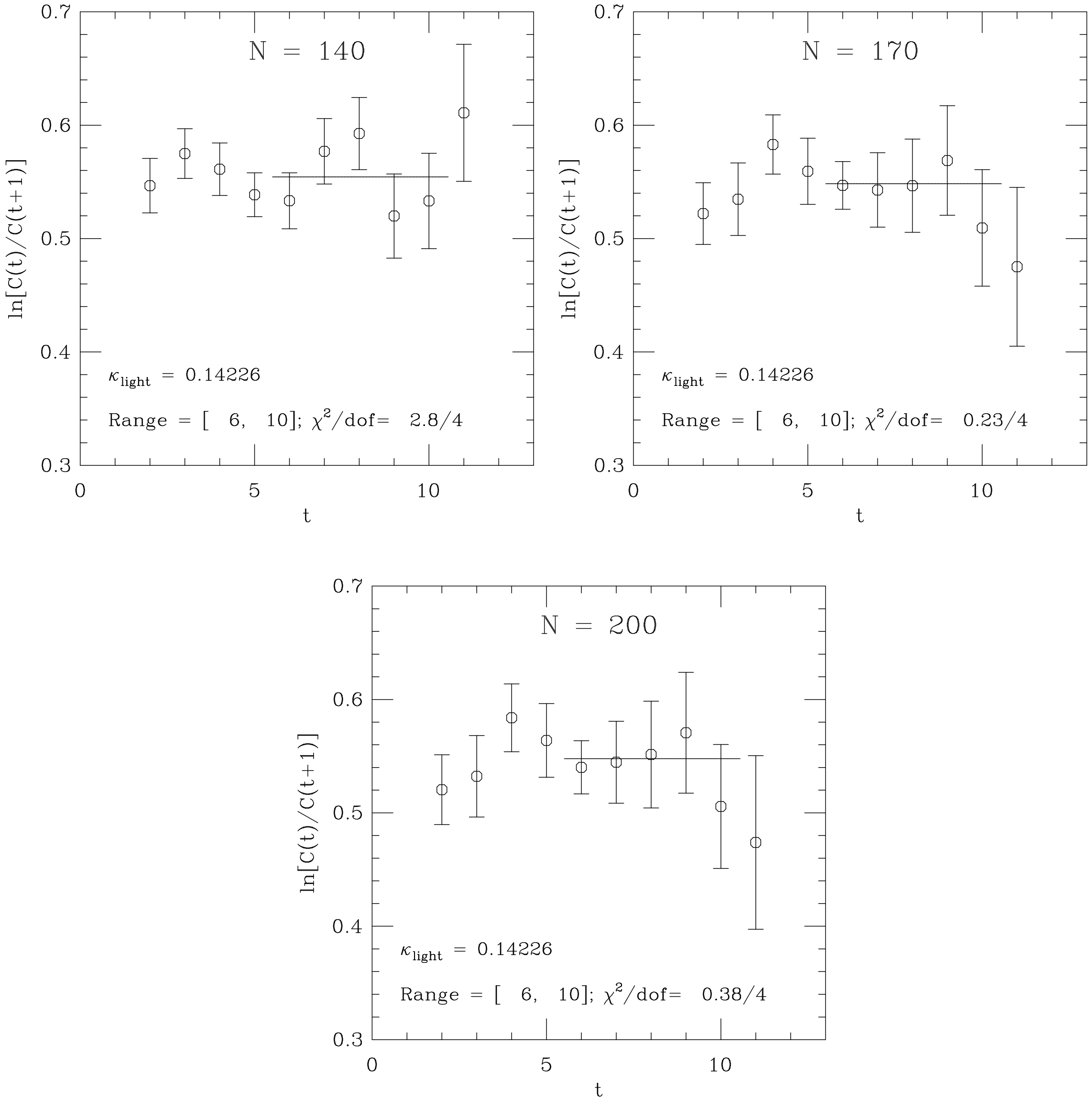

Figure C.6: Effective mass plots, $\ln[C(t)/C(t+1)]$ versus t, for SS correlators at light $\kappa = 0.14226$ using INV smearing for iterations of the Jacobi algorithm $N = 140, 170, 200$ on a subset of 30 configurations.

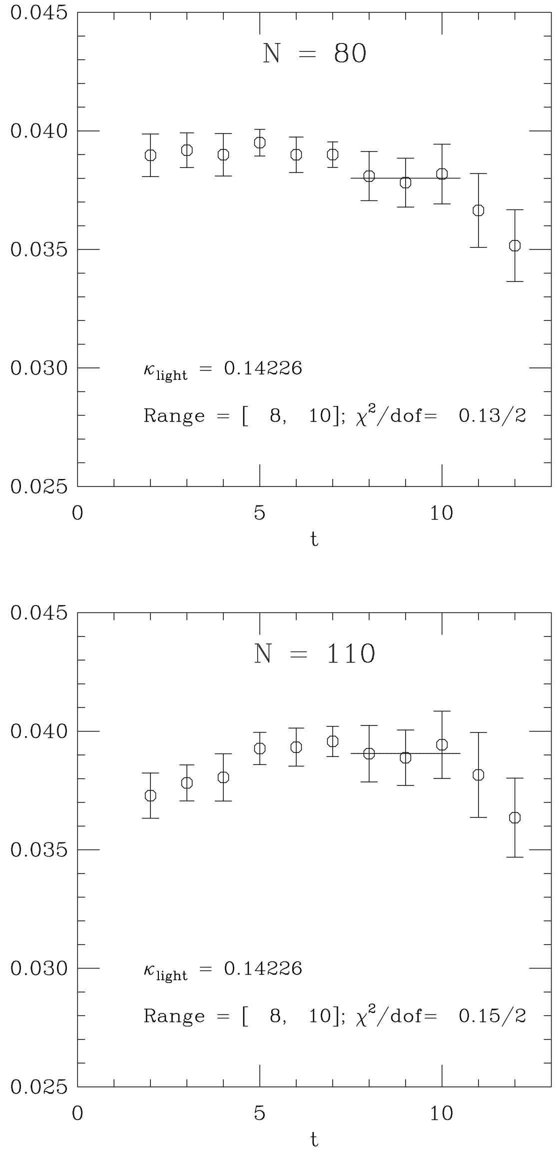

Figure C.7: Plots of the ratio $C^{\rm LS}(t)/C^{\rm SS}(t)$ versus t at light $\kappa = 0.14226$ using INV smearing for iterations of the Jacobi algorithm $N = 80, 110$ on a subset of 30 configurations.

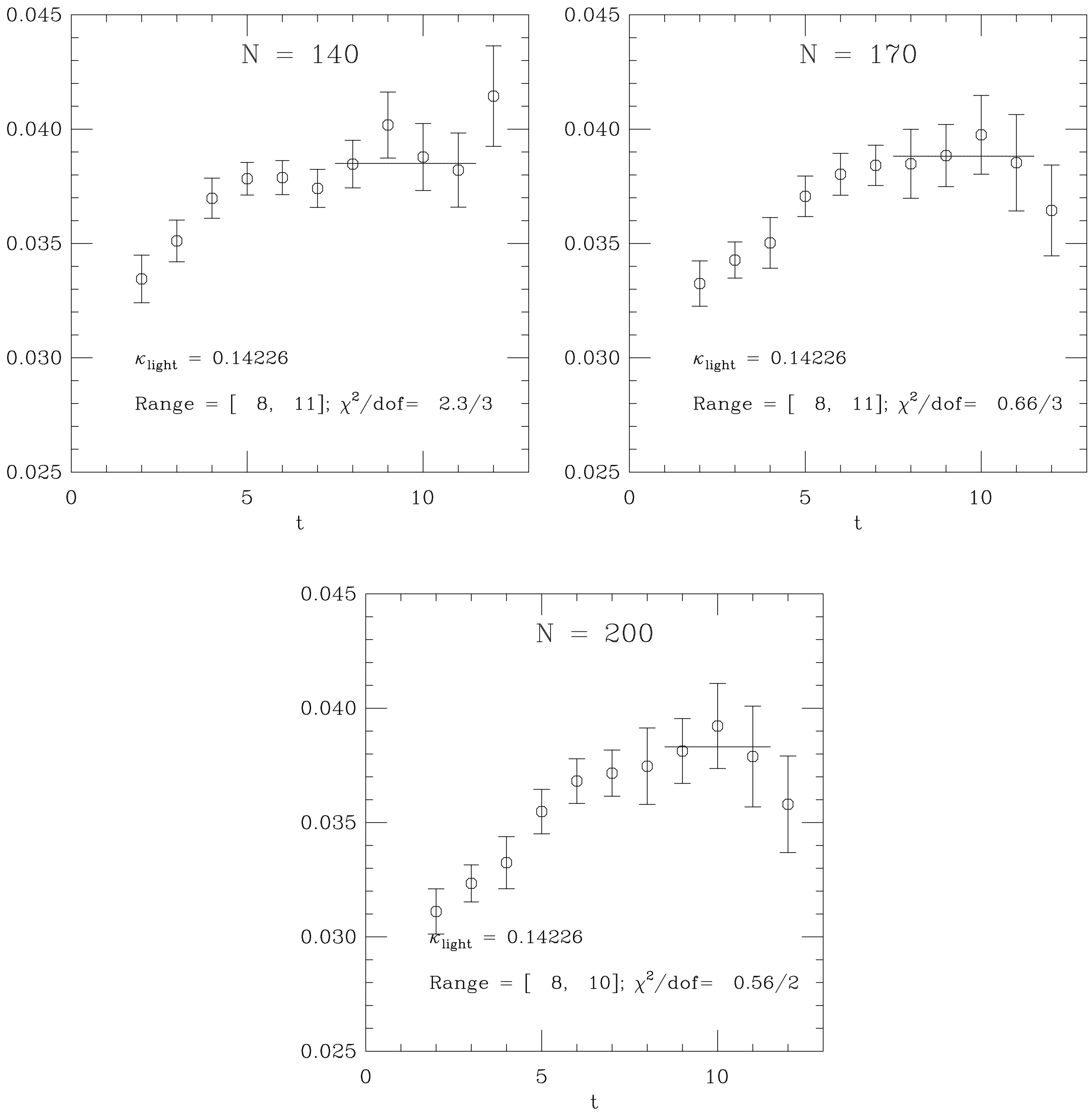

Figure C.8: Plots of the ratio $C^{\text{LS}}(t)/C^{\text{SS}}(t)$ versus t at light $\kappa = 0.14226$ using INV smearing for iterations of the Jacobi algorithm $N = 140, 170, 200$ on a subset of 30 configurations.

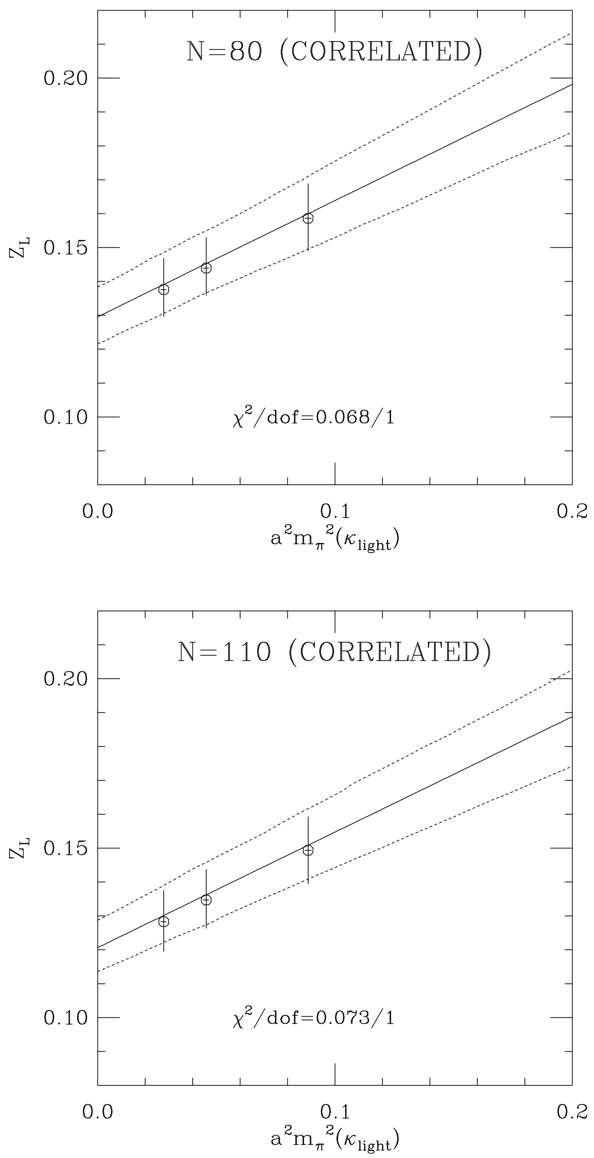

Figure C.9: Chiral extrapolations of Z_L, fitted from method I, using INV smearing for iterations of the Jacobi algorithm $N = 80, 110$ on a subset of 30 configurations. The dashed lines in the plots are the 68% errors on the fit parameters.

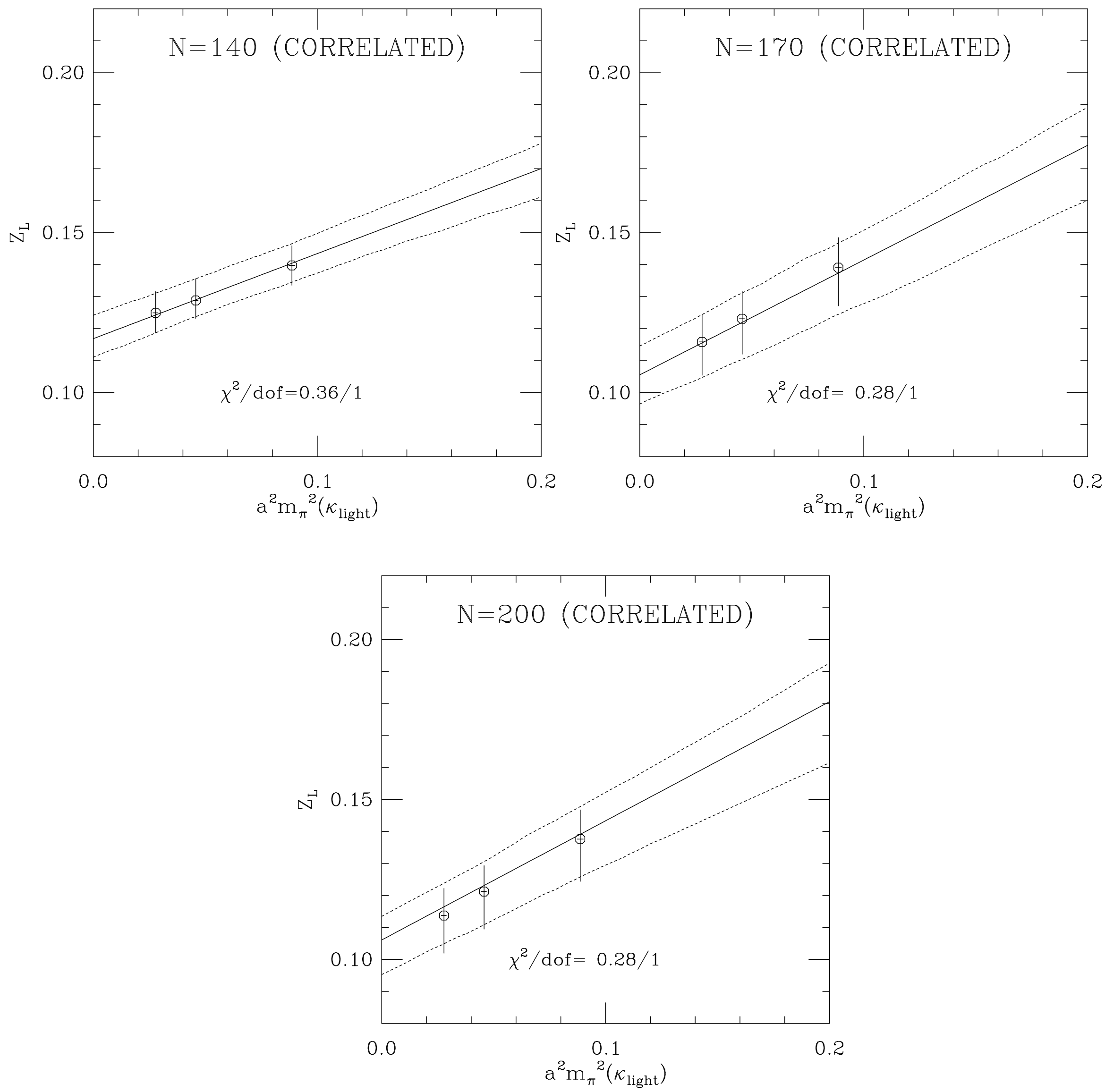

Figure C.10: Chiral extrapolations of Z_L, fitted from method I, using INV smearing for iterations of the Jacobi algorithm $N = 140, 170, 200$ on a subset of 30 configurations. The dashed lines in the plots are the 68% errors on the fit parameters.

References

[1] N. Cabibbo, Phys. Lett. **10**, 531 (1963).

[2] M. Kobayashi and K. Maskawa, Prog. Theor. Phys **49**, 652 (1973).

[3] R. D. Peccei, in *CP Violation*, edited by C. Jarlskog (World Scientific, Singapore, 1989).

[4] C. Jarlskog, Phys. Rev. Lett. **55**, 1039 (1985).

[5] Particle Data Group, Phys. Rev. D **50**, (1994).

[6] L. Wolfenstein, Phys. Rev. Lett. **51**, 1945 (1983).

[7] J. F. Donoghue, E. Golowich, and B. R. Holstein, *Dynamics of the Standard Model* (Cambridge University Press, Cambridge, 1992).

[8] R. Forty, in *Proceedings of the XXVII Int. Conf. on High Energy Physics, Glasgow, UK, 20-27 July, 1994*, edited by P. J. Bussey and I. G. Knowles (Institute of Physics Publishing, Bristol and Philadelphia, 1995), Vol. 1, p. 171.

[9] M. Lautenbacher, in *Proceedings of the XXVII Int. Conf. on High Energy Physics, Glasgow, UK, 20-27 July, 1994*, edited by P. J. Bussey and I. G. Knowles (Institute of Physics Publishing, Bristol and Philadelphia, 1995), Vol. 2, p. 747.

[10] A. J. Buras, in *Proceedings of the XXVII Int. Conf. on High Energy Physics, Glasgow, UK, 20-27 July, 1994*, edited by P. J. Bussey and I. G. Knowles (Institute of Physics Publishing, Bristol and Philadelphia, 1995), Vol. 2, p. 1307.

[11] A. J. Buras, hep-ph/[9503262] (1995).

[12] A. Ali and D. London, Z. Phys. C **65**, 431 (1995).

[13] C. Bernard, in *From Actions to Answers*, edited by T. DeGrand and D. Toussaint (World Scientific, Singapore, 1990).

[14] M. K. Gaillard and B. W. Lee, Phys. Rev. Lett. **33**, 108 (1974).

[15] T. Inami and C. S. Lim, Prog. Theor. Phys **65**, 297 (1981), ibid **65** (1981) 1772.

[16] A. J. Buras, M. Jamin, and P. H. Weisz, Nucl. Phys. B **347**, 491 (1990).

[17] B. Grinstein *et al.*, Nucl. Phys. B **380**, 369 (1992).

[18] M. Neubert, Phys. Rep. **245**, 259 (1994).

[19] T. Mannel, W. Roberts, and Z. Ryzak, Nucl. Phys. B **368**, 204 (1992).

[20] H. Georgi, Phys. Lett. B **240**, 447 (1990).

[21] E. Eichten, Nucl. Phys. B (Proc. Suppl.) **4**, 170 (1988).

[22] A. F. Falk, B. Grinstein, and M. E. Luke, Nucl. Phys. B **357**, 185 (1991).

[23] M. E. Luke and A. V. Manohar, Phys. Lett. B **286**, 348 (1992).

[24] X. Ji and M. J. Musolf, Phys. Lett. B **257**, 409 (1991).

[25] H. D. Politzer and M. B. Wise, Phys. Lett. B **208**, 504 (1988).

[26] B. Grinstein, Nucl. Phys. B **339**, 253 (1990).

[27] R. F. Streater and A. S. Wightman, *PCT, Spin and Statistics and All That* (W. A. Benjamin, New York, 1964).

[28] I. Montvay and G. Münster, *Quantum Fields on a Lattice* (Cambridge University Press, Cambridge, 1994).

[29] K. G. Wilson, Phys. Rev. D **10**, 2445 (1974).

[30] J. F. Cornwell, *Group Theory in Physics, Vols. 1,2* (Academic Press, London, 1984).

[31] H. J. Rothe, *Lattice Gauge Theories* (World Scientific, Singapore, 1992).

[32] K. G. Wilson, in *New Phenomena in Subnuclear Physics*, edited by A. Zichichi (Plenum, New York, 1975).

[33] J. Kogut and L. Susskind, Phys. Rev. D **11**, 395 (1975).

[34] H. B. Nielsen and M. Ninomiya, Nucl. Phys. B **185**, 20 (1981).

[35] L. H. Karsten and J. Smit, Nucl. Phys. B **183**, 103 (1981).

[36] H. W. Hamber and C. M. Wu, Phys. Lett. B **136**, 255 (1984).

[37] G. Heatlie *et al.*, Nucl. Phys. B **352**, 266 (1991).

[38] B. Sheikholeslami and R. Wohlert, Nucl. Phys. B **259**, 572 (1985).

[39] N. Metropolis *et al.*, J. Chem. Phys. **21**, 1087 (1953).

[40] F. Butler *et al.*, Phys. Rev. Lett. **70**, 2849 (1993).

[41] S. R. Sharpe, in *CP Violation and the Limits of the Standard Model*, edited by J. Donoghue (World Scientific, Singapore, 1995).

[42] A. D. Simpson, Ph.D. thesis, University of Edinburgh, 1991.

[43] S. Güsken, Nucl. Phys. B (Proc. Suppl.) **17**, 361 (1990).

[44] S. L. Adler and R. Dashen, *Current Algebras and Applications to Particle Physics* (W. A. Benjamin, New York, 1968).

[45] UKQCD Collaboration, C. R. Allton *et al.*, Phys. Rev. D **49**, 474 (1994).

[46] R. M. Baxter, Ph.D. thesis, University of Edinburgh, 1993.

[47] G. Lepage and P. Mackenzie, Phys. Rev. D **48**, 2250 (1992).

[48] E. Eichten, Nucl. Phys. B (Proc. Suppl.) **26**, 391 (1992).

[49] C. Bernard, C. M. Heard, J. Labrenz, and A. Soni, Nucl. Phys. B (Proc. Suppl.) **26**, 384 (1992).

[50] UKQCD Collaboration, R. M. Baxter *et al.*, Phys. Rev. D **49**, 1594 (1994).

[51] C. Bernard, J. N. Labrenz, and A. Soni, Phys. Rev. D **49**, 2536 (1994).

[52] P. B. Mackenzie, Nucl. Phys. B (Proc. Suppl.) **30**, 35 (1993).

[53] A. S. Kronfeld, Nucl. Phys. B (Proc. Suppl.) **30**, 445 (1993).

[54] C. T. Davies *et al.*, Phys. Rev. Lett. **73**, 2645 (1994).

[55] C. T. H. Davies, Nucl. Phys. B (Proc. Suppl.) **42**, 319 (1995).

[56] UKQCD Collaboration, C.T.H. Davies *et al.*, Nucl. Phys. B (Proc. Suppl.) **34**, 437 (1994).

[57] A. A. Khan, Nucl. Phys. B (Proc. Suppl.) **42**, 382 (1995).

[58] S. Collins, Nucl. Phys. B (Proc. Suppl.) **42**, 395 (1995).

[59] UKQCD Collaboration, C. R. Allton *et al.*, Nucl. Phys. B **407**, 331 (1993).

[60] R. Sommer, Nucl. Phys. B **411**, 839 (1994).

[61] UKQCD Collaboration, (H. Wittig), Nucl. Phys. B (Proc. Suppl.) **42**, 288 (1995).

[62] UKQCD Collaboration, D. S. Henty *et al.*, Phys. Rev. D **51**, 5323 (1995).

[63] UKQCD Collaboration, A. K. Ewing *et al.*, Submitted to Phys. Rev. D .

[64] E. Eichten and B. Hill, Phys. Lett. B **234**, 511 (1990).

[65] E. Eichten and B. Hill, Phys. Lett. B **240**, 193 (1990).

[66] A. Borrelli and C. Pittori, Nucl. Phys. B **385**, 502 (1992).

[67] O. F. Hernández and B. R. Hill, Phys. Lett. B **289**, 417 (1992).

[68] D. Richards, Private Communication .

[69] S. Gusken, Phys. Lett. B **227**, 266 (1989).

[70] UKQCD Collaboration, C. R. Allton *et al.*, Phys. Rev. D **47**, 5128 (1993).

[71] APE Collaboration, P. Bacilieri *et al.*, Phys. Lett. B **214**, 115 (1988), nucl. Phys. B 317, (1989) 509.

[72] M. L. Paciello *et al.*, Phys. Lett. B **289**, 405 (1992).

[73] J. Mandula and M. Ogilvie, Phys. Lett. B **248**, 158 (1990).

[74] V. N. Gribov, Nucl. Phys. B **139**, 1 (1978).

[75] APE Collaboration, C. R. Allton *et al.*, Phys. Lett. B **236**, 295 (1994).

[76] A. Duncan *et al.*, Phys. Rev. D **51**, 5101 (1995).

[77] T. Draper and C. McNeile, Nucl. Phys. B (Proc. Suppl.) **34**, 453 (1994).

[78] T. Draper, C. McNeile, and C. Nenkov, Nucl. Phys. B (Proc. Suppl.) **42**, 325 (1995).

[79] C. R. Allton, Nucl. Phys. B **437**, 641 (1995).

[80] APE Collaboration, C. R. Allton *et al.*, Nucl. Phys. B (Proc. Suppl.) **42**, 385 (1995).

[81] C. Alexandrou *et al.*, Nucl. Phys. B **414**, 815 (1994).

[82] APE Collaboration, C. R. Allton *et al.*, Nucl. Phys. B **413**, 461 (1994).

[83] C. R. Allton *et al.*, Nucl. Phys. B **349**, 598 (1991).

[84] J. M. Flynn, O. F. Hernández, and B. R. Hill, Phys. Rev. D **43**, 3709 (1991).

[85] O. F. Hernández and B. R. Hill, Phys. Lett. B **237**, 95 (1990).

[86] G. Martinelli *et al.*, Nucl. Phys. B **414**, 815 (1995).

[87] A. Abada *et al.*, Nucl. Phys. B **376**, 172 (1992).

[88] S. R. Sharpe, Nucl. Phys. B (Proc. Suppl.) **34**, 403 (1994).

[89] W. H. Press, S. A. Teukolsky, W. T. Vetterling, and B. P. Flannery, *Numerical Recipes in C* (Cambridge University Press, Cambridge, 1992).

[90] C. Michael, Phys. Rev. D **49**, 2616 (1994).

[91] C. Michael, Phys. Rev. D **51**, 3745 (1995).

[92] D. Seibert, Phys. Rev. D **49**, 6240 (1994).